CHAPTER 1

INTRODUCTION

1.1 BACKGROUND

Gas turbines play an important role in many modern industries. The two prominent industries that come to mind are the aircraft industry and the power generation industry [1,2]. In addition to these well-established industries, gas turbines are used today for varying industrial heating applications [3]. The aircraft industry is the biggest user of gas turbines, and this is due to their advantages of range, speed and comfort [4]. It is also possible to increase the efficiency of gas turbines by using combined heat and power or the cogeneration concept [5,6]. This concept is regarded as one way of saving the already depleted fossil fuel energy.

Although gas turbines offer important advantages, they have to fulfil performance requirements, some of which are conflicting and non-linearly related [4]. These performance requirements are related to the exit temperature profile, exhaust emissions, pressure loss, thermo-acoustic waves and noise, stability and structural integrity [2]. Unfortunately, almost all of the above performance requirements are related to the effective operation of the combustor [2]. Since the performance requirements are sometimes conflicting, the design of a gas turbine combustor is a challenging task. In the aircraft industry, the difficulty in designing the combustor is exacerbated by the constraints of space and weight [7].

One of the bigger challenges in gas turbine design is to achieve a desired exit temperature profile at the combustor exit. Exit temperature profile is one of the most critical parameters that affect the temperature distribution over the turbine blades [2]. The fact that the exit temperature profile has drastic effects on the life of turbine blades, and hence affects the maintenance costs, makes it a critical design requirement

[8]. The need to increase the power output and efficiency of the gas turbine also necessitates an increase in the combustor exit temperature, which puts more pressure on the design requirements [8].

In the early days of gas turbine combustor design, a number of empirical relations in conjunction with semi-empirical techniques supported by experiments were the main design approaches [9,10]. Design optimisation was based on a trial-and-error method where the approach was to repetitively test different variants of the combustor until a suitable arrangement was found. This approach was costly and time-consuming because of multiple rig testing performed in order to reach a correct design [11]. With advances in computer power, the role played by simulation codes (computational fluid dynamics software) in combustor development changed the design process remarkably, and these codes have now become a valuable part of an overall integrated design system [12]. But a lot had to be done on the validation of the codes with experimental data.

In terms of design optimisation, computational fluid dynamics still has some disadvantages similar to that of the previous experimental method. It is still costly to run repetitive trial-and-error computational simulations in trying to get satisfactory performance requirements [7]. These trial-and-error parametric variations are also influenced by the skill and past experience of the designer. The use of computational fluid dynamics tools, even though these are not perfect and still have serious deficiencies [12], resulted in a giant leap in terms of design capability, costs and lead time [13,14].

Having recognised that computational fluid dynamics has drastically reduced experimental costs and lead time [13,14], what remains is to find a solution for its inherent trial-and-error parametric approach in design optimisation. This requires that while the advantages of both experimental and computational fluid dynamics in design optimisation approaches are being exploited, these approaches should be complemented by a mechanism that would search for the optimum design. A tool that can achieve this is a suitable mathematical optimisation algorithm [15,16]. Mathematical optimisation has been applied to numerous design problems, many of which are in the area of computational structural mechanics [17-19]. In this regard, however, combustion has not been a popular candidate due to a lack of viable

analytical equations for and complexity in modelling the process [20]. Nevertheless, the practice of coupling computational fluid dynamics to mathematical optimisation has recently been shown to be capable of producing designs, which can be called optimum within reasonable computational time [21].

In engineering, mathematical optimisation or so-called "automated or numerical" optimisation usually implies the application of an optimisation algorithm integrated into a numerical simulation software package for the automated optimal modification of design variables. As already stated, for complex problems such as the design of a combustion system, optimisation tools have not been widely used to date. But now, with the availability of powerful high-speed computers, the repetitive simulation of the combustion process has become feasible, which makes the design of a combustion system a suitable candidate for mathematical optimisation [22].

Mathematical optimisation tools can be grouped into two classes, being single-objective and multi-objective methods [23]. The decision on which method to use depends on the number of criteria involved, but for determining the global minimum of a specific performance parameter, such as the combustor exit temperature profile considered in this study, a single-objective algorithm is preferable [20]. Although Paschereit et al. [20] used a multi-objective method, it is suggested in the same work that for determining a global minimum of a specific performance, a single-objective algorithm is preferable.

Technical product design optimisation involves at least two aspects: first, the product design has to be described in terms of a set of design variables and secondly, evaluation tools (computational fluid dynamics software) are required for the evaluation of the design properties or objective function. The optimisation algorithm points to new possibly improved designs, which are automatically evaluated with the analysis tools such as computational fluid dynamics. Depending on the resulting objective values, the process continues until a certain termination criterion is fulfilled.

It is useful to automate the tuning of the design variables using optimisation techniques in order to support the designer in his/her task. The multidisciplinary

design optimisation approach, particularly its application to optimisation of the combustor exit temperature profile, remains a topic to be researched.

The aim in this study, therefore, is to combine computational fluid dynamics and mathematical optimisation in order to optimise the combustor exit temperature profile, with respect to design variables which will be chosen to be combustor parameters that directly affect the combustor exit temperature profile. The mathematical optimisation process will be constrained such that certain performance parameters are not violated. In the past, deficiencies in performing optimisation without the use of numerical optimisation techniques hindered the progress in combustor design and hindered the achievement of the maximum performance point for a given technology and increased the time and cost to achieve a desired set of the performance target [12].

The principal aim of this work is to investigate the feasibility of using a gradient-based approximation method for the computationally efficient optimisation of a combustor exit temperature profile. The particular methodology used here entails the use of computational fluid dynamics and the successive approximation method [24,25] to produce an optimum combustor exit temperature profile. This suggested method originates from the fact that the trial-and-error methods commonly used for optimising the combustor exit temperature profile do not guarantee near-optimal solutions [2], and are also extremely time-consuming and costly.

3.1 REVIEW OF RELATED LITERATURE

Until the 1970s, combustor design was considered more an art than a science. It was mostly based on trial-and-error methods where the approach was to repetitively test different variants of the combustor until a suitable arrangement could be reached [12]. It made use of a few empirically based design rules [26,27] and relied on repeated testing to achieve a suitable design. Anand and Priddin [12] highlighted that some 75% of all hardware costs were spent on the trial-and-error design cycle.

Combustor exit temperature design optimisation is a critical area in the design of a gas turbine combustor. The maximum combustor exit temperature is governed by the

working temperature of the highly stressed turbine blades [8]. The temperature must not be allowed to exceed a certain critical limit. This value depends on the creep strength of the materials used in the construction of the turbine blade and the required working life of the turbine blade. It is also very important that the temperature distribution of the combustor exit temperature conforms to a target profile that is also governed by the turbine blades [4].

Few studies, however, have focused on how the combustor exit environment affects the performance of the turbine. Shang *et al.* [28] conducted some tests on the influence of the inlet temperature distortion on rotor blades. It is reported that the radial temperature distortion results in significant augmentation of local blade heat transfer. Nusselt numbers 10% higher than those measured with uniform conditions within the tip region and 50% higher within the hub region were reported and similar trends are reported in references [29] to [31]. The investigation of Krishnamoorty *et al*. [32] also revealed that the cooling effectiveness can be reduced by as much as 10% as a result of temperature distortions. Higher combustor exit temperatures require complex turbine blade cooling systems causing additional component losses. With better design optimisation methods of the combustor exit temperature, it would be possible to increase the power output and efficiency of gas turbines by increasing the pressure ratio and exit temperature. This has the advantages of decreasing the specific fuel consumption and, consequently, the reduction of the size and weight of the engine can be very considerable, particularly in the aircraft industry [4].

Design optimisation of the combustor exit temperature profile was attempted first by applying dilution hole design procedures [2,26]. Methods that use a similar procedure based on empirically derived expressions are reported by Lefebvre [2]. These methods that follow later in the manuscript are the Cranfield approach in equation (1.3) and the NASA approach in equation (1.4). From these equations, it is evident that optimisation of the combustor exit temperature profile is a function of the momentum flux ratio, and this controls jet penetration and mixing efficiency.

It is known that the injection holes in the combustor are varied to achieve the desired zone air-fuel ratio to limit the emissions level, to achieve proper mixing of the injection flows with the combustion zone, as well as the desired combustor exit

temperature profile [2]. All the principles that contribute to the ease of controlling and optimising the combustor exit temperature profile depend on the principles of swirling flows and jet mixing. These kinds of flows promote the mixing of fuel and air and the mixing of combustion products with fresh air. Failure to achieve zone objectives during combustion leads to the difficulty in controlling or optimising the combustor exit temperature profile.

The mixing associated with jets in cross-flow plays a critical role in optimising the combustor exit temperature profile. It should be noted that in practical combustors, the amount of air available for dilution is usually what remains after the requirements of combustion and wall cooling have been met [5]. Under these conditions, where variation in dilution airflow rate is not an option available to the designer, any change in momentum-flux ratio *(J)* will necessitate a change in orifice diameter if optimum penetration and mixing are to be met. Though there are many factors governing jet mixing, the key factors are the momentum-flux ratio, length of the mixing path, and the number, size and initial angle of the jets. A procedure for the design of dilution holes that can achieve optimum combustor exit temperature profile is given by [2] as shown below:

For a single round jet, Lefebvre [2] found that the maximum penetration is given by

$$Y_{\max} = 1.15 d_j J^{0.5} \sin\theta \qquad (1.1)$$

Here, Y_{max}, d_j, J and θ are maximum jet penetration, diameter of the jet, momentum-flux ratio and initial jet angle, respectively.

Due to blockage penetration of multiple jets in producing a local increase in mainstream velocity, Lefebvre [2] recommended the following equation for maximum penetration of round jets into a tubular liner:

$$Y_{\max} = 1.15 d_j J^{0.5} \dot{m}_g / \left(\dot{m}_g + \dot{m}_j \right) \qquad (1.2)$$

$\dot{m}_g$ and $\dot{m}_j$ are air mass flow rate and jet mass flow rate, respectively.

Two methods for dilution hole design have been discussed in [2]. The first one is the Cranfield design method that utilises the equation below.

$$\dot{m}_j = (\pi/4) n d_j^2 \rho_3 U_j \qquad (1.3)$$

Here, n, ρ_3 and U_j are number of holes, density at the combustor inlet plane, and velocity of the jet, respectively. This method utilises equation (1.2) to determine the jet diameter, d_j, and substitutes it in equation (1.3) to find the optimum number of holes, n.

The second method is the NASA design method, which utilises the following equation:

$$n_{opt} = \pi (2J)^{0.5} / C \qquad (1.4)$$

Where, n_{opt} is the optimum number of holes and C is an empirical constant.

These two methods differ in the sense that one stresses the importance of the hole size and the other stresses the importance of hole spacing. Unfortunately, the two methods do not always produce the same results [2]. If J is increased by increasing U_j, then the two methods make the same recommendations with regard to how the number, size and spacing of the holes should be changed for optimum penetration. However, if J is increased by reducing U_g, then the two approaches give different results.

Lefebvre and Norster [33] derived another method of obtaining the optimum number and size of dilution holes, for the attainment of the most uniform distribution of the exhaust gas temperature. The method is purely empirical and relevant data has to be obtained from charts. The dilution hole diameter is obtained from the following equation [33]:

$$d_h^{\,2} = \frac{4(1-k_{opt})A}{\pi n}\left(\frac{A_d}{A_a}\right) \qquad (1.5)$$

d_h, k_{opt}, A, A_d, and A_a are dilution hole diameter, optimum ratio of flame tube area to casing area, combustor casing area, area of dilution hole and annulus area, respectively.

The above methods do not guarantee the optimum solution, but have proved very successful in preliminary design. The reason why the above methods do not guarantee an optimum solution is that they do not employ any searching criteria for the optimum. Failure of the above methods to achieve the optimum makes the optimisation process depend so much on trial-and-error rig testing, which is very costly and time-consuming.

Anand and Priddin [12] highlighted that some 75% of all hardware costs were spent on these trial-and-error design cycles. The design methods stated above appear to contain an inherent defect in that the calculated value of number of holes is not necessarily a whole number. Lack of efficient design tools made the issues of design optimisation even more complicated, costly and time-consuming [12].

Advances in experimental and theoretical research on gas turbine combustors resulted in better understanding of the physical processes taking place inside the combustor [34,35]. This better understanding in conjunction with the powerful computational hardware made possible the development of numerical techniques capable of simulating, with relatively high accuracy, most of the phenomena encountered inside a combustor. Based on these techniques, design optimisation techniques have been made more systematic and efficient [36,37].

Computational fluid dynamics has become an alternative tool with which to assess different combustor designs [38-40]. The use of simulation tools, even though these are not perfect and still have serious deficiencies, resulted in a giant leap in terms of design capability, costs and lead time [12,13]. These codes have been utilised for design analysis studies after validating them with reliable experimental data [41-43]. The complexity of turbulence causes serious problems in the modelling of turbulence [44,45]. Though there are some models that can compute turbulence better, their practical application is sometimes limited by the immense and totally impractical number of nodes required allowing accurate description of turbulence. Mathematical modelling of turbulent combustion is faced with problems of modelling turbulent flow

and chemical kinetics as well as the interaction between the flow and the chemical reactions [46].

Due to the use of simulation tools, the design of the Adour 915 (Hawk retrofit program) was performed in a short time with only five tests required as compared with 40 to 50 for previous programs [12]. Jones *et al.* [14] also reported more than a 60% reduction of direct operating costs, 70% increase in thrust-weight ratio, 90% reduction in soot, 90% reduction in smoke, 90% reduction in UHC, 90% reduction in CO and 40% reduction of NOx emissions due to advances in simulation tools. The incorporation of computational fluid dynamics into design cycles had the result of making it possible to assess designs before rig testing.

Attempts were made to use computational fluid dynamics to optimise the combustor exit temperature profile by modelling jets in cross-flow and the results are reported in references [47] and [48]. The studies concluded that mixing is a strong function of momentum-flux ratio, mainstream swirl strength, and various ratios of geometric spacing, hole diameter and duct height. Other researchers [36,37,49] also performed parametric computational fluid dynamics studies to try and optimise the combustor exit temperature profile, with particular interest in dilution hole pattern.

The parametric nature of the computational fluid dynamics optimisation approach could also be viewed as lacking the ability to achieve the optimal design. This is due to the fact that parameter variation depends so much on the skill and experience of the designer. The most promising results on combustor exit temperature profile optimisation are from the work of Catalano *et al*. [50,51]. In these papers, progressive optimisation was used with computational fluid dynamics to optimise a duct after-burner. The combination of the two tools exploited the analysis speed of computational fluid dynamics, while an optimisation algorithm searched for design variables that produce optimum results. While the method was found to be more efficient, the theory of cross-flow jet mixing as applied to the combustor exit temperature optimisation could not be applied, because the work was performed on the afterburner without wall injections.

The availability of reliable experimental data has made possible statistical methods to be used for assessing performance. Becz and Cohen [52] have used proper orthogonal decomposition to quantitatively assess mixing performance of non-reacting jets in cross-flow. This method has similarities with other methods [47] and [48] which determine mixing efficiency from momentum-flux ratio. The proper orthogonal decomposition statistically predicts mixing performance from experimental data. The prediction made by Becz and Cohen [52] were consistent with the results of Holdemann *et al.* [47]. This method required experimental data in order to perform statistical analysis, therefore, it can be costly due to a number variants required to generate experimental data.

Most of the studies cited above [36,37,47,48] confirm that the most important flow variable influencing the extent of jet mixing in cross-flow is the momentum-flux ratio. This momentum-flux ratio is a function of the diameter of the injection holes and number of the injection holes, such that any change in these parameters creates a corresponding change to the momentum-flux ratio. While most of the literature confirms the importance of the momentum-flux ratio for mixing, the problem is a way of obtaining the optimum momentum-flux ratio for a certain desired combustor exit temperature profile. It has been pointed out that the empirically derived expressions when used in conjunction with experiments are both costly, time-consuming and do not achieve what can be called optimum designs.

It is also recognised that while computational fluid dynamics contributed a lot by reducing costs and lead times through its ability to perform the flow analysis, the decision on which the parametric variation is based also relies heavily on the skill and experience of the designer. The deficiencies in the above methods show that it is necessary to investigate mathematical optimisation as a tool that makes parameter variations easier by employing an optimum searching mechanism. A combination of computational fluid dynamics and mathematical optimisation is viewed as a possible revolutionary technique that can take the optimisation process further [21].

Research into the application of optimisation algorithms to the design and optimisation of combustors is gaining momentum. The concept of using an optimisation algorithm to design a combustor was first proposed by Despierre *et al*.

[53] and most recently references [6] and [7] reported some success. Their approaches focused on the use of genetic algorithms in conjunction with a one-dimensional semi-empirical code at the preliminary design stages. The one-dimensional simulation codes have limitations in that they use a non-parametric description of the combustor geometry, which is cumbersome and cannot be modified easily. In addition, one-dimensional codes cannot describe such processes as mixing in a more refined and physical way, so they need to be complemented by computational fluid dynamics tools [7].

Though combustor exit temperature is one of the design objectives, only its quality in terms of pattern factor was used as a design objective. This does not say anything about the proximity of the combustor exit temperature profile to the target profile. Another drawback is that genetic algorithms in their nature cannot produce results that can be called "optimum", because the results they reach are a compromise between many conflicting objectives subject to many constraints [54]. Since the results produce a set of possible solutions, the user can find an entire set of Pareto optimisation solutions, and the decision about which is the best is taken by the decision maker. In this way, they are only good when used during the preliminary design phase. The preferred candidate for fine-tuning a specific performance objective such as combustor exit temperature profile would be a single-objective optimisation algorithm [22]. However, this single-objective optimisation can be a function of many different objectives. This has been commonly used through different techniques such as the simple weighted sum [55], and goal-attained or target vector optimisation [56].

1.3 NEED FOR THE STUDY

With particular emphasis on cross-flow jet mixing for combustion application, there is a need for further research in the methods that can improve the optimisation of a combustor exit temperature profile. In order to develop higher-performance, more efficient, longer-life stages, combustor design must take into account combustor exit temperature non-uniformities. From the literature study, it can be concluded that optimisation of the combustor exit temperature profile still remains a difficult task. The optimisation is made more important due to the fact that the hot path components such as turbine blades are affected by the non-uniform combustor exit temperature profile. This non-uniform combustor exit temperature profile shortens the life of the

turbine blades, puts pressure on blade cooling technologies and results in high maintenance costs.

The currently applied optimisation methods are extremely time-consuming, costly and do not achieve a near-optimal solution. They also inhibit the improvement of the engine power output and thermal efficiencies, by limiting the highest exit temperature possible. Technological advancement has brought gradual improvements, with computational fluid dynamics contributing a great deal to the design optimisation. With the advent of computational fluid dynamics, it has been possible to perform analysis on parametric design variants until a satisfactory design is reached before rig testing has to be done. This helped by reducing costs and decreasing lead times. However, the fact still remains that the optimisation methodologies applied to date cannot be called "optimum", because the existing methods for parameter variation depends too arbitrarily on the skill and experience of the designer. This represents a limitation to the technology that needs to be overcome. A possible way is to implement a tool that can do the search for the optimum design prior to computational fluid dynamics analysis and rig testing. Thus, the techniques of mathematical optimisation come into play to make up for this deficiency. A combination of computational fluid dynamics and mathematical optimisation can produce unexpected improvements in design if implemented in the design optimisation loop. The un-expected improvements can be such things as reducing design lead time and achieving design targets that are not achievable with the current design methods.

1.4 AIM OF THE PRESENT WORK

The use of optimisation techniques for combustors may ease the pressure on the combustor designer by automating the optimisation of some performance parameters of the combustor, giving more time to the designer to concentrate on the technical tasks rather than the tuning of the design. More importantly, these techniques can also reduce cost and lead time and can lead to optimum designs, as shown in the literature study.

The aim of this thesis is to propose, develop and implement a design optimisation methodology, based on a mathematical gradient-based technique, that will allow for

the optimisation of the combustor exit temperature profile. This study also represents the first step towards optimisation of critical non-analytical performance objectives such as the combustor exit temperature profile, by the use of numerically approximated objective functions in an iterative mathematical optimisation process. This will be achieved by combining computational fluid dynamics and mathematical optimisation tools to perform the optimisation of mixing in order to optimise the combustor exit temperature profile. This means that the design parameters become design variables and that the performance trends with respect to these variables are automatically taken into account by the optimisation algorithm.

In the current study, none of the equations stated in the literature study are used directly in the optimisation application. The approximated combustor exit temperature profile obtained from computational fluid dynamics simulations is used in the computation of the objective function.

1.2 ORGANISATION OF THE THESIS

The thesis consists of the following chapters:

3 Chapter 2 gives the appropriate literature pertaining to the main features of a gas turbine combustor and discusses how these features can be used to improve the performance of the combustor. This allows for determining the possible roles these features may play in deciding on the optimisation variables. The constraints that would be necessary for design optimisation are also discussed.

4 Chapter 3 presents the appropriate literature on the conservation equations of reacting flows. The derivation of these equations from mass, species or energy balances is not discussed. Conservation and transport are dealt with in connection with the non-premixed combustion. The multiphase equations between gas and spray droplets are also discussed.

5 Chapter 4 briefly reviews the main types of optimisation techniques that can be considered for optimising the combustor. The only algorithm that is

discussed in detail is the Dynamic-Q algorithm since it is the method of choice for this study.

6 Chapter 5 validates the analysis part (computational fluid dynamics) of the proposed methodology, by comparing the simulation results with experimental results of an experimental combustor. The proposed design optimisation methodology is then discussed.

7 Chapter 6 applies the methodology developed to three different optimisation case studies in order to show that the optimisation methodology is a viable alternative in the design of gas turbine combustors.

8 Chapter 7 provides the conclusion drawn from this study and also makes recommendations and discusses the possibility of future research in this field.

CHAPTER 2

BACKGROUND TO GAS TURBINE COMBUSTION

2.1 PREAMBLE

The literature on gas turbine combustion and design is well-known [2,4,57]. Therefore, this section reviews only the main features (parameters) of a gas turbine combustor, and how these features can be used to improve the performance of the combustor in terms of improving the combustor exit temperature profile. This will determine the role these features can play as possible optimisation variables. The constraints that would be necessary when optimising the combustor exit temperature profile will also be discussed.

2.2 THE BASIC FEATURES OF A GAS TURBINE COMBUSTOR

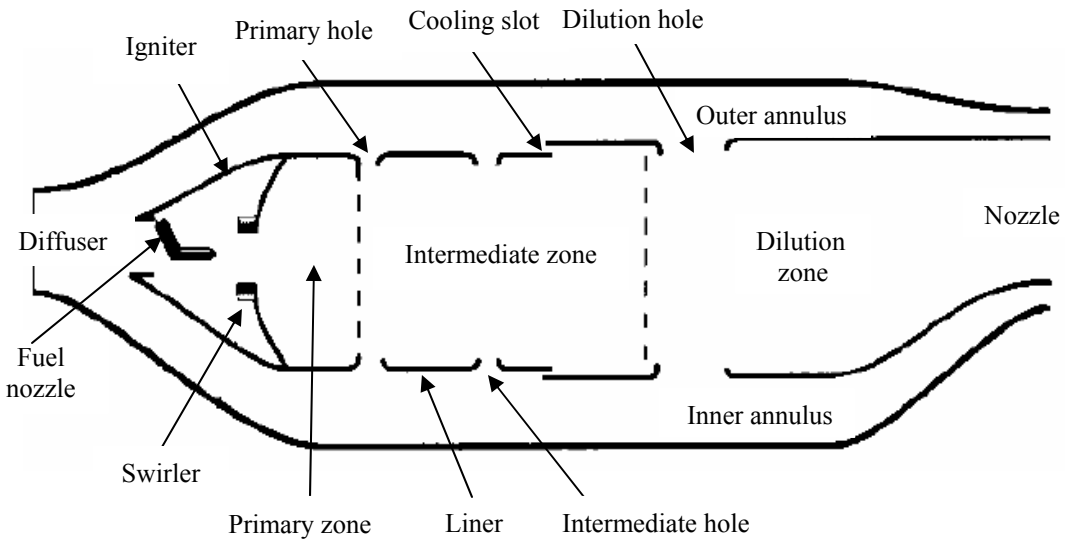

Figure 2.1. The basic features of a gas turbine combustor

Figure 2.1 is a schematic section of an annular combustor, which will be located circumferentially around the body of the gas turbine. Though an annular combustor is

shown in the figure, it is representative of the main features of all types of combustors and their processes [2].

2.2.1 Diffuser

The purpose of the diffuser is to reduce the high compressor outlet velocity to a level suitable for introduction to the combustor while (1) avoiding a high pressure drop, (2) allowing a stable flame, and (3) providing for a recovery of dynamic pressure [57]. The compressor outlet velocities may reach 150 m/s [2] or higher and it will be difficult to burn fuel at these high velocities without the diffuser and apart from combustion problems, the pressure loss will be excessive. The drop in velocity because of the diffusion process is converted to a rise in static pressure.

2.2.2 Liquid fuel injection

The liquid fuels employed in gas turbines must first be atomised before being injected into the combustion zone. Fortunately, atomisation is easy to accomplish; for most liquids, all that is needed is a high relative velocity between the liquid to be atomised and the surrounding air or gas [58,59]. Pressure atomisers accomplish this by discharging the liquid at high velocity into a relatively slow-moving stream of air. An alternative approach is to expose a slow-moving liquid in a high-velocity air stream, and this is known as air blast atomisation. The spray will consist of droplets with a wide range of diameters, and the degree of atomisation is usually expressed in terms of a mean droplet diameter. If the droplets are too small, they will not penetrate far enough into the air stream and if they are too large, the evaporation time may be too long [35]. The effective minimum supply pressure is that which will provide the required degree of atomisation. This shows that the spray parametric effects can have some effect on gas turbine combustion. A more uniform fuel distribution in the dome has been found to lead to uniform temperatures in the dome, which subsequently leads to low NOx and uniform exit temperature [60]. A study by Su and Zhou [61] has also shown that as the Sauter mean diameter of the spray increases, the exit temperature distribution deteriorates, and

injection angles are required to have sprays located within the swirling recirculation. The temperature distribution was also found to improve as the injection velocity of fuel sprays increases.

2.2.3 Swirler

The swirler imparts a high swirl into the flow to induce a strong recirculation region in the primary zone [35,62,63]. The swirler works in conjunction with the primary wall jets in providing recirculation. Recirculation is created when sufficient tangential momentum is provided by the vanes to cause vortex breakdown. The swirl enables the residence time in the primary zone to be lengthened without making this region excessively long. It also promotes good mixing of air and fuel through turbulence. The swirler creates recirculation in the core region by imparting high rotation to the flow and provides better mixing because of strong shear regions, high turbulence and rapid mixing rates. The amount of the recirculating flow in the primary zone defines the quality of the mixing in the primary zone and influences re-light. The amount of recirculating flow can be estimated using the following rule of thumb [7]:

$$\dot{m}_r = \sum \dot{m}_{bp} + \frac{1}{2}\sum \dot{m}_{po} + \frac{1}{3}\sum \dot{m}_{cool} \qquad (2.1)$$

Even though this representation is oversimplistic and not representative of the modern combustor with a strong swirl, it is often used in the preliminary design stage [7]. Large swirl numbers are known to lead to recirculation and longer residence times for the fuel, with shorter flames and higher temperatures close to the base of the combustor, enabling flame stabilisation over a wider range of equivalence ratios than with small numbers [63,64]. This subsequently enhances fuel-air mixing and rate of heat generation. Swirl has been found to play a major role in the particle dispersion process [35,65]. Sankaran and Menon [35] reported that increase in swirl creates a significant lateral dispersion of particles. Analysis by Squires and Eaton [65] has also shown that the droplets tend to accumulate in regions of low vorticity and this accumulation increases with the increase

in the swirl number. This type of preferential accumulation has serious implications for higher combustion efficiency and lower pollutant emissions. Since most of the droplets evaporate before reaching the flame in high swirl, the fuel vapour from the droplets forms a cloud and burns like a gaseous diffusion flame [66]. For practical application, this issue is important since combustion and subsequent heat release can be either vaporising controlled or mixing controlled in a spray combustion system (depending on local conditions). Therefore, the design of spray combustors needs to incorporate the two issues since these mechanisms can significantly impact the overall performance.

2.2.4 Cooling air

Combustors use cooling air for durability of the liner and participation of cooling air in the reaction is considered to be negligible [57]. The cooling air is introduced through a variety of cooling slots such as convection, film and transpiration [7,65]. The detrimental effects of the air film cooling techniques on combustor performance are well-known [57]. The injection of large amounts of cool air at the surface of the combustor walls, combined with a corresponding reduction in the amount of air available for mixing in the dilution zone, produces an uneven radial temperature distribution in the outlet of the combustor. Another undesirable effect of film cooling air in the primary zone is to chill the combustion process and thereby reduce combustion efficiency. Due to lower heat release and lower inlet temperature at the atmospheric pressure, it is normally considered unnecessary to use cooling air for the wall of the laboratory combustor [57]. The absence of cooling air allows better-defined boundary conditions that are easily modelled, as well as simplifying the design.

2.2.5 Primary zone

The function of the primary zone is to sustain the flame and to provide optimum temperature, turbulence and time necessary to achieve efficient combustion of fuel [2,64]. The primary zone has air admission holes around the line to provide jet mixing as shown in Fig. 2.1. In the primary zone, good mixing promotes efficient combustion and

minimum pollution formation. The primary zone has different behaviours depending on the jet design. As described by Rudoff [57], either large-scale recirculation with a small number of jets, or small-scale recirculation, with a large number of jets may be utilised. The average zone air-fuel ratio (AFR) corresponds to the ratio of total air mass flow to fuel mass flow in the given zone as given by equation 2.2 [7]. It is one of the crucial parameters controlling combustion. The combustion temperature and hence the pollutant emissions are strongly dependent on the AFR, therefore it should be controlled precisely throughout the whole combustion zone [58,7]. However, this zone-averaged AFR does not constrain the local AFR values and depends largely on the mixing. Therefore, constraining the mixing will put a constraint on the local AFR distribution.

$$AFR_{avg} = \frac{\dot{m}_{air}}{\dot{m}_{fuel}} \qquad (2.2)$$

The design optimisation of the primary zone is very important for the performance of a gas turbine combustor. Most of the important combustor boundary conditions that control emissions and the rate of heat release are in the primary zone. These parameters relate to the swirler strength, spray distribution, inlet air pressure and temperature and primary hole injections [2,63]. All these flow and burner parameters have varying effects on the performance of the burner [62,63,65,66,67]. Some effects relate to the degree of swirl and fuel injection in the performance of the combustor and are given in sections 2.2.2 and 2.2.3. Inlet pressure has been reported to have some effects on combustion efficiency, NOx concentration and exit temperature [67].

2.2.6 Intermediate (secondary) zone

In the intermediate zone, the gas is diluted with air bled through the intermediate holes [2,4]. This air induces further turbulence and supplies more oxygen to complete the burning of soot formed during primary combustion. The air will also lower gas temperature to reduce the amount of NOx formed at high temperatures during primary combustion. The penetration of the jets should be less so that quenching does not occur

too rapidly [57]. At higher altitudes, or at the lower pressure of the laboratory scale combustor, reactions are slower and the secondary zone can also provide additional residence time for combustion.

2.2.7 Dilution zone

In the dilution zone, the gas is further diluted by air admission through the dilution holes to reduce the temperatures to those acceptable to the gas turbine blades [48]. The design of the dilution zone is such that the combustor exit temperature profile will match the turbine blade thermal stresses. The quality of the exit temperature in terms of pattern factor and profile factor has to be controlled in the dilution zone. Different variations of size, number and location of the dilution holes are used to control the combustor exit temperature [48,68]. The investigations in references 48 to 68 have confirmed that mixing efficiency strongly depends on the momentum-flux ratio of the streams, and an optimum momentum-flux ratio can be determined by investigating different configurations.

2.3 OPTIMISATION PARAMETERS FOR COMBUSTOR EXIT TEMPERATURE PROFILE

The temperature attained by gases at the outlet of the combustor is dependent on its history from the time it emerges from the compressor. During its passage through the combustor, its temperature and composition changes rapidly under the influence of combustion, heat transfer and mixing processes, none of which are perfectly understood [2]. Therefore, the temperature distribution of the gases entering the dilution section is controlled by processes in the primary and secondary zones. Because of the proximity of secondary and tertiary air jets to the combustor exit and the turbulent mixing of jets with combustion products of the primary zone, large fluctuations in temperature and mixture fraction values are expected to be present at the combustor exit [68]. Such fluctuations in temperature and scalar flow field are believed to be responsible, in part, for the so-called “hot streaks” at the combustor exit, and these are represented by the maximum individual

temperature at the combustor exit (T_{4max}). These hot streaks represent a drop in combustion efficiency and can also potentially cause damage to turbine vanes and blades. Figure 2.2 is used to provide some explanation of terms in the combustor exit temperature profile.

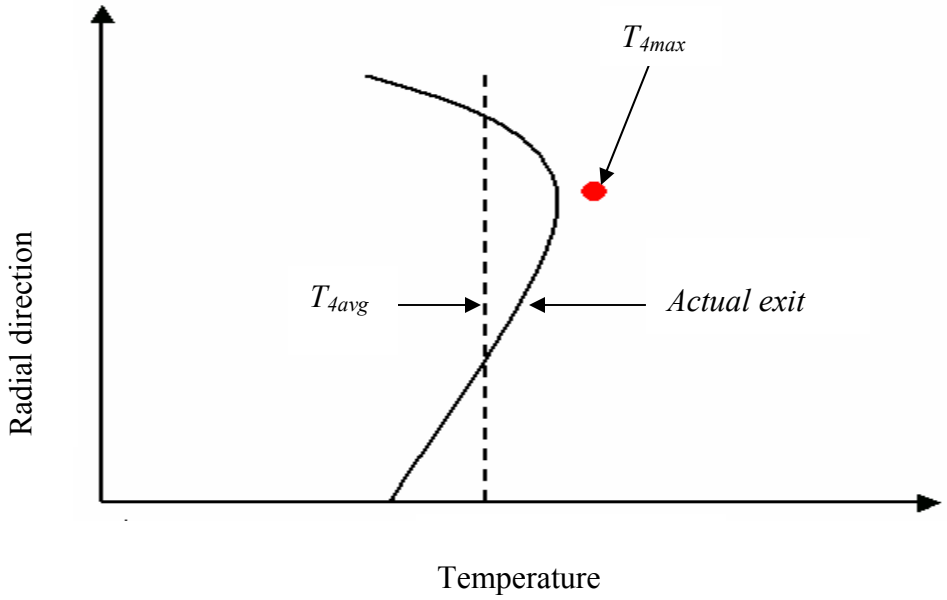

Figure 2.2. Explanation of terms in exit temperature profile parameters

The most important temperature parameters are those that affect the power output of the engine and the life and durability of the hot sections [68]. As far as the overall engine performance is concerned, the most important temperature is the turbine inlet temperature T_{4avg}, which is the mass-flow-weighted mean of all the exit temperature recorded for one standard combustor. The quality of combustor exit temperatures distribution is generally expressed in terms of two non-dimensional parameters, viz., profile factor and pattern factor, which can be defined as [48]:

$$\text{Pattern factor} = \frac{\left(T_{4\max} - T_{4avg}\right)}{\left(T_{4avg} - T_3\right)} \qquad (2.3)$$

and

$$\text{Profile factor} = \frac{\left(T_{4\,peak} - T_{4avg}\right)}{\left(T_{4avg} - T_3\right)} \qquad (2.4)$$

where T_{4max} is the maximum individual temperature at combustor exit, T_{4avg} is the average temperature at combustor exit, T_{4peak} is the maximum temperature in average radial profile at combustor exit and T_3 is the average temperature at combustor inlet.

A combustor exit temperature with a good profile is necessary for the acceptable performance of turbine blades. The turbine blades are normally highly stressed because of associated stresses due to centrifugal forces, aerodynamic forces, and thermal stresses. Blade failure can occur due to (a) creep, (b) thermal fatigue and (c) surface oxidation and corrosion [8]. Creep life tends to be a function of "bulk" metal temperature. Thermal fatigue is principally controlled by the peak temperature and temperature gradients in the blade. Surface oxidation tends to be a function of the peak metal temperatures that occur at thin sections, usually at the leading and trailing edges of the blade. The three processes mentioned above can adversely affect the service life of the blades, and therefore, in order to prolong the service life of turbine blades, it is necessary to optimise the combustor exit temperature profile.

Optimisation of the combustor exit temperature profile is normally achieved by having dilution holes to reduce the exit temperature to the turbine blades' operating temperature, and also to shape the temperature profile as shown in Fig. 2.2. Since the temperature attained by gases at the combustor exit is dependent on its history from the time it emerges from the compressor, it has been discussed in sections 2.2.3 to 2.2.7 that all the combustor geometric parameters (swirler and injections holes) can be used as optimisation variables for the combustor exit temperature profile. The optimisation of the combustor exit temperature profile is performed after the preliminary design, and during that stage most of the combustor performance requirements are satisfied. Therefore, optimisation of the combustor exit temperature profile can only create small changes or no changes at all to other performance requirements, and any probable change would be controlled by design constraints [69].

A common procedure for optimising the combustor exit temperature profile is the use of combustor parameters related to the dilution holes [32,37]. But this does not rule out the possibility of using some other parameters such as the primary holes, secondary holes and

swirler, because the flow field in the dilution zone is dependent on what happens upstream was discussed in sections 2.2.1 to 2.2.7. As the geometries of injection holes and swirler are varied, the flow field in the combustor also changes requiring the use of appropriate design constraints on the affected performance parameters. This practice mostly affects the combustor pressure loss due to its close coupling to injection velocities and the injection hole diameter [2].

Pressure loss can be regarded as the sum of the loss due to combustion (hot loss) and the flow resistance through the liner (friction loss). Any pressure drop between inlet and outlet of the combustor leads to both an increase in specific fuel consumption and reduction in specific power output and, therefore, it is essential to keep pressure loss to a minimum [4]. However, higher liner pressure loss is beneficial to the combustion and dilution processes, because it gives high injection air velocities and step penetration and high levels of turbulence, which promotes good mixing and can result in a shorter liner [2]. Also an increase in air velocities can reduce the aerodynamic performance of the combustor. During the design of a combustor, three different ratios of pressure drop are taken into consideration [7]. These are the overall pressure drop, diffuser pressure drop and the flame tube pressure drop. The flame tube pressure drop can be subdivided into the outer-wall and inner-wall pressure drops. For the purpose of this work, where the inner-flame tube is considered, the inner-wall pressure drop [7] is given by [7].

$$\Delta P_{overall} = \frac{P_3 - P_4}{P_3} \qquad (2.5)$$

2.4 CONCLUSION

Some background on gas turbine combustor design features has been given, including description parameters necessary for the optimisation of the combustor exit temperature profile and the associated constraints. The key geometric parameters for the performance of the combustor have been identified and some of these parameters will be used as design variables for the optimisation process described in Chapter 5. This chapter has

also shown how each of these geometric parameters affects the performance of the combustor, especially the combustor exit temperature.

CHAPTER 3

NUMERICAL COMBUSTION

3.1 PREAMBLE

This chapter presents the conservation equations for reacting flows. The derivation of these equations from mass, species or energy balances will not be treated. Conservation and transport equations will be dealt with in connection with the non-premixed combustion only. The multi-phase equations between gas and spray droplets will also be discussed in this chapter.

3.1.1 Conservation of momentum

In combustion, multiple species react through multiple chemical reactions. The mathematical model of combustion processes is based on the Navier-Stokes equations [70]. The chemical reactions are considered as source terms in the continuity equation for each species.

Consider the gas mixture including N species. Let ρ_k be the density for each species k ($k = 1,\ldots,N$); $\rho = \sum \rho_i$ is the density of the mixture; $Y_k = \frac{\rho_k}{\rho} = \frac{m_k}{m}$ is the mass fraction; and u_i is the three-dimensional velocity field.

The momentum equation is the same in non-reacting (equation 3.1) and reacting flows (equation 3.2).

$$\frac{\partial}{\partial t}\rho u_j + \frac{\partial}{\partial x_i}\rho u_i u_j = -\frac{\partial p}{\partial x_j} + \frac{\partial \tau_{ij}}{\partial x_i} \qquad (3.1)$$

$$\frac{\partial}{\partial t}\rho u_j + \frac{\partial}{\partial x_i}\rho u_i u_j = -\frac{\partial p}{\partial x_j} + \frac{\partial \tau_{ij}}{\partial x_i} + \rho \sum_{k=1}^{N} Y_k f_{k,j} \qquad (3.2)$$

where $f_{k,j}$, is the volume force acting on species k in direction j. Even though equation 3.2 does not include explicit reaction terms, the flow is modified by combustion. Temperature variation causes changes in dynamic viscosity (μ) and density (ρ). As a consequence, the local Reynolds number varies much more than in non-reacting flow.

Going from non-reacting flow to combustion requires solving for N more variables. The N increases the number of conservation equations to solve, because of the addition of the number of species. The behaviour of reacting flows is different from non-reacting flows, because combustion modifies density and the respective velocities of flow.

3.1.2 Mass conservation

The total mass conservation is given in equation 3.3.

$$\frac{\partial \rho}{\partial t} + \frac{\partial \rho u_i}{\partial x_i} = 0 \qquad (3.3)$$

Equation 3.3 is unchanged when comparing non-reacting and reacting flows, because combustion does not generate mass.

The mass conservation for a species k with diffusion velocities is written as follows:

$$\frac{\partial \rho Y_k}{\partial t} + \frac{\partial}{\partial x_i}\left(\rho\left(u_i + V_{k,i}\right)Y_k\right) = \dot{w}_k \qquad (3.4)$$

where $V_{k,i}$ is the i component of the diffusion velocity V_k of species k and w_k is the reaction rate of species k.

where $\sum_{k=1}^{N} Y_k V_{k,i} = 0$, and $\sum_{k=1}^{N} \dot{w}_k = 0$

The task for solving equation 3.4 is difficult, because solving for diffusion velocities is complex [70] so most codes use a simplified approach based on Fick's law as shown in equation 3.5.

$$\frac{\partial \rho Y_k}{\partial t} + \frac{\partial}{\partial x_i}\left(\rho\left(u_i + V_i^{\,c}\right)Y_k\right) = \frac{\partial}{\partial x_i}\left(\rho D_k \frac{\partial Y_k}{\partial x_i}\right) + \dot{w}_k \qquad (3.5)$$

$$and \quad V_i^{\,c} = \sum_{k=1}^{N} D_k \frac{\partial Y_k}{\partial x_i}$$

where D_k is the diffusion coefficient of species k into the mixture.

Fick's law is a convenient approximation for diffusion velocities because the Lewis numbers of individual species usually vary by small amounts in flame fronts. Since Lewis numbers change slightly through the flame front, using diffusion velocities based on Fick's law and constant Lewis numbers provide a reasonable approximation of the reacting species.

3.1.3 Conservation of energy (sum of sensible and kinetic energies)

The energy equation is shown in equation 3.6.

$$\frac{\partial \rho E}{\partial t} + \frac{\partial}{\partial x_i}\left(\rho u_i E\right) = \dot{w}_T - \frac{\partial q_i}{\partial x_j} + \frac{\partial}{\partial x_j}\left(\sigma_{ij} u_i\right) + \dot{Q} + \rho \sum_{k=1}^{N} Y_k f_{k,i}\left(u_i + V_{k,i}\right) \qquad (3.6)$$

where $\dot{Q}$ is the external heat source term and q is the heat flux.

Equation 3.6 is necessary for solving heat addition and heat transfer effects. Additions can be made to the energy equation in the form of a source term that includes heat addition and losses by means of conduction and radiation, as well as volumetric heat addition from an exothermic reaction.

Energy conservation equations have multiple forms, but not all the forms are implementable in classical computational fluid dynamics, and the most preferred forms are the forms with sensible energies or enthalpies. The simplified forms which are commonly used in combustion codes are: constant pressure flames, equal heat capacities for all species and constant heat capacity for a mixture.

3.2 TURBULENT NON-PREMIXED COMBUSTION

In non-premixed combustion, fuel and oxidiser enter the combustor in distinct streams, so that there is no reactant mixing before reactants enter the combustion zone. For this reason, they are simpler to design and safer to operate when compared with premixed combustion, because they do not exhibit propagation speeds and do not flash back, and they are located where the fuel and oxidiser meet. Without propagation speed, a non-premixed flame is unable to impose its own dynamics on the flow field and is more sensitive to turbulence. Diffusion flames are also more sensitive to stretch than turbulent

premixed flames and are more likely to quench by turbulent fluctuations, and flamelet assumptions are not justified as often.

In combustion modelling, non-premixed combustion is more challenging and difficult to understand. The main reason is that reacting species have to reach the flame front by molecular diffusion and while that is happening, their diffusion speeds may be strongly modified by turbulence motions. However, in many combustion codes, chemical reaction is assumed to be fast, or infinitely fast, when compared with transport processes. Most mechanisms described for turbulent premixed flames are also found in non-premixed flames [71].

Turbulence may be characterised by fluctuations of all local properties and occurs for sufficiently large Reynolds numbers, depending on the system geometry. The main effect of turbulence on combustion is to increase the combustion rate. Elementary concepts of turbulence can be found in Hinze [70].

3.3 TURBULENT COMBUSTION MODELLING APPROACHES

The three main numerical approaches used in turbulence combustion modelling are: Reynolds-averaged Navier-Stokes (RANS) equations, direct numerical simulation (DNS) and large eddy simulation (LES). In RANS, equations describe mean flow fields and this approach is limited to practical industrial simulations. In DNS, all characteristic length and times scales are resolved, but the approach is limited to academic applications. In LES, larger scales are explicitly computed whereas the effects of smaller ones are modelled. For the purpose of this research, only RANS will be dealt with in more detail.

3.3.1 RANS in turbulence modelling

The balance equations for the mean quantities in RANS simulations are obtained by averaging the instantaneous balance equations. This averaging procedure introduces

unclosed quantities that have to be modelled with turbulent combustion models. Classical assumptions used to average the conservation equations are as follows [71,72]:

- the thermodynamic pressure is constant and Mach numbers are small
- species heat capacities are equal and constant *($C_{pk} = C_p$)*
- molecular diffusion follows Fick's law and molecular diffusivities D_k are equal *($D_k = D$)*
- Lewis numbers are equal
- fuel and oxidising streams are separately introduced into the combustion chamber with reference state (T_F^0, Y_F^0) for fuel and (T_O^0, Y_O^0) for oxidiser.

Under these assumptions, for a single one-step chemical reaction in adiabatic flows, fuel *(Y_F)* and oxidiser *(Y_O)* mass fractions, and temperature *(T)* are linked [71] through the mixture fraction *z* given in equation 3.7:

$$z = \frac{sY_F - Y_O + Y_O^0}{sY_F^0 + Y_O^0} = \frac{\frac{C_p}{Q}(T - T_O^0) + Y_F}{\frac{C_p}{Q}(T_F^0 - T_O^0) + Y_O^0} = \frac{\frac{sC_p}{Q}(T - T_O^0) + Y_O - Y_O^0}{\frac{sC_p}{Q}(T_F^0 - T_O^0) - Y_O^0} \qquad (3.7)$$

In flames where the second and the fourth assumptions (stated above) are not satisfied (multi-step chemistry, heat losses), mixture fraction variables are based on atomic elements and are linked to species mass fractions.

In Reynods averaging, any quantity f may be split into mean $(\overline{f})$ and fluctuating component (f') such that $(f = \overline{f} + f')$ and the same equation for Favre averaging becomes $(f = \tilde{f} + f'')$. Since Reynolds averaging for variable density flows introduces many other unclosed correlations between any quantity f and density fluctuations $\left(\overline{\rho' u_i'}\right)$, to avoid this difficulty, mass-weighted averages (called Favre averages) are usually preferred [71,72].

The Favre-averaged balance equations [71] become:

Mass

$$\frac{\partial \overline{\rho}}{\partial t} + \frac{\partial}{\partial (x_i)} (\overline{\rho} \tilde{u}_i) = 0 \qquad (3.8)$$

Momentum

$$\frac{\partial \overline{\rho} \tilde{u}_i}{\partial t} + \frac{\partial}{\partial x_i} (\overline{\rho} \tilde{u}_i \tilde{u}_j) + \frac{\partial \overline{p}}{\partial x_j} = \frac{\partial}{\partial x_i} \left(\overline{\tau}_{ij} - \overline{\rho u_i'' u_j''} \right) \qquad (3.9)$$

Chemical species

$$\frac{\partial (\overline{\rho} \tilde{Y}_k)}{\partial t} + \frac{\partial}{\partial x_i} (\overline{\rho} \tilde{u}_i \tilde{Y}_k) = -\frac{\partial}{\partial x_i} (\overline{V_{k,i} Y_k} + \overline{\rho u_i'' Y_k''}) + \overline{\dot{w}} \text{ for k } = 1, \ldots, \text{N}, \qquad (3.10)$$

Enthalpy

$$\frac{\partial \overline{\rho} \tilde{h}_s}{\partial t} + \frac{\partial}{\partial x_i} (\overline{\rho} \tilde{u}_i \tilde{h}_s) = \overline{\dot{w}} + \overline{\frac{Dp}{Dt}} + \frac{\partial}{\partial x_i} \left(\overline{\lambda \frac{\partial T}{\partial x_i}} - \overline{\rho u_i'' h_s''} \right) + \overline{\tau_{ij} \frac{\partial u_i}{\partial x_j}} - \frac{\partial}{\partial x_i} \left(\overline{\rho \sum_{k=1}^{N} V_{k,i} Y_k h_{s,k}} \right) \qquad (3.11)$$

where $\overline{\frac{Dp}{Dt}} = \frac{\partial \overline{p}}{dt} + u_i \overline{\frac{\partial p}{\partial x_i}} = \frac{\partial \overline{p}}{dt} + \tilde{u}_i \frac{\partial \overline{p}}{\partial x_i} + \overline{u_i'' \frac{\partial p}{\partial x_i}}$

Equations 3.8 to 3.11 are formerly identical to the classical Reynolds-averaged equations for constant density flows. Comparisons have shown that simulation differences between Reynolds-averaged equations ($\overline{f}$) and Favre-averaged equations ($\tilde{f}$) are negligible, however, most experimental techniques (thermocouple readings) give Reynolds averages.

3.3.2 Unclosed terms in Favre-averaged balance equations

The resulting problem of finding additional equations or conditions to make up for these unknown equations has come to be called the closure problem. The objective of turbulent combustion modelling is to propose closures for the unknown quantities in equation 3.8 to 3.11.

Reynolds stresses $\left(\widetilde{u_i'' u_j''}\right)$

These equations [71] are closed by turbulence models and the closure may also be done directly or by deriving balance equations for the Reynolds stresses. Since most combustion works are based on the classical turbulence models developed for non-reacting flows, such as the k-ε model, the equations are simply rewritten in terms of Favre averaging. Heat release rates are normally assumed to have no effect on Reynolds stresses.

Species $\left(\widetilde{u_i'' Y_k''}\right)$ **and enthalpy** $\left(\widetilde{u_i'' h_s''}\right)$ **turbulent fluxes**

These fluxes are generally closed using a classical gradient assumption [70,71]:

$$\overline{\rho}\widetilde{u_i'' Y_k''} = -\frac{\mu_t}{S_{ckt}}\frac{\partial \tilde{Y}_k}{\partial x_i} \qquad (3.12)$$

where μ_t is turbulent viscosity, estimated from turbulent model, and Sc_k a turbulent Schmidt number for species *k*.

3.3.3 Classical turbulence models for the Reynolds stresses

These turbulence models have been developed for non-reacting flows and are written in terms of classical unweighted Reynolds averages [70]. Their extension to reacting flows remains an open question, but is generally conducted by simply replacing Reynolds averages by Favre averages in the model expressions as done here.

Following the turbulence viscosity assumption proposed by Boussinesq [70], the turbulent Reynolds stresses are generally described [70] using the viscous tensor (τ_{ij}) expression retained for Newtonian fluids:

$$\overline{\rho u_i'' u_j''} = \bar{\rho} u_i'' Y_k'' = -\mu_t \left(\frac{\partial \tilde{u}_i}{\partial x_j} + \frac{\partial \tilde{u}_j}{\partial x_i} - \frac{2}{3}\delta_{ij} \frac{\partial \tilde{u}_k}{\partial x_k} \right) + \frac{2}{3}\bar{\rho} k \qquad (3.13)$$

where μ_t is a turbulent dynamic viscosity ($\mu_t = \bar{\rho}\nu_t$ and ν_t is the kinematic viscosity). The right side has been added to recover the correct expression for the turbulent kinetic energy k [1] as:

$$k = \frac{1}{2}\sum_{k=1}^{3} \widetilde{u_k'' u_k''} \qquad (3.14)$$

In order to account for the transport of turbulence, models have been developed which employ transport equations for quantities characterising turbulence. It has thus become customary to classify turbulence by the number of transport equations used for turbulence quantities. The resulting nomenclature is explained in Table 3.1. These approaches evaluate the turbulent viscosity, μ_t, and are: algebraic expressions that do not require any additional terms (zero-equation model), one-equation models, two-equation models and Reynolds stress models.

Name	**Number of turbulent transport equations**	**Turbulence quantities transported**
Zero-equation models	0	None
One-equation models	1	k, turbulent kinetic energy
Two-equation models	2	k and ε
Stress/flux models	6	$\overline{u_i u_j}$ components
Algebraic stress models	2	k and ε used to calculate $\overline{u_i u_j}$

Table 3.1. Classes of turbulence models

The zero-equation models include such models as the Prandtl mixing length model [73]. These models are based on algebraic expression and are generally computationally inexpensive, but their accuracy is insufficient. One-equation models incorporate a closure of the balance equation for turbulent kinetic energy *(k)*. The turbulent length scales in these models are correlated with algebraic equations. The results produced are normally satisfactory but not better than the zero-equation models. In two-equation turbulence models, a second equation is coupled with the turbulent kinetic energy equation used in the one-equation models**.** The second equation models, for example, the rate of change of either dissipation *(ε)*, turbulent length scale *(L)*, or vorticity *(ω)*. The most popular is the *k-ε* model [70,71], which has many derivatives in an attempt to improve its deficiencies [74]. Since the *k-ε* model has been used in this work, it will be discussed in more detail and its strengths and weaknesses will be pointed out.

3.3.4 Standard *k-ε* turbulence model

In the standard the *k-ε* model, the effects of turbulence are represented by an isotropic "eddy" or "turbulent" viscosity which is evaluated using two quantities: turbulent kinetic energy *(k)* and its rate of dissipation *(ε)*. *k* and *ε* are obtained from the solutions of "modelled" transport equations [75].

In this approach, due to the work of Jones and Launder [75], the turbulent viscosity is estimated as:

$$\mu_t = \bar{\rho} C_\mu \frac{k^2}{\varepsilon} \tag{3.15}$$

where the turbulent kinetic energy k and its dissipation rate ε are described by closure balance equations:

$$\begin{aligned} \frac{\partial}{\partial t}(\bar{\rho}k) + \frac{\partial}{\partial x_i}(\bar{\rho}\tilde{u}_i k) &= \frac{\partial}{\partial x_j}\left[\left(\mu + \frac{\mu_t}{\sigma_k}\right)\frac{\partial k}{\partial x_j}\right] + P_k - \bar{\rho}\varepsilon \\ \frac{\partial}{\partial t}(\bar{\rho}\varepsilon) + \frac{\partial}{\partial x_i}(\bar{\rho}\tilde{u}_i \varepsilon) &= \frac{\partial}{\partial x_j}\left[\left(\mu + \frac{\mu_t}{\sigma_\varepsilon}\right)\frac{\partial \varepsilon}{\partial x_j}\right] + C_{\varepsilon 1}\frac{\varepsilon}{k}P_k - C_{e2}\bar{\rho}\frac{\varepsilon^2}{k} \end{aligned} \tag{3.16}$$

The source term, P_k, is given by:

$$P_k = -\bar{\rho}\widetilde{u_i'' u_j''}\frac{\partial \bar{u}_i}{\partial x_j} \tag{3.17}$$

and the Reynolds stresses $\bar{\rho}\widetilde{u_i'' u_j''}$ are determined using Boussinesq expression in equation 3.13: The standard k-ε model is usually employed with five constants as recommended by Launder and Spalding [76]. Simple flow situations were analysed to obtain the values from measured data under controlled laboratory conditions. The constants are usually:

$$C_\mu = 0.09 \quad ; \quad \sigma_k = 1.0 \quad ; \quad \sigma_\varepsilon = 1.3 \quad ; \quad C_{\varepsilon 1} = 1.44 \quad ; \quad C_{\varepsilon 2} = 1.92$$

3.3.5 Strengths and weaknesses of the standard k-ε turbulence model

The strengths of the model are that the model is robust and cost-efficient to use.

The weaknesses are that the constants are taken from simple, steady, high Reynolds number flows; the model is hard to be extended to low Reynolds number (Re< $5*10^4$); and since isotropic eddy viscosity (μ_t is a scalar), the model assumes that one length scale (and one velocity scale) is appropriate for all directions.

In general, it is known that the two equation closures are based on the linear constitute law (the Boussinescq assumption). In the Boussinescq assumption, gradient diffusion approximation is typically employed to close the Reynolds stresses. For this reason, poor predictions are expected when the non-linearity of the flow field is remarkable, such as in the presence of chemical reactions and swirling flows (combustors). This linear relation should be replaced with a non-linear relation between the Reynolds stresses and the local mean velocity field. The assumptions made in the closure schemes for turbulence also affect turbulence-chemistry interactions, and further assumptions are made in the reaction model used [71]. The isotropic assumption in the k-ε model does not apply to practical flows very often, but strong anisotropic features are prevalent. Such phenomena can be incorporated through models such as the Algebraic stress model (ASM) or the Reynolds stress model (RSM) which is a second-order modelling [73].

3.4 TURBULENCE CHEMICAL REACTION INTERACTIONS

Before deriving any models, challenges in the reaction rate term $\overline{\dot{w}}_f$ modelling should be emphasised. First, from the mathematical point of view, the strong non-linearity of the Arrhenius law with temperature makes averaging a difficult issue, because the average of the strong non-linearity function cannot be estimated using the value of the function for the mean values. Modelling the reaction rate term $\overline{\dot{w}}_k$ is the key difficulty in turbulent non-premixed combustion simulations. Most of the theoretical arguments derived for laminar diffusion flames can be repeated to the structure of the turbulent diffusion flame and in such a flame the two problems to solve are [71]:

- A mixing problem providing the average mixture fraction field $\tilde{z}(x_i,t)$ and some of its higher moments (for example $\widetilde{z''^2}$)
- A flame structure problem where species mass fractions, Y_k, temperature, T, and reaction rate, $\bar{\dot{w}}_k$, are expressed as functions of z.

The complexity added by turbulence, compared with laminar diffusion flames, comes from the averaging procedures. To determine average values, the mean value of z is not sufficient: higher z moments are needed and, if possible, a full probability density function (pdf) of z. When the pdf of z, $p(z)$ is known, averaged species mass fraction ($\tilde{Y}_k$), averaged temperature ($\tilde{T}$) or averaged reaction rates ($\bar{\dot{w}}_k$) are given by:

$$\bar{\rho}\tilde{Y}_k = \int_0^1 \left(\overline{\rho Y_k \middle| z^*}\right) p(z^*)dz^* \quad ; \quad \bar{\rho}\tilde{T} = \int_0^1 \left(\overline{\rho T \middle| z^*}\right) p(z^*)dz^* \tag{3.18}$$

$$\bar{\dot{w}} = \int_0^1 \left(\overline{\dot{w} \middle| z^*}\right) p(z^*)dz^* \tag{3.19}$$

where $\left(\overline{Q \middle| z^*}\right)$ denotes the conditional average of quantity Q for a given value of the mixture fraction $z = z^*$, depending on z^* and various quantities such as the scalar dissipation rate. $p(z^*)$ is the z-probability density function. According to equations 3.18 and 3.19, two different levels are available to model turbulent non-premixed flames, and they are the primitive variable approach and the reaction rate approach.

3.4.1 Primitive variable method

In the primitive variable method, assumptions are made on the flame structure (from flamelet libraries) or through balance equations (such as conditional moment closures) to provide conditional quantities such as $\overline{\rho Y_k \middle| z^*}$ and $\overline{\rho T \middle| z^*}$ [71]. In simple terms, the

primitive variables solve for $\tilde{z}$ and deduce $\tilde{T}$ and $\tilde{Y}_k$ from the information stored. The species mass fractions and temperature balance equations are no longer required and mean reaction rates ($\overline{\dot{w}}_k$) are not modelled. The RANS codes solve only for flow variables ($\overline{\rho}, \tilde{u}_i, ...$) and mixture fraction variables ($\tilde{z}, \widetilde{z''^2}, ...$) to estimate, directly or indirectly, the probability density function ($p(z^*)$). The primitive variable method is less time-consuming than the reaction rate approach, because species mass fractions are no longer required. The method can be applied to both infinitely fast chemical reactions and finite chemical reaction assumptions.

3.4.2 Reaction rate method

In the reaction rate method, balance equations for species mass fractions and, eventually, for temperature, are solved. The reaction rates, $\overline{\dot{w}}_k$, have to be modelled or have to use laminar flame stored data for $\overline{\dot{w}|z^*}$. In simple terms, reaction rates solve for $\overline{\dot{w}}_k$ taking $\overline{\dot{w}|z^*}$ from the stored data and advance $\tilde{T}$ and $\tilde{Y}_k$ from balance equations. Under infinitely fast chemical reactions, two approaches have been proposed to model reaction rates in a turbulent non premixed flame and they are the eddy-dissipation-concept [77] and the flame structure analysis [71]. This concept directly extends the eddy-break-up concept to non-premixed combustion. Since assuming infinitely fast chemical reactions is not always adequate, a way of incorporating more chemical reactions into turbulent combustion models is needed. This is done by assuming a finite rate chemical reaction, whereby the link between flow variables and mixture fraction is no longer unique but depends on the Damkohler number [72,78]

3.5 NEAR-WALL TURBULENCE MODELLING

The turbulence models described above cannot be applied without modifications in the near-wall region. The wall function approach and the near-wall model approach are the two existing options for modelling the near wall. The wall function approach [74,79]

contains the standard wall functions and the non-equilibrium wall functions. The non-equilibrium wall functions are not used in this work and, therefore, are not discussed.

3.5.1 Wall functions

For the wall functions approach, the viscosity-affected region is not resolved and, instead it is bridged by the wall functions. The wall functions consist of an empirical description of the mean velocity and temperature profiles in the wall boundary layer and formulas for the near-wall turbulence quantities (*k-ε, etc)*.

The log-law for the mean velocity is given by equation 3.20;

$$U^* = \frac{1}{k}\ln\left(Ey^*\right) \qquad (3.20)$$

where $U^* \equiv \frac{UC_\mu^{1/4}k^{1/2}}{\tau_w/\rho}$, $\qquad y^* \equiv \frac{\rho C_\mu^{1/4}k^{1/2}y}{\mu}$

and E is an empirical constant (= 9.81).

The log-law for temperature; is given by

$$T^* = \sigma_t\left(U^* + P\right) \qquad (3.21)$$

where $T^* \equiv \frac{\left(T - T_w\right)\rho c_p C_\mu^{1/4}k^{1/2}}{q''}$

In the *k*-ε models implemented in FLUENT [74], the *k* equation is solved in the whole domain including the wall-adjacent cells. The boundary condition for *k* imposed at the wall is:

$$\frac{\partial k}{\partial n} = 0 \qquad (3.22)$$

where *n* is the local coordinate normal to the wall.

The production of kinetic energy, G_k, and its dissipation rate, ε, at the wall-adjacent cells, which are the source terms in the k-equation, are computed on the basis of a local equilibrium hypothesis. Under this assumption, G_k and ε are assumed to be equal in the wall-adjacent control volume.

Thus, G_k is computed [74] from:

$$G_k \approx \tau_w \frac{\partial U}{\partial y} = \tau_w \frac{\tau_w}{k\rho C_\mu^{1/4} k^{1/2} y_p} \qquad (3.23)$$

and ε is computed [5] from:

$$\varepsilon = \frac{C_\mu^{1/4} k_p^{3/2}}{k y_p} \qquad (3.24)$$

The equation is not solved at the wall-adjacent cells, but instead is computed using equation 3.24.

The wall functions are valid for $y^+ > 30$-60 (up to about 400, even though a value close to the lower bounds is most desirable) where y^+ is defined as:

$$y^+ \equiv u_\tau y / \nu \qquad (3.25)$$

And μ_τ is defined as: $\mu_\tau \equiv \left(\tau_w / \rho\right)^{1/2}$

Wall functions are economical, robust and reasonably accurate. However, there are certain situations [74] in which the wall function approach becomes inadequate:

- when low Reynolds numbers or near-wall effects are pervasive (e.g. flow through a small gap, flows with low Reynolds numbers, and flows near transition);

- when there is transpiration (blowing/suction) through the wall;
- when strong body forces are present (e.g. flow near rotating disks, and flow under strong buoyancy effects);
- when the flow is highly three-dimensional in the near-wall region (e.g. Ekman layers, strongly skewed three-dimensional boundary layers).

In such situations, the two-layer zonal model provides an alternative to the wall function approach. In this approach, the near-wall region is resolved all the way down the wall. The turbulence models ought to be valid throughout the near-wall region. The flow is divided into two regions; i.e. the viscosity-affected near-wall region and the fully turbulent core region. The high Reynolds number k-ε models are used in the turbulent core region. In the viscosity-affected region, only the k-equation is solved**.**

3.6 FLAME AND WALL INTERACTION

Flame and wall interactions are found in most practical industrial systems where they induce various effects on the overall efficiency and pollutant formation of the flame but also on the lifetime of combustion chambers. The interactions influence combustion and wall heat fluxes in a significant manner and constitute a difficult challenge for combustion studies. These phenomena are applicable to both premixed and non-premixed combustion in the same manner. Studying the interaction between flames and walls is extremely difficult from an experimental point of view, because all interesting phenomena occur in a very thin zone near the wall [79,80**]**. In most cases, the only measurable quantity is the unsteady heat flux through the wall, which is an indirect measurement of the phenomena taking place in the gas phase. Figure 3.1 shows how the interactions between flames and walls take place.

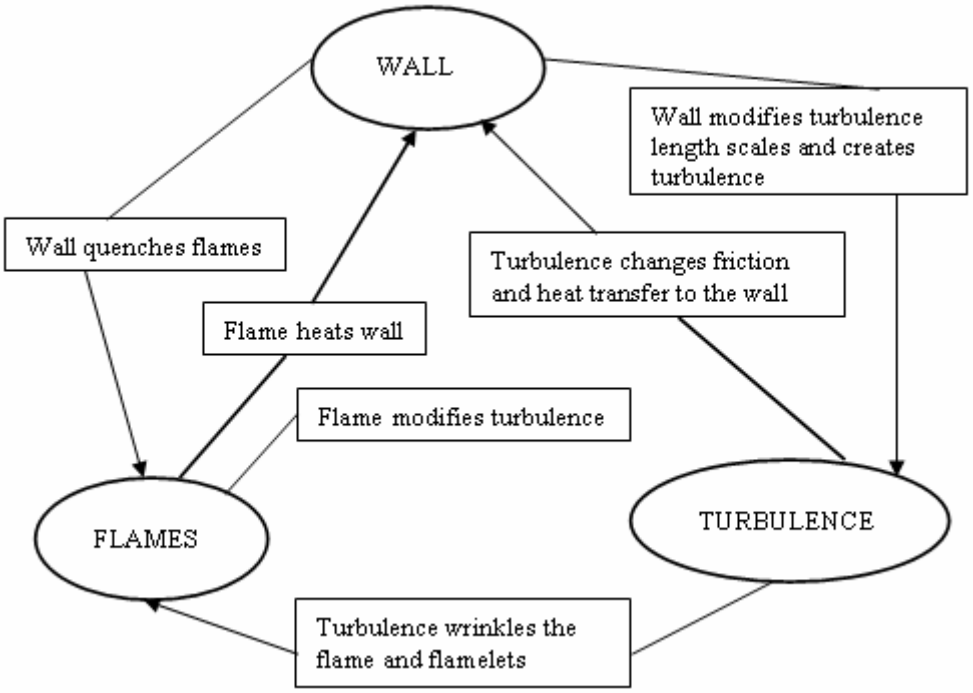

Figure 3.1. Interactions between walls, flame and turbulence [71]

The following are the effects of flame wall interactions [71]:

1. Walls quench the flamelets which come too close to them, and this is directly associated with an enthalpy loss from the flow to the wall so that adiabatic assumption used in many models fails. Due to the quenching of the flame, unburned hydrocarbons form on the walls, and this is a source of pollutants and reduced performance.

2. Flame elements induce very large heat fluxes to the wall, before quenching, and this controls the maximum levels of heat fluxes to be considered for cooling.

3. The walls modify turbulence scales and therefore, near-wall effects must be included in turbulence models. For non-reacting flow, law-of-the-wall extensions are used. The law-of-the-wall extensions derived for non-reacting flows poses danger when used with reacting flow. The most obvious

limitation of combustion models near walls is that turbulent length scales decrease near walls, and these scales can become smaller than the flame thickness so that the flamelet models should not be used anymore.

3.7 SPRAY MODELLING

A significant portion of the current total energy demand has been met by the combustion of liquid fuels. For efficient combustion to occur, intimate mixing of fuel and air is a necessity. Therefore, the study of the mixing process in an evaporating spray is important. In some cases, mixing can be separated from combustion, but most often combustion of the spray proceeds concurrently with mixing, which makes the physiochemical process more closely coupled.

Theoretical modelling and numerical evaluation of sprays require information on the distribution of droplet sizes and velocities produced by the injector. The spray formation process, however, complicates this specification, since it involves complicated processes such as breakup of primary jets, secondary droplet breakup, and collisions between drops. Different models have been developed for spray combustion processes [72,81], i.e. empirical correlations, droplet ballistic models, stirred reactor models, locally homogeneous models and separated flow (two-phase flow) models.

Among all of the above models, the two-phase flow model is the most logical approach, since the effects of exchange of mass, momentum and energy between the liquid and gas phases are included in the analysis. Moreover, it is not limited to extremely small droplets. However, due to limitation of computer storage and cost of computations, researchers developing separated flow models have made no attempt to accurately model the details of the flow field around individual drops. Therefore, the exchange processes between phases must be modelled independently. Usually, a set of empirical correlations for droplet drag, heat and mass transfer is employed.

In general, there are three different approaches to separated flow analyses for evaporating and combusting sprays [72].

1. *Particle-source-in cell model, or discrete-droplet model.* In this model, a finite numbers of groups of particles are used to represent the entire spray. The motion and transport of representative samples of discrete drops are tracked through the flow field using a Lagrangian formulation, while the Eulerian formulation is used to solve the governing equations for the gas phase. The effect of droplets on the gas phase is taken into account by introducing appropriate source terms in the gas-phase conservation equations.

2. *Continuous droplet model.* In this model, a distribution function is used to evaluate the statistical distributions of drop temperature, concentration, etc. The transport equation for the distribution function is solved along with the gas conservation equations to provide all the properties of the spray.

3. *Continuum-formulation model.* In this model, the motion of both drops and gas is treated as though they were interpenetrating continua. A continuum formulation of the conservation equations for both phases is used to model spray combustion and evaporating problems. In this approach, the governing equations for the two phases are similar; however, there are many difficulties in describing the droplet heat-up process, the turbulent stresses, and the turbulent dispersion of droplets.

For the purposes of this research, only the Particle-source-in-cell model will be discussed, for the reason that it is the most logical approach and used mostly in computational fluid dynamics applications.

3.7.1 Particle-source-in-cell model, or discrete droplet model

In this approach, the entire spray is divided into many representative samples of discrete drops whose motion and transport through the flow field are found using a Lagrangian formulation in determining the drop life history, while a Eulerian formulation is used to solve the governing equations for the gas phase [82]. Depending on the consideration of the effect of turbulent fluctuations on particle motion and the method of the velocity differences (slip) between the phases, discrete droplet models are further subdivided into deterministic separated flow models and stochastic separated flow models.

In deterministic separated flow models, the slip and finite interphase transport rates are considered, but effects of turbulence on interphase transport rates are ignored. Droplets are assumed to interact only with the mean gas motion. In the deterministic separated flow formulation, particles following deterministic trajectories are found by solving their Lagrangian equation of motion. Spray models of this type usually employ the standard drag coefficient for spheres and ignore virtual mass and Basset forces. These approximations are appropriate for high void fractions and high liquid-gas density ratios [80].

It is generally assumed that the spray is diluted in these models. This implies that although particles interact with the gas phase, they do not interact with each other. Therefore, droplet collisions are ignored, and empirical correlations determined for single drops in an infinite medium are used to estimate interphase transport rates.

Although the deterministic separated flow model described above considers the interphase slip between particles and the continuous phase, the effects of turbulent fluctuations on particle motion are ignored. Several stochastic separated flow models have been developed to treat both slip and the effects of turbulent fluctuations [72].

Computational fluid dynamics analysis of the fuel film dynamics and atomisation process has not reached a sufficiently matured state for the design purposes. Therefore,

experiments have to be performed on combusting spray in order to characterise the spray for computational fluid dynamics modelling. Due to experimental limitations, most measurements of drop size and velocity distributions have generally been made at some distance from the injector [82]. This so-called initial station is usually in the dilute portion of the spray. Both experimental and theoretical studies of the dense spray region are needed in future to understand the jet breakup process as well as to accurately specify the flow conditions at the selected station near the injector exit.

Despite the fact that a commercial code has been used for combustion simulations in the study, the equations on the application of physical submodels have been considered on a more general basis. The physical submodels are not discussed in terms of the FLUENT code [74], but instead a more general approach, which can be followed by any code, has been used. This is due to the fact that the processes that take place in spray phenomena are similar, but the only difference is the kinds of equations used or assumptions made during the development of a certain code. This considers the spray phenomena as undergoing the following processes: turbulent dispersion, breakup, drop coalescence and collision, mass transfer, heat transfer and turbulence modification.

3.7.2 Liquid phase equations

The liquid fuels employed in combustors must first be atomised before being injected into the combustion zone. Fortunately, atomisation is easy to accomplish; by quantifying the relative velocities between the liquids to be atomised and the surrounding air or gas. The Lagrangian method is used in the liquid-phase modelling and fuel is assumed to be injected into the combustor as a fully atomised spray which consists of spherical droplets. Liquid sprays are represented by a discrete particle technique, in which each computational particle represents a number of droplets of identical size, velocity and temperature. In the absence of any fundamental mechanism or model to build a theory of drop size distribution, a number of functions have been proposed based on either probability or purely empirical considerations. Those in general use include log-normal, Nukiyama-Tanasawa, Rossin-Rammler and the upper limit distribution [58].

The path of a particle introduced in the computational domain is usually computed in a Lagrangian reference frame, using momentum balance. The momentum equation for a spherical particle can be expressed with only Stokes drag forces and body forces. Other forces (virtual mass and other) can be neglected if the ratio of ρ_A to ρ_D is in the order 0.001 [83]. The equation takes the following form.

$$\frac{du_D}{dt} = -\frac{\rho_A}{\rho_D}\frac{3}{4}\frac{C_D}{D}\left|u_A - u_D\right|\left(u_A - u_D\right) + g \qquad (3.26)$$

with for the drag coefficient C_D:

$$C_D = \begin{cases} 24\left(1+0.15\,\mathrm{Re}_D{}^{0.687}\right)/\mathrm{Re}_D & \mathrm{Re}_D \le 10^3 \\ 0.44 & \mathrm{Re}_D > 10^3 \end{cases} \qquad (3.27)$$

The droplet trajectory is now computed in time, using a predefined step size, by integrating the velocity vector. The two phases (air and droplets) do not necessarily interact, and a very dilute spray can be thought of as having no effect at all on the carrier phase. If the spray cannot be considered dilute, it affects the properties of the carrier fluid. In this case, the spray is dense enough to affect the carrier flow field via momentum exchange between the droplets and the carrier fluid. Considering that a spray consists of a huge number of drops, it is common practice to gather similar droplets (same diameter, initial velocity and liquid properties) in a parcel and calculate the trajectory of the parcel to represent that category of drops. This approach known as the discrete droplet model [84] is widely used in computational fluid dynamics software.

3.7.2.1 Turbulent dispersion

Turbulent dispersion is the spreading of drops over the flow field due to droplet-eddy interaction. When using a RANS turbulence model, the turbulence kinetic energy, k, is assumed to be isotropic and the fluctuating velocity to have a Gaussian distribution with

standard deviation $(2k/3)^{1/2}$. As turbulence is a chaotic process, an '"eddy" passing through a certain point can be thought of as being a realisation of the probability density function of the velocity fluctuation at that point. The droplet thus passes through a certain point in space where the instantaneous carrier fluid velocity, u_A, is determined by the average bulk velocity U_A and a randomly sampled fluctuation u'_A *or* $u_A = U_A + u'_A$.

A droplet will interact with an eddy for a certain time, τ_{INT}, or, in other words, the same sampled velocity fluctuation will be used for a certain number of computational time steps. When this interaction time is passed, a new sample will be taken from the probability density function of the velocity fluctuation. The interaction time is the minimum of the time scales of two possible events:

- The droplet travels with the eddy until the eddy dies and τ_E is the eddy life-time.
- The droplet traverses the eddy because it has enough momentum relative to the main airflow. This event has the transit time scale τ_{TR}.

These time scales are respectively defined by the following equations [84];

$$\tau_E = \frac{L_E}{\left|u'_A\right|}$$

$$\tau_{TR} = -\tau_D \ln\left(1 - \frac{L_E}{\tau_D \left|u_A - u_D\right|}\right) \qquad (3.29)$$

$$\tau_{INT} = \min\left(\tau_E, \tau_{TR}\right)$$

where the drop relaxation time τ_D is

$$\tau_D = \frac{4}{3}\frac{\rho_D D}{\rho_A C_D \left|u_A - u_D\right|} \qquad (3.30)$$

3.7.2.2 Drop breakup

Drop breakup is the reduction of drop size due to the interaction with the high-speed airflow. This feature is not available in every commercial computational fluid mechanics code, but will be discussed in this work. The model by Gosman and Ioannides [85] is considered here. Several breakup regimes are distinguished. The Weber number and the Ohnesorge number relate these regimes to the initial drop conditions. The latter dimensionless number represents the effect of drop viscosity on breakup. Other useful relations are the droplet Reynolds number and the critical drop diameter. These are based on the critical value of the Weber number, which is defined when breakup no longer occurs**.** The breakup rate of a drop is then defined as [85]:

$$\frac{d_D}{dt} = -\frac{D - D_{CR}}{\tau_B} \tag{3.31}$$

With the characteristic breakup time defined as:

$$\tau_B = \frac{5}{1-(Oh/7)\left|u_{O,R}\right|}\left(\frac{\rho_D}{\rho_A}\right)^{1/2} \qquad We > 12 \tag{3.32}$$

3.7.2.3 Turbulence modification

Turbulence modification is the phenomenon that the airflow turbulence level changes under the influence of discrete phases. It either increases or reduces the turbulence level. The production of turbulence is attributed to vortex shedding behind large droplets and the dissipation of turbulence happens when drops extract energy from the mean flow turbulence to settle to bulk air velocity. Most commercial computational fluid dynamics codes do not include turbulence modification.

3.7.2.4 Drop collisions and coalescence

Droplet collisions and coalescence, as well as aerodynamic breakup, can also be included in spray modelling. The current treatment is as given by Su and Zhou [61]. If the collision impact parameter, b, that is, the distance between droplet centres, is less than a critical value, b_{cr}, the droplets coalescence; and if it exceeds the critical value, the droplets maintain their sizes and temperatures but undergo velocity changes. The sizes, velocities and temperatures of droplets after collisions are obtained in terms of the conservation of mass, momentum and energy. The critical impact parameter, b_{cr}, for a collision between two droplets with subscript 1 and 2 is given by

$$b_{cr}^2 = \left(r_{D1} + r_{D2}\right)^2 \min\left(1.0, 2.4 f\left(v\right)/We\right) \qquad (3.33)$$

where $f(v) = v^3 - 2.4v^2 + 2.7v$, σ_D is the droplet surface tension coefficient, and

$$v = \max(r_{D1}, r_{D2}) / \min(r_{D1,}\, r_{D2})$$

When the droplet's distortion exceeds unity, it breaks up into a distribution of smaller droplets. The droplet's distortion y is given by

$$y(t) = We/12 + e^{-1/t_D}\left((y(0) \_ We/12)\cos wt + \frac{1}{\omega}\left(y(o) + \frac{y_0 - We/12}{t_D}\right)\sin \omega wt\right) \qquad (3.34)$$

Where, We, is the Weber number, the viscous damping time $t_D = 2\rho_D r^2 / 5\mu_l$, and the square of the oscillation frequency $\omega^2 = 8\sigma/\rho_D r^3 - 1/t_D^2$. After breaking of the droplet, the following distribution is assumed for the radii:

$$g(r) = \frac{1}{r} e^{-r/\bar{r}} \qquad (3.35)$$

where the mean radius $\bar{r} = r/(7+3\rho_D r^3 y^2/8\sigma)$. The magnitude of product droplet velocities differ from that of the parent droplet by a velocity magnitude, *w*, and with direction randomly distributed in a plane normal to the relative velocity vector between the parent droplet and gas. The quantity, *w*, is given by:

$$w = \frac{1}{2} r \frac{dy}{dt} \tag{3.36}$$

The number of mass droplets associated with the computational particle is adjusted from the conservation of mass.

3.7.2.5 Heat and mass transfer

Heat and mass transfer occur with evaporating sprays. To calculate droplet mass and heat transfer with the surrounding gas, a uniform temperature model of a single droplet is used. The evaporation rate is given by the Frossling correlation [86].

$$\frac{dr_D}{dt} = \frac{(\rho D)_g}{2\rho_D r_D} \frac{Y_{Ds} - Y_D}{1 - Y_{Ds}} Sh_D \tag{3.37}$$

where $(\rho D)_g$ is fuel vapour diffusivity in gas. Y_{Ds} is the fuel vapour mass fraction at the droplet's surface and $Y_D = \rho_D / \rho_g$. Sh_D is the Sherwood number given by

$$Sh_D = \left(2.0 + 0.6\,\mathrm{Re}_D^{0.5}\, Sc_D^{0.5}\right) \frac{\ln(1+B_D)}{B_D} \tag{3.38}$$

and $Sc_D = \mu_g / (\rho D)_g$ and $B_D = (Y_{Ds} - Y_D)/(1 - Y_{Ds})$.

The rate of droplet temperature change is determined by the conservation energy equation at the droplet surface.

$$\rho_D \frac{4}{3}\pi r_D^3 C_p \frac{dT_D}{dt} - \rho_D 4\pi r_D^2 L_D \frac{dr_D}{dt} = 4\pi r_D^2 Q_D \qquad (3.39)$$

where C_p is the droplet-specific heat, L_D is the latent heat of vaporisation, and Q_D is the rate of heat conduction to the droplet surface per unit area, which is given by the Ranz-Marshall correlation.

$$Q_D = \frac{K_g (T_g - T_{D)}}{2r_D} Nu_D \qquad (3.40)$$

where the Nusselt number is given by

$$Nu_D = \left(2.0 + 0.6\,\mathrm{Re}_D^{0.5}\,\mathrm{Pr}_D^{0.5}\right)\frac{\ln(1+B_D)}{B_D} \qquad (3.41)$$

and the Prandtl number $\mathrm{Pr}_D = \mu_g C_{pg} / K_g$, K_g is the gas thermal conductivity.

The changes of mass, momentum and energy of droplets from the above calculations are then added into the source terms of the governing equations. The momentum exchange is treated by implicit coupling procedures to avoid the prohibitively small time steps that would otherwise be necessary. The accurate calculation of mass and energy exchange is ensured by automatic reduction in the time step when the exchange rates become large.

3.8 CONCLUSION

This chapter presented the conservation equations for turbulent reacting flows in non-premixed combustion. Different turbulent modelling techniques have been discussed, particularly the *k*-ε model since it will be used in this study. The interaction of chemical reactions and turbulence has also been discussed. Since combustion is a two-phase flow involving mixing of air and fuel, spray modelling has also been discussed. Different ways of spray modelling have been discussed in this chapter, but only the discrete droplet model has been discussed in detail due to its suitability to this study.

CHAPTER 4

THE DYNAMIC-Q OPTIMISATION METHOD

4.1 PREAMBLE

This section discusses in detail the Dynamic-Q method of Snyman and Hay [24], since it has been the method of choice used in this study.

4.2 MATHEMATICAL OPTIMISATION

Mathematical optimisation is the process of finding either a minimum or a maximum of a specified function by adjusting the variables of that function with a mathematical algorithm**.** The function can be linear or non-linear, and subject to certain constraints. Sometimes the function does not even have a known analytical form, increasing the complexity of the problem. In mathematical optimisation, first the product design has to be described in terms of a set of variables and secondly, evaluation tools are required for evaluation of the design properties.

4.2.1 Constrained optimisation

Consider the constrained optimisation problem of the general mathematical form:

$$\min f(\mathbf{x});\ \mathbf{x}=\left[x_1,x_2,...,x_i,...,x_n\right]^T,\ \mathbf{x}\in R^n$$

$$\text{subject to constraints: } \begin{matrix} g_j(\mathbf{x})\le 0;\ \ j=1,2,...,m \\ h_k(\mathbf{x})=0;\ \ k=1,2,...,p<n \end{matrix} \qquad (4.1)$$

where $f(\mathbf{x})$, $g_j(\mathbf{x})$ and $h_k(\mathbf{x})$ are scalar functions of the n-dimensional vector $\mathbf{x}$.

The function $f(\mathbf{x})$ is the objective function that is being minimised. The $g_j(\mathbf{x})$ denote the inequality constraint functions and $h_k(\mathbf{x})$ the equality constraint functions. The

components x_i, $i = 2,\ldots,n$ of $\boldsymbol{x}$ are called the design variables. The optimum vector $\boldsymbol{x}$ that solves problem 4.1 is denoted by the vector

$$\mathbf{x}^* = \left[x_1^*, x_2^*, \ldots, x_n^*\right]^T \qquad (4.2)$$

with corresponding lowest function value $f(\boldsymbol{x}^*)$ subject to the given inequality and equality constraints.

The optimisation problem formulated in (4.1) may be solved using many different gradient-based methods, such as the successive approximation sequential quadratic programming (SQP) method, or stochastic methods such as genetic algorithms. Genetic algorithms are often found to be too expensive in terms of the number of function evaluations (simulations) when compared with SQP [87-88]. The method of choice for the work done here is the relatively new gradient-based and successive approximation Dynamic-Q method [24]. The Dynamic-Q method has been extensively tested by Snyman and Hay [24] and was found to offer equal competitiveness to that of SQP. Dynamic-Q was also found to be superior to SQP at handling problems with severe noise by Els and Uys [89]. Dynamic-Q was successively applied to a mixed integer problem by Visser and De Kock [90], and this is of particular interest since the problem considered in this study is also of mixed integer nature.

In this study, the Dynamic-Q method [24] is used and will, therefore, be discussed in detail. The Dynamic-Q method is capable of handling general constrained optimisation problems. The method consists of applying the dynamic trajectory optimisation algorithm [91] to successive spherically quadratic approximations of the actual optimisation problem.

4.2.2 Dynamic-Q method

The Dynamic-Q algorithm uses the LFOP algorithm outlined by Snyman [91] to handle constrained problems by means of a penalty function approach. For any general optimisation problem of the form (4.1), the associated penalty function

formulation, which transforms the constrained problem to an unconstrained problem, is: min *Q(**x**)* with respect to ***x***, where

$$Q(\mathbf{x}) = f(\mathbf{x}) + \sum_{j=1}^{m} \rho_j g_j^2(\mathbf{x}) + \sum_{k=1}^{p} \beta_k h_k^2(\mathbf{x}) \qquad (4.3)$$

$$\text{where } \rho_j = \begin{cases} 0 & \text{if } g_j(\mathbf{x}) \leq 0 \\ \alpha_j & \text{if } g_j(\mathbf{x}) > 0 \end{cases}$$

For simplicity, the penalty parameters α_j and β_k usually take on the same large positive value $\alpha_j = \beta_k = \mu$. It can be shown that as μ tends to infinity, the unconstrained minimum of *Q(**x**)* yields the solution to the constrained optimisation problem. The LFOP dynamic trajectory method applied to the penalty function formulation of the constrained problem in three phases is called the LFOPC algorithm [92,93].

PHASE 0: Given some starting point $\mathbf{x}^0$, apply LFOP with some overall penalty parameter $\mu = \mu_0 (= 10^2)$ to $Q(\mathbf{x}, \mu_0)$ to give $\mathbf{x}^*(\mu_0)$.

PHASE 1: With $\mathbf{x^0} := \mathbf{x}^*(\mu_0)$, apply LFOP with increased overall penalty parameter $\mu = \mu_0 (= 10^4) >> \mu_0$ to $Q(\mathbf{x},\mu_1)$ to give $\mathbf{x}^*(\mu_1)$. Identify the set of n_a active constraints corresponding to the set of subscripts $I_a = (u1, u2, ..., un_a)$ for which $g_{uj}(\mathbf{x}^*(\mu_1)) > 0, \quad j = 1, 2, ..., n_a$.

PHASE 2: With $\mathbf{x^0} := \mathbf{x}^*(\mu_1)$, apply LFOP to

$$\min_x Q_a(\mathbf{x}, \mu_1) = \sum_{j=1}^{n_a} \mu_1 g_{uj}^2(\mathbf{x}) + \sum_{k=1}^{p} \mu_1 h_k^2(\mathbf{x}) \qquad (4.4)$$

to give $\mathbf{x}^*$.

4.2.3 Constructing the successive approximate spherical quadratic subproblems

The spherically quadratic approximation of a function is used in this study to approximate the functions that are not analytically known and/or computationally expensive to evaluate. The approximated functions are used to construct a subproblem *P(i)* at design iteration *i*. The approximated functions can be the objective function and/or the constraint functions depending on the optimisation problem being investigated. The computational time for optimisation is, therefore, reduced by replacing computationally expensive functions by simpler approximate functions obtained from a few expensive function evaluations (simulations). The way these successive subproblems are constructed will now be discussed in detail [25,94].

The Taylor expansion of a function $f(\mathbf{x})$ in the region of the current design point $\mathbf{x}^{(i)}$ is given by:

$$f(\mathbf{x}) = f(\mathbf{x}^{(i)}) + \nabla^T f(\mathbf{x}^{(i)})(\mathbf{x}-\mathbf{x}^{(i)}) + \frac{1}{2}(\mathbf{x}-\mathbf{x}^{(i)})^T H(\mathbf{x}^{(i)})(\mathbf{x}-\mathbf{x}^{(i)}) + H.O.T \qquad (4.5)$$

where $H(\mathbf{x}^{(i)})$ is the Hessian matrix at point $\mathbf{x}^{(i)}$ and $H.O.T$ is the higher-order terms in the expansion. The vector $\mathbf{x}^{(i)}$ is the current design point. The Hessian matrix is defined as

$$H(\mathbf{x}) = \begin{bmatrix} \frac{\partial^2 f}{\partial x_1^2} & \frac{\partial^2 f}{\partial x_1 \partial x_2} & \cdots & \frac{\partial^2 f}{\partial x_1 \partial x_n} \\ \frac{\partial^2 f}{\partial x_2 \partial x_1} & \frac{\partial^2 f}{\partial x_2^2} & \cdots & \frac{\partial^2 f}{\partial x_2 \partial x_n} \\ \vdots & \vdots & & \vdots \\ \frac{\partial^2 f}{\partial x_n \partial x_1} & \frac{\partial^2 f}{\partial x_n \partial x_2} & \cdots & \frac{\partial^2 f}{\partial x_n^2} \end{bmatrix}(\mathbf{x}) = \nabla^2 f(\mathbf{x}) \qquad (4.6)$$

If the higher-order terms are ignored, the value of *f* at a point $\mathbf{x}$ in the region of $\mathbf{x}^{(i)}$ is given approximately by:

$$f(\mathbf{x}) \approx f(\mathbf{x}^{(i)}) + \nabla^T f(\mathbf{x}^{(i)})(\mathbf{x} - \mathbf{x}^{(i)}) + \frac{1}{2}(\mathbf{x} - \mathbf{x}^{(i)})^T H(\mathbf{x}^{(i)})(\mathbf{x} - \mathbf{x}^{(i)}) \qquad (4.7)$$

The gradient vector $\nabla f(\mathbf{x}^{(i)})$ in equation (4.7), may be approximated using a first-order forward differencing scheme. This first-order gradient approximation needs some special consideration and will be discussed in the following sub-section.

Since the function *f*, or its derivatives, may not be analytically known, the second-order derivatives need also to be calculated using a finite difference approximation, e.g. a forward differencing scheme. Furthermore, if the calculation of the function is computationally expensive to evaluate (as is the case with computational fluid dynamics), the calculation of the Hessian matrix becomes extremely expensive computationally. The way the Hessian matrix is approximated in the Dynamic-Q method now follows.

Taking $\mathbf{A}^{(i)}$ as the approximation of the Hessian matrix, the spherically quadratic approximation $\tilde{f}(\mathbf{x})$ to the function, *f(**x**)* is given by:

$$\tilde{f}(\mathbf{x}) = f(\mathbf{x}^{(i)}) + \nabla^T f(\mathbf{x}^{(i)})(\mathbf{x} - \mathbf{x}^{(i)}) + \frac{1}{2}(\mathbf{x} - \mathbf{x}^{(i)})^T \mathbf{A}^{(i)}(\mathbf{x}^{(i)})(\mathbf{x} - \mathbf{x}^{(i)}) \qquad (4.8)$$

where the approximation of the Hessian matrix $(\mathbf{A}^{(i)})$ is given by

$$\mathbf{A}^{(i)} = \text{diag}(a^{(i)}, a^{(i)}, ..., a^{(i)}) = a^{(i)}\mathbf{I} \qquad (4.9)$$

and $\mathbf{I}$ is the identity matrix.

The appropriate curvature $a^{(i)}$ used in the construction of the approximate Hessian matrix is calculated by using function and gradient information at the design point $\boldsymbol{x}^{(i)}$ and the previous design point, point $\boldsymbol{x}^{(i-1)}$. The value of $a^{(i)}$ defines the amount of curvature of the spherical quadratic approximation. During an optimisation run, the point $\boldsymbol{x}^{(i-1)}$ is the previous design point where the gradient and the function are already known. The initial value, $a^{(i)}$, depends on the specific optimisation problem being considered. In this study, a value of zero was chosen for the construction of the first subproblem. This implies that the first approximation has no curvature.

The same procedure is used to get spherical quadratic approximations $\tilde{g}_j(\mathbf{x})$ and $\tilde{h}_k(\mathbf{x})$ to $g_j(\mathbf{x})$ and $h_k(\mathbf{x})$ which then becomes:

$$\begin{aligned}\tilde{g}_j(\mathbf{x}) &= g_j(\mathbf{x}^{(i)}) + \nabla^T g_j(\mathbf{x}^{(i)})(\mathbf{x}-\mathbf{x}^{(i)}) + \\ &\quad \frac{1}{2}(\mathbf{x}-\mathbf{x}^{(i)})^T \mathbf{B}_j(\mathbf{x}^{(i)})(\mathbf{x}-\mathbf{x}^{(i)}), \quad j=1,\ldots,m \\ \tilde{h}_k(\mathbf{x}) &= h_k(\mathbf{x}^{(i)}) + \nabla^T h_k(\mathbf{x}^{(i)})(\mathbf{x}-\mathbf{x}^{(i)}) + \\ &\quad \frac{1}{2}(\mathbf{x}-\mathbf{x}^{(i)})^T \mathbf{C}_k(\mathbf{x}^{(i)})(\mathbf{x}-\mathbf{x}^{(i)}), \quad k=1,\ldots,p\end{aligned} \tag{4.10}$$

with the Hessian matrices B_j and C_k taking on simple forms

$$\begin{aligned}\mathbf{B}_j &= b_j \mathbf{I} \\ \mathbf{C}_k &= c_k \mathbf{I}\end{aligned} \tag{4.11}$$

It is specified that $\tilde{f}(\mathbf{x})$ interpolates $f(\boldsymbol{x})$ at $\boldsymbol{x}^{(i)}$ and $\boldsymbol{x}^{(i-1)}$ and that the gradient of $\tilde{f}(\mathbf{x})$ matches that of $f(\boldsymbol{x})$ at $\boldsymbol{x}^{(i)}$, then equation (4.9) can be rewritten to give $a^{(i)}$ as follows:

$$a^{(i)} = \frac{2\left\{f(\mathbf{x}^{(i-1)}) - f(\mathbf{x}^{(i)}) - \nabla^T f(\mathbf{x}^{(i)})(\mathbf{x}^{(i-1)} - \mathbf{x}^{(i)})\right\}}{\left\|\mathbf{x}^{(i)} - \mathbf{x}^{(i-1)})\right\|^2} \tag{4.12}$$

This may be called the backward interpolation spherical approximation to $f(\boldsymbol{x})$ at $\boldsymbol{x}^{(i)}$.

Another way to calculate $a^{(i)}$ is to specify that $\tilde{f}(\mathbf{x})$ interpolates *f(x)* at $\boldsymbol{x}^{(i)}$ and $\boldsymbol{x}^{(i-1)}$ and that the gradient of $\tilde{f}(\mathbf{x})$ matches that of *f(x)* at $\boldsymbol{x}^{(i-1)}$ and not at $\boldsymbol{x}^{(i)}$ as above. This gives the following expression:

$$a^{(i)} = \frac{2\left\{f(\mathbf{x}^{(i)}) - f(\mathbf{x}^{(i-1)}) - \nabla^T f(\mathbf{x}^{(i-1)})(\mathbf{x}^{(i-1)} - \mathbf{x}^{(i)})\right\}}{\left\|\mathbf{x}^{(i)} - \mathbf{x}^{(i-1)})\right\|^2} \qquad (4.13)$$

By averaging the curvature of the backward interpolation quadratic function as in equation (4.12), and forward interpolation quadratic approximation as in equation (4.13), an averaged expression for $a^{(i)}$ can be obtained [95,96]. In this study use was made of equations (4.12), and it gives more stable values for the curvature.

4.2.4 Gradient approximation of objective and constraint functions

The Dynamic-Q method of Snyman needs the gradients of the objective and constraint functions. Different methods can be used for calculating these gradients, and these methods have certain advantages and disadvantages when using computational fluid dynamics to construct the gradient. One such method is the forward differencing scheme.

A forward differencing scheme is used to approximate the gradient vector of the objective function $(\nabla f(\mathbf{x}^{(i)}))$ which is used in the spherical quadratic approximation discussed in sub-section 4.2.3. The components of the gradients are calculated as follows:

$$\frac{\partial f(\mathbf{x})}{\partial x_i} = \frac{f(\mathbf{x} + \Delta\mathbf{x_i}) - f(\mathbf{x})}{\Delta x_i}, \quad i = 1, 2, ..., n \qquad (4.14)$$

where

$$\Delta\mathbf{x}_i = \left[0, 0, ..., \Delta x_i, ..., 0\right]^T \qquad (4.15)$$

The components of the gradients of the inequality and equality constraint functions used in the spherical quadratic approximation are approximated in a similar manner and are given in equation (4.16).

$$\frac{\partial g_i(\mathbf{x})}{\partial x_i} = \frac{g_i(\mathbf{x}+\Delta\mathbf{x}_i) - g_i(\mathbf{x})}{\Delta x_i} \quad i = 1,\ldots,m$$
$$\frac{\partial h_i(\mathbf{x})}{\partial x_i} = \frac{h_i(\mathbf{x}+\Delta\mathbf{x}_i) - h_i(\mathbf{x})}{\Delta x_i} \quad i = 1,\ldots,p \qquad (4.16)$$

again with

$$\Delta\mathbf{x}_i = \left[0,0,\ldots,\Delta x_i,\ldots,0\right]^T \qquad (4.17)$$

A new computational fluid dynamics simulation is required to approximate each of the components. Thus $n+1$ computational fluid dynamics simulations are to be performed at each optimisation iteration. The restart feature of the computational fluid dynamics package can be used to reduce the computation time required to obtain the computational fluid dynamics solutions. In some cases, the amount of iterations required to obtaining a converged computational fluid dynamics solution for a perturbed set of design variables ($\boldsymbol{x}+\Delta x_i$), can be reduced by a factor of 10, when using the restart feature of the computational fluid dynamics package [49].

In many optimisation problems, additional simple side constraints of the form $\hat{k}_i \le x_i \le \check{k}_i$ occur. Constants $\hat{k}_i$ and $\check{k}_i$, respectively, are lower and upper bounds for variables x_i. Since these constraints are of a simple form (having zero curvature), they need not be approximated in the Dynamic-Q method and are instead explicitly treated as special linear inequality constraints in the application of LFOP.

As a further aid in controlling convergence, intermediate move limits are imposed on the design variables during the minimisation of the subproblem. For each approximate subproblem *P(i)*, these move limits take the form of additional inequality constraints [97]. These inequality constraints are described by

$$x_j - x_j^{(i-1)} - \delta_j \le 0, \qquad x_j^{(i-1)} - x_j - \delta_j \le 0, \qquad j=1,2,\ldots,n \qquad (4.18)$$

where $\delta_j>0$ are user-specified move limits.

The Dynamic-Q algorithm can now be stated as follows [24]:

1. Choose a starting point $\boldsymbol{x}^1$ and move limits δ_j, $j:=1,2,...,n$ and set $i:=1$.
2. Evaluate $f(\boldsymbol{x}^i)$, $g_j(\boldsymbol{x}^i)$ and $h_j(\boldsymbol{x}^i)$ as well as $\nabla f(\boldsymbol{x}^i)$, $\nabla g_j(\boldsymbol{x}^i)$ and $\nabla h_j(\boldsymbol{x}^i)$. If termination criteria are satisfied then set $\boldsymbol{x}^* := \boldsymbol{x}^i$ and stop.
3. Construct a local approximate subproblem $P[i]$ with corresponding penalty function $Q(\boldsymbol{x})$ at $\boldsymbol{x}^i$ (as in (4.3)), using approximations for the objective and constraint functions given by (4.8) - (4.13).
4. Solve the approximated subproblem $P[i]$ to give $\boldsymbol{x}^{*i}$ by using LFOPC [92].
5. Set $i := i + 1$, $\boldsymbol{x}^i := \boldsymbol{x}^{*(i-1)}$ and return to Step 2.

4.2.5 Particular strengths of Dynamic-Q

The particular choice of spherically quadratic approximations in the Dynamic-Q algorithm has implications for the computational and storage requirements of the method. Since the second derivative of the objective function and constraints is approximated using function and gradient data, the $O(n^2)$ calculations and storage locations, which would usually be required for the second order derivatives, are not needed. The computational and storage resources for the Dynamic-Q method are thus reduced to O(n). At most, $4+m+p+r+s$ n-vectors need to be stored (where m, p, r, s are the number of inequality and equality constraints and the number of lower and upper limits of the variables, respectively) [24]. The savings become significant when the number of variables becomes large. Therefore, Dynamic-Q is ideally suited for optimisation of engineering problems with a large number of design variables.

The LFOPC algorithm [92] implemented in Dynamic-Q to solve the sequence of subproblems $P(i)$ requires only gradient information and no explicit line searches or function evaluations are performed, and these together with the fundamental physical principles as shown by Snyman [91,92], ensure that the algorithm is very robust. A further desirable feature is that, if there is no feasible solution to the problem, the

LFOPC algorithm in Dynamic-Q will still find the best possible compromised solution without breaking down. Therefore, Dynamic-Q usually converges to a solution from an infeasible remote point without the need to use searches between the subproblems as is the case with SQP.

The Dynamic-Q method requires very few settings by the user. The only settings needed are: convergence criteria, specification of maximum number of iterations, number of constraints (inequality and equality) and limits (lower and lower) and specification of step limit and perturbation size.

4.2.6 Approximation of derivatives for noisy functions

Noise may appear in both the experimentally and numerically derived functions. In experimental functions, noise may be caused by errors due to environmental influences and in computational fluid dynamics functions, noise may be caused by grid changes, incomplete convergence and numerical accuracy of the computer. These noisy functions may pose problems when approximating the derivatives using the forward differencing schemes as discussed by De Kock [96,98]. Due to the noise in the function, gradient approximations with too small Δx may be highly inaccurate. Therefore, choosing a larger Δx will ensure that the noise is effectively smashed out and does not detrimentally influence the global gradient of the function to the same extent. However, choosing a very large Δx will also result in an inaccurate gradient approximation. De Kock [96,98] has pointed out that a larger Δx may cause the optimisation problem not to converge and cause the design variables to rock back and forth near the optimum. The perturbation sizes were taken as 10% of the range of variables used.

4.3 CONCLUSION

This chapter focused on mathematical optimisation. Mathematical optimisation was formerly defined and Dynamic-Q, the method of choice for this study, was discussed in detail. The effect of numerical noise on gradient-based algorithms was also considered.

CHAPTER 5

DESIGN OPTIMISATION METHODOLOGY

5.1 PREAMBLE

In this chapter, a preliminary work was performed in which computational fluid dynamics simulations were validated against accurate and reliable experimental results. After the preliminary work was performed, the design optimisation methodology proposed for the study was developed. All the tools that have been used for the development of the methodology are discussed here. The other important aspect is the discussion of the coupling between all the tools that made it possible to achieve the design optimisation methodology.

5.2 MODEL VALIDATION

The model validation is performed by comparing computational fluid dynamics predictions with measurements for a suitable test case. The results for this test will pave the way for a design optimisation study on a more realistic model of a combustor. A commercial code FLUENT [74] has been used to validate the simulation results against experimental results.

To ensure that computational fluid dynamics modelling is correct, it is necessary to validate the simulation results against accurate and reliable experimental results. This validation process assures the user that the code can be used with confidence for simulations and the user can use the code in the correct manner to solve the problem. The ability to reproduce the experimental results gives the designer a margin of confidence in the simulation code.

In this validation study, simulation results are compared with experimental results of a Berl combustor model [41]. Different turbulence models will be used to assess their accuracy when calculating reacting flows in a combustor.

5.2.1 Validation error control

In any simulation case, it is extremely important to make sure that the errors of the obtained solutions are sufficiently small. The errors can be caused by human factors (mistakes), setting of wrong boundary conditions, discretisation (truncation errors), iterative errors (algebraic errors) and model errors. The first two must be avoided as far as possible by careful work. The last two errors will always be present in numerical calculations, but they should be minimised, so that they are small compared with the model error. The model error is the difference between the correct value (analytical solution or exact measurements) and the exact solution of the turbulence model. As this error is case-dependent and model-specific it is interesting to quantify it for different classes of problems.

A rule of thumb [41] is that the iterative and the discretisation errors should not be larger than 10% of the model error. That is, if the model error is 10% of a mean quantity, the iterative and discretisation errors should not be larger than 1% each. The method used to determine if the errors are small enough is listed below and further explanations follow below the list:

1. Obtain converged solution on a relatively coarse initial grid.
2. Refine the grid globally and perform new calculations.
3. Compare the converged solutions of the two grids.
4. If the difference is too large, refine the grid again globally and perform new calculations. Compare the solutions of the previous grids.
5. Continue like this until the difference between the two finest grids are small enough, maximum 10% of the model error.

The comparison of the converged solutions of different grids was done to check the discretisation errors. If the solution of grid one is compared with the solution of grid two (grid one refined once globally), the error is somewhere between 1/3 to 1 times the difference of the solutions (Δe), i.e. the correct solution for the specific turbulence model is 1/3*Δe to 1*Δe away from the solution of the finest grid. 1/3*Δe

corresponds to an error proportional to h^2 ($O(h^2)$) (h is the mesh size) and 1*Δe corresponds to an O(h) discretisation.

5.2.2 Test case

The test case study was performed following "Best Practice Advice for Combustion and Heat Transfer" [99]. However, critical model configurations have been made where necessary. The above reference observes the fact that stringent environmental legislation requires very low NOx and CO, a more efficient methodology to design a cleaner system is needed, and computational fluid dynamics reduces experimental costs. In this reference, there are some references to documented underlying flow regimes in a knowledgeable base, one of which is "Bluff Body Burner for CH_4H_2 turbulent combustion".

The validation was performed on the unstaged natural gas flame in a 300 kW industrial burner shown in Fig. 5.1. The experimental results of this work were collected from a FLUENT validation case [41]. The burner features 24 radial fuel ports and a bluff centre-body. Air is introduced through an annular inlet and movable swirl blocks are used to impart swirl. Figure 5.2 shows the computational grid of the combustor.

In this test case, it is important to estimate how well different turbulence models in the program predicts the swirling flow and heat transfer in the combustor. Calculations were carried out for the following turbulence models, using a second-order discretisation scheme:

- Standard *k*-ε model (*k*-ε)
- RNG *k*-ε model (RNG)
- Realizable *k*-ε (RLZ)
- Reynolds stress method (RSM)

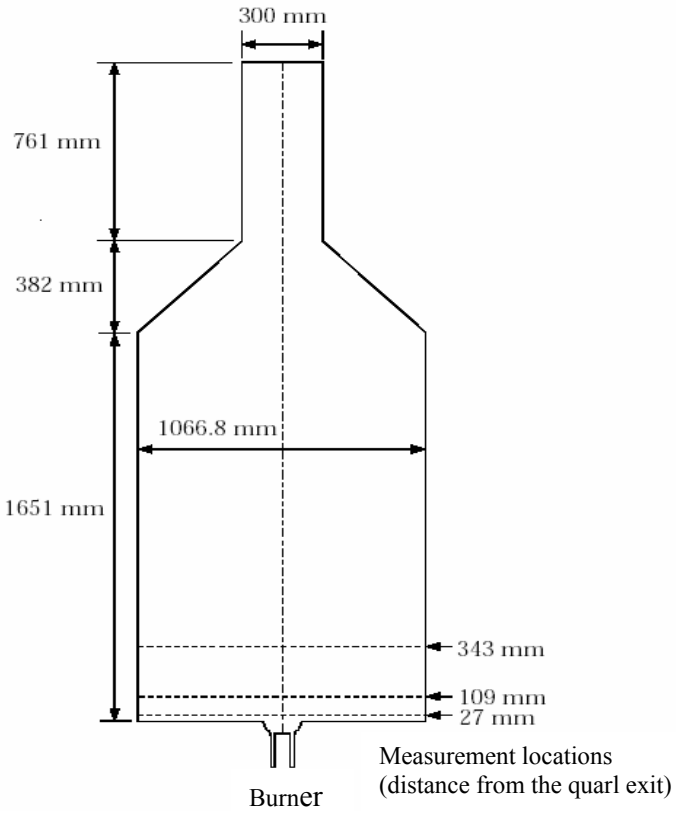

Figure 5.1. Two-dimensional view of a Burner

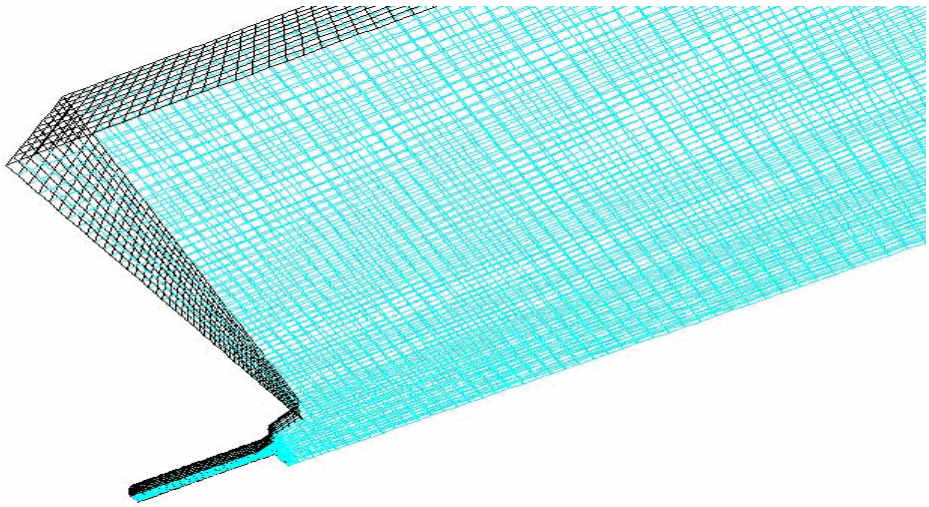

Figure 5.2. Meshed volume of the Burner

The simulations code solves the equations for conservation of momentum, conservation of mass, energy and species concentrations. The reaction was modelled with a mixture fraction/pdf model and radiation was modelled with a P-1 model. The standard wall functions were used with all the models.

Since it was the model error that was important to determine, the calculations were performed to minimise the iterative errors and discretisation errors, i.e. make sure the solutions were converged and independent of the grid.

5.2.3 Case set-up

A commercial computational fluid dynamics code [74] for turbulent reacting flows was used to carry out all flow analyses discussed in this case. There are three-dimensional features (radial fuel ports), hence a three-dimensional model (1/24 sector of the combustor) was considered in all numerical computations.

The flow also includes strong streamline curvatures, as well as vortices and boundary layer separation. All RANS-based models available in FLUENT were used for the case study. The mixture fraction/pdf was used to model chemical reactions. In this approach, the transport equations for mixture fraction and its variance are solved, instead of the species equations. The density and the component concentrations are derived from the predicted mixture fraction and the variance distributions. This approach applies specifically to the simulation of turbulent diffusion flames.

To reduce the computational efforts, further simplifications have been considered: the effects of the buoyancy forces have been neglected, so that only the symmetric portion of the domain was analysed; the pressure variations are so small that the flow has been considered as incompressible and wall functions have been used to model the near-wall region.

As a requirement of the mixture fraction/pdf model, a pdf file was set-up with a PrePDF processor. Then the pdf file was imported into FLUENT to set-up the FLUENT case file. The pdf file contains a look-up table needed by the mixture fraction/pdf model in Fluent. The equilibrium mixture for calculation with pdf model was assumed to consist of 13 different species and radicals: CH_4, C_2H_6, C_3H_8, C_4H_{10}, CO_2, N_2, O_2, H_2O, CO, H_2, O, OH and H.

5.2.4 Boundary conditions

The boundary conditions for the simulations are given in Table 5.1 to 5.3.

Boundary	T (K)	Emissivity
Walls near the inlet duct	312	0.6
Bluff body front wall	1173	0.6
Inlet duct insert (oblique)	1173	0.6
Quarl wall (oblique)	1273	0.6
Furnace bottom wall	1100	0.5
Furnace cylinder wall	1280	0.5
Furnace top wall (hood)	1305	0.5
Chimney wall	1370	0.5

Table 5.1. Wall thermal conditions

	Air	Gas
Mean axial velocity (m/s)	31.35	0
Radial velocity (m/s)	0	157.25
Mean tangential velocity (m/s)	20.97	0
Temperature (K)	312	308
Turbulence intensity (%)	17	5
Turbulence length scale (m)	0.0076	0.0009

Table 5.2. Inlet flow boundary conditions

	Oxidiser	Fuel
Mole fraction of CH_4	0	0.965
Mole fraction of C_2H_6	0	0.017
Mole fraction of C_3H_8	0	0.001
Mole fraction of C_4H_{10}	0	0.001
Mole fraction of CO_2	0	0.003
Mole fraction of N_2	0.79	0.013
Mole fraction of O_2	0.21	0.013

Table 5.3. Mole fractions in the inlet

5.2.5 Results and discussions

Velocity profiles

The comparisons of velocity profiles were made along three lines across the combustor at axial distances of 27 mm, 109 mm and 343 mm from the quarl body. The quantities on which comparisons are made are velocity profiles and temperature profiles for numerical predictions and measurements results.

In Figures 5.3, 5.4 and 5.5, the axial velocity is plotted against the crosswise direction. The figures include results for the four turbulence models tested in this test case: i.e. standard *k-ε* model, realizable *k-ε* model, RNG model and RSM model. The results in Fig. 5.3 show that the curves for *k-ε*, RNG and RLZ have good agreement with the measurements in shape. RNG predicted the axial velocity close to the measurements in the recirculation zone, but RLZ and *k-ε* deviated a little from RNG. However, RNG has a higher peak than RLZ and *k-ε*. RSM has not predicted any recirculation at this location, where all other models have shown some recirculation. At a greater radius, the models gave the results close to the measurements, except RSM. All the models under-predicted the strength of the reverse flow velocity near the centreline. The peak velocities are also over-predicted.

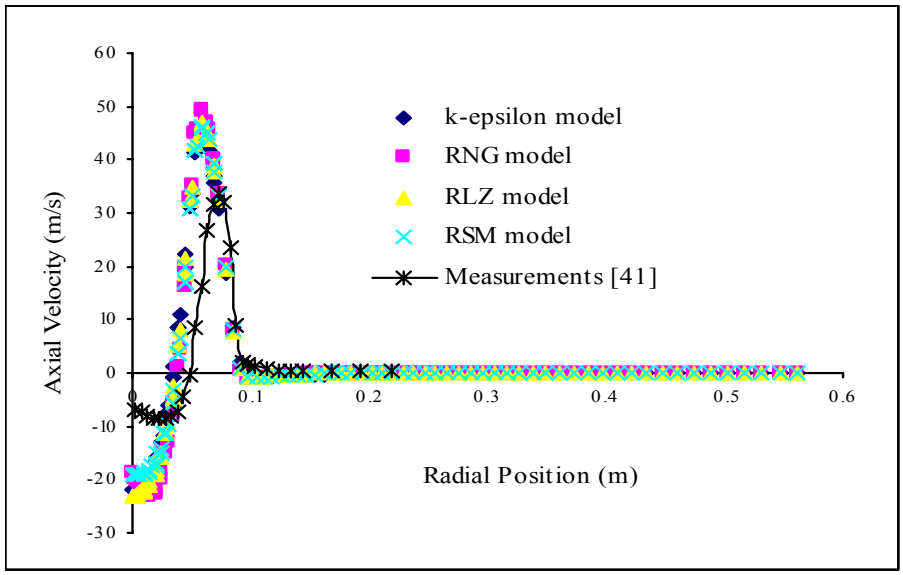

Figure 5.3. Axial velocity at 27 mm from the quarl exit

In Fig. 5.4 all the models have predicted recirculation and they predicted curves with the same shape as the measurements. The *k-ε* model has performed better than other models. It has predicted velocities close to measurements near the centreline. For all the models, as the results move away from the centreline, the predictions deteriorate. All the models, except the RNG model under-predicted the strength of the swirl near the centreline. The peak velocity has been over-predicted by all the models, with peaks appearing at a smaller radius. In Fig. 5.5, all the models have performed unsatisfactorily. The curves have larger differences in shape, magnitude and location of peaks.

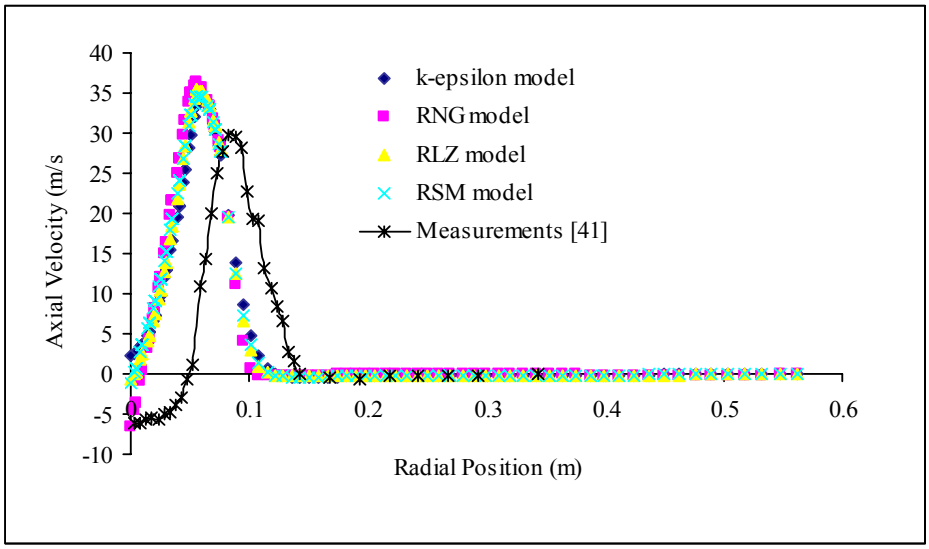

Figure 5.4. Axial velocity at 109 mm from the quarl exit

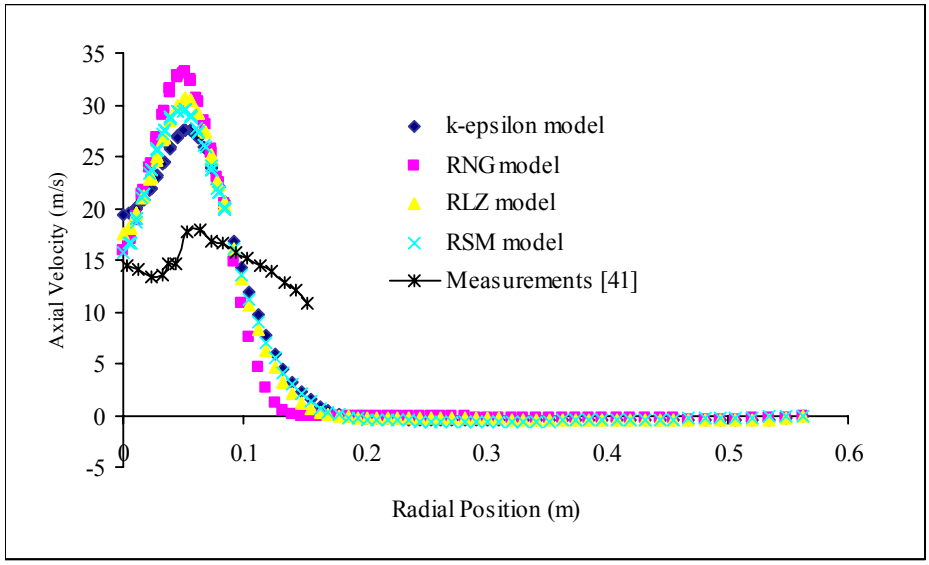

Figure 5.5. Axial velocity at 343 mm from the quarl exit

In all three figures (Fig. 5.3, 5.4 and 5.5) discussed above, it was expected that the RSM and RLZ models would perform better than other models as they are strongly recommended by FLUENT [74] for the kind of flows in the combustor. As expected, RSM took more time to converge, the reason being that the model has many equations to solve. The RNG and *k-ε* were expected to perform not as well as RSM and RLZ, but the opposite happened. The reason might be that the flow is not highly swirled (S = 0.56), because RSM and RLZ are highly recommended for highly swirled flows (S > 0.6).

Temperature profiles

Temperature calculations are very important in combustion. For a swirling flow, the calculations are more difficult. In order to calculate correct temperature distributions in reacting flows, the model used should be able to calculate "correct" velocities in non-reacting flows and this gives some problems for most of the models. Figure 5.6 shows the temperature contours in the combustor from which the plots of temperature at different locations were derived.

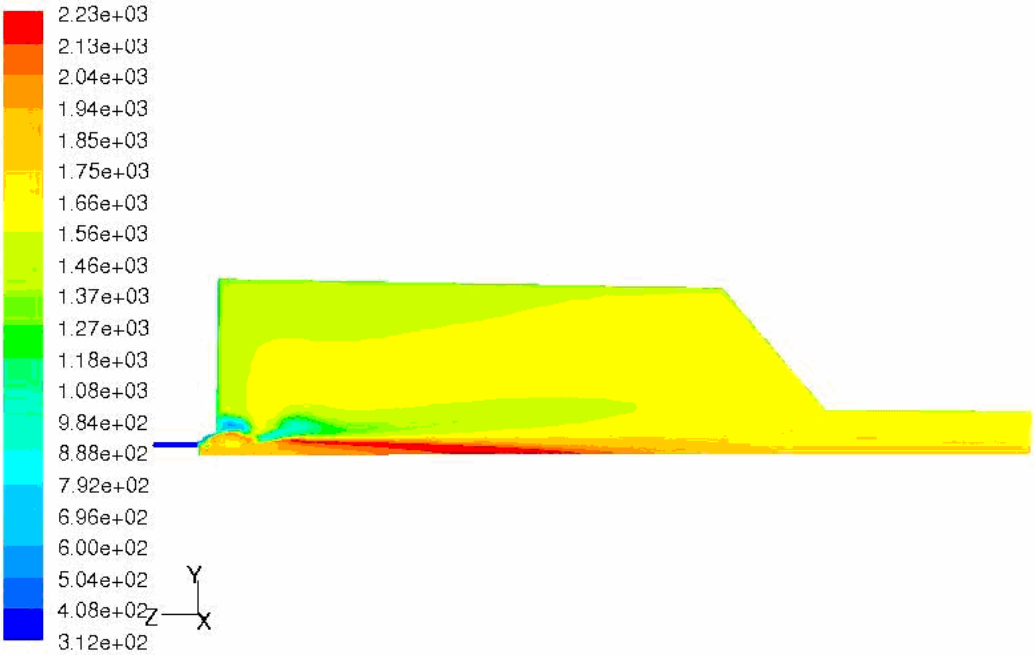

Figure 5.6. Flow field showing temperature (K) contours

Figures 5.7, 5.8 and 5.9 show curves of temperature plotted against radius for the three axial locations (27 mm, 109 mm and 343 mm). In Fig. 5.7, the models have predicted the temperature satisfactorily near the centreline. RSM and RNG performed better than other models. All the models have over-predicted the peak temperatures. However, all the curves have the same shape as the curve for measurements. The pdf model used shows the presence of sharp spikes, and the cause can be an inherent limitation of the model [41]. The limitation results from peak temperature predictions in a narrow region where the stoichiometry is achieved according to the mixture field [41].

In Fig. 5.8, the three models also performed even better near the centreline, with RSM and RNG performing better than other models. But the same spiky behaviour of the pdf model is evident. Peak temperatures have been over-predicted by all the models. However, the predicted curves resemble the experimental curve fairly. In Fig. 5.9 all the models performed unsatisfactorily, and this is consistent with the velocity predictions with all the models for Fig. 5.9.

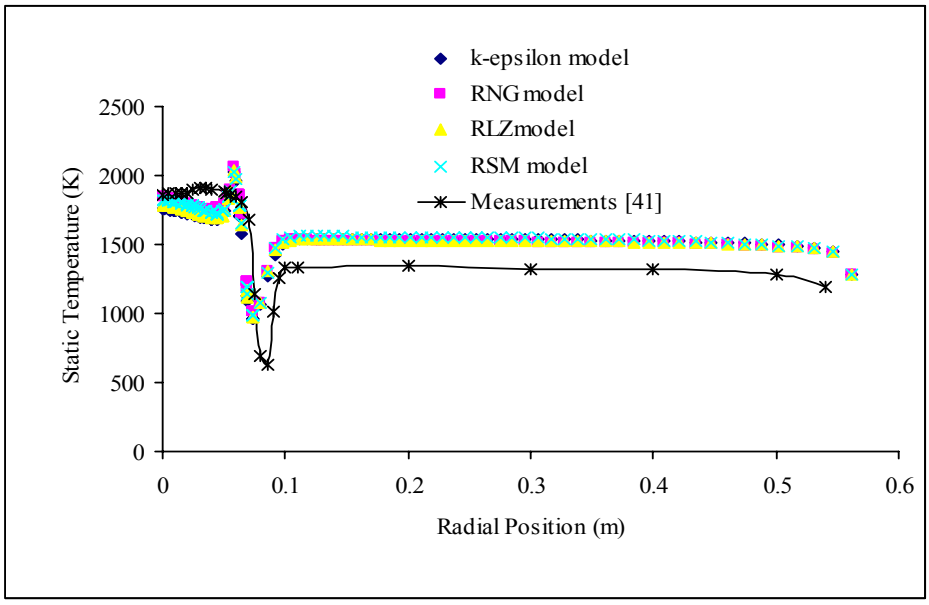

Figure 5.7. Temperature at 27 mm from the quarl exit

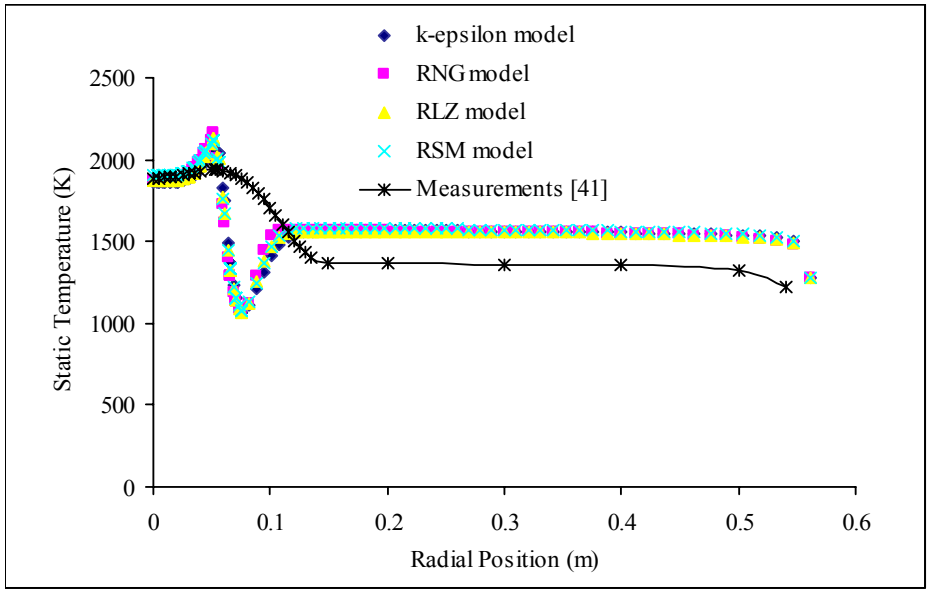

Figure 5.8. Temperature at 109 mm from the quarl exit

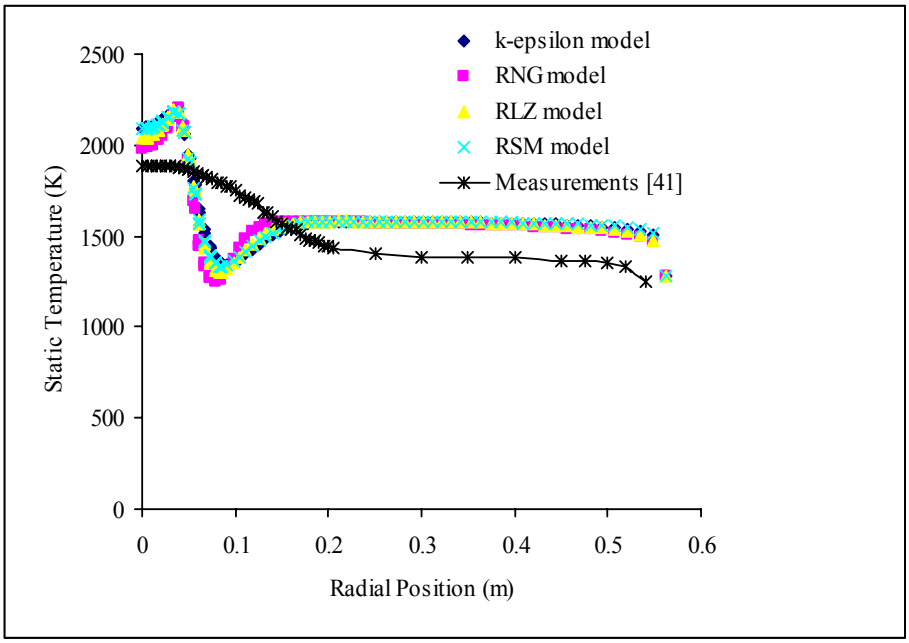

Figure 5.9. Temperature at 343 mm from the quarl exit

The difference between the measurements and predictions on the location x-axis = 0 (in the vicinity of the wall) is minimal for all the locations (i.e. 27 mm, 109 mm and 343 mm) and falls within 200 K, which is a 10% difference. When looking at the temperature profiles there are differences in both minimum and maximum temperature shown by measurements and predictions. Nonetheless, the profiles represent each other favourably. A similar relationship has been shown by reference [41], when using the same combustor to model flow and heat transfer. The predictions show a longer and thinner flame than as observed in measurements. The minimum temperature recorded has been significantly over-predicted by 290 K at location 27 mm, and this exists at the sharp spike.

5.2.6 Conclusions

The agreement between the measurements and computational fluid dynamics results is satisfactory, when considering limitations of computational fluid dynamics models used as explained later in section 5.2.7. Similar differences between predictions and measurements were reported by other researchers [34,40,47]. Therefore, the models are of sufficient accuracy to be used for the design optimisation study. The turbulence models investigated have varying strengths as indicated in the discussions. A guide as

to which model to use and where to use the model can be based on the amount of accuracy required and how fast the results are required. Globally, it is possible to conclude that the models are of adequate accuracy and robust enough in the simulation of diffusion flames.

5.2.7 Results discrepancies

The results for both velocities and temperature profiles can be looked at in a qualitative rather than quantitative manner. The main reason is that the curves for numerical simulations and measurements do follow each other, but the deviations are in some cases large. The same results were found by FLUENT News [41], in which a similar case was used then for that study. The reasons for deviations are many and range from descritisation to the models used, but in this case, the reasons basically originating from the models will be looked at, as they affect the results more. In general, it is known that the two equation closures are based on linear constitute law (the Boussinescq assumption).

In the Boussinescq assumption, gradient diffusion approximation is typically employed to close the Reynolds stresses. For these reasons, poor predictions are expected when the non-linearity of the flow field is high, such as in the presence of chemical reactions and swirling flows. This linear relation should be replaced with a non-linear relation between the Reynolds stresses and the local mean velocity field. The assumptions made in the closure schemes for turbulence also affect turbulence-chemical reaction interactions, and further assumption made are also in the reaction model used. It is well-known that predictions of temperature are mostly based on good predictions of velocities, and in the above results, simulations of temperature deviate even more than velocity simulations and the same findings were reported by Mongia [9] and Gulati *et al*. [48].

The temperature curves have spikes which create high peaks, however, there is no clear explanation of what causes them, but FLUENT News [41], where the same case has been used for modelling turbulent combustion, assumed that the spikes appeared because of inherent pdf model problems, as they did not appear in the finite-rate reaction model of the same case.

5.3 IMPLEMENTATION OF DESIGN OPTIMISATION METHODOLOGY

In order to successfully achieve a set of targets, a designer has to define the shape of the combustor, select its features and optimise all the parameters controlling the performance of the combustor. The optimisation phase is relatively time-consuming and it currently involves trial-and-error approaches to define the combustor configuration that offers the best performance parameters and satisfies the design constraints. The trial-and-error approaches have been found to be costly and time-consuming and hardly achieve the design targets. A combination of computational fluid dynamics and mathematical optimisation is expected to solve the problems related to the trail-and error approaches. In this, way a parametric model is run several times with computational fluid dynamics guided by an optimisation algorithm, such that an optimal solution in terms of performance can be found.

Though discussions have been done on possible optimisation objectives related to the performance of the combustor in section 2.3, the current study focused on optimising the combustor exit temperature profile only. The developed design optimisation methodology will be used to optimise the combustor exit temperature profile. The design optimisation methodology applies geometric parameters such as injection holes and swirler as optimisation design variables. The process involves varying these features with a mathematical optimiser and simulating the performance with computational fluid dynamics until convergence is achieved.

In order to perform the design optimisation, one must first be confident that the modelling techniques used can accurately predict the physical processes being modelled, ascertain its limitations and cultivate one's ability to perform the modelling. This is due to the fact that the optimisation results can be as good as the accuracy of the modelling. For this reason, a validation study was performed on a well-researched Berl combustor [41], and the results are reported in section 5.2. Generally, it is concluded from the results that the standard k-ϵ model is of adequate accuracy to be used for simulation of combustor reacting flows. The model is also robust enough, and therefore, well-suited to the present design optimisation study.

This chapter focused on explaining the design optimisation methodology and how it has been used to achieve the design optimisation of a combustor exit temperature profile. The benefits of a good combustor exit temperature profile have been discussed in sections 2.3.4, 2.4 and 2.5.4.

5.4 NUMERICAL TOOL FOR FLOW ANALYSIS

The commercial software code developed by FLUENT Inc [74] was used to perform the numerical analyses in this study. The FLUENT selected pre-processor, GAMBIT, acts both as a geometry modeller and mesh generator.

The computational fluid dynamics code solves the gas equations in Eulerian form whereas the droplets are treated in a Lagrangian formulation with discrete trajectories. The spherical droplets evaporate according to the uniform temperature model [86] and interchange enthalpy, mass, and momentum with the gas phase and vice versa, as explained in section 3.7. The main local temperature is calculated along the lines of the assumed probability density function (pdf) approach (f-g model) [100] by weighting the mixture fraction-dependent thermodynamic equilibrium temperature with an assumed pdf. This two-parameter solely depends on the local average of the mixture fraction whose variance is assumed to be a β-function. This approach applies specifically to the simulation of turbulent diffusion flames.

Turbulence was modelled using the standard k-ε model along with wall functions for treatment of near-wall regions. The limitations of the standard k-ε model to capture regions which include strong stream-wise curvatures, as well as vortices and boundary layer separation are well-known, but for the purposes of this design optimisation study, the model proved to be appropriate due to its robustness and speed as shown in section 5.2 and by other researchers [35,36].

The use of this model was also necessitated by the fact that the work involves many computational fluid dynamics simulations that take long to converge. To reduce the computational effort, further simplifications have been considered, namely: the effects of buoyancy forces have been neglected, so that only a periodic portion of the domain

is analysed. Furthermore, the pressure variations are so small that the flow has been considered incompressible. Due to the fact that this is an atmospheric combustor, whereby soot particles will be small in diameter, radiation has also been neglected [2].

As a requirement of the mixture fraction/pdf model, a pdf file was set up with the PrePDF processor. The pdf file was then imported into Fluent to set up the Fluent case file. The pdf file contains a look-up table needed by the mixture fraction/pdf model. The equilibrium mixture for calculation with pdf model was assumed to consist of nine different species and radicals: $C_{13}H_{24}$, CO_2, N_2, O_2, H_2O, CO, H_2, O and OH.

Since FLUENT was a commercial computational fluid dynamics code applicable to a wide range of engineering problems, it was necessary to customise the physical submodels and numerical methods and to streamline the boundary condition specification for the current application.

For continuous-phase calculations, the segregated, implicit, pressure-based semi-implicit method for pressure-linked equations (SIMPLE), and an algebraic multi-grid solver are used [74]. In this application, numerical accuracy provided by first-order approximation was insufficient, so second-order accurate approximations were used. In numerical mathematics terms, this was performed by introducing differences that provide additional terms otherwise appearing in the truncation error. The second-order upwind scheme for all scalar equation was used for discretisation.

5.5 GEOMETRIC MODEL

The configuration considered in this study was a can-type atmospheric combustor (Fig. 5.10) developed by Morris [101], for combustion research. The combustor has 10 curved swirler (45°) passages, six primary holes, 12 secondary holes and 10 dilution holes. The combustor has a length of 174.8 mm and a diameter of 82.4 mm. The fuel nozzle has been modelled with a discrete droplet model.

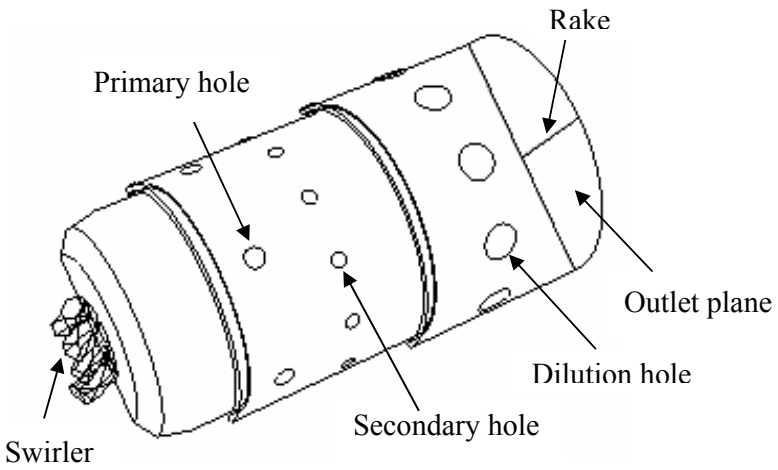

Figure 5.10. Three-dimensional model of the combustor

Since the configuration was symmetrical, only half of the geometry was modelled. Due to the complexity of the geometry and automation required by the optimisation method, the physical domain has been discretised by an unstructured tetrahedral mesh (Fig. 5.11). It was found from a sensitivity study that 500 000 computational cells provided an adequate compromise between accuracy and speed. Further refinement of the mesh beyond 500 000 computational cells did not give any realisable difference, the computational time was acceptable. Particular care was taken on refining the mesh where the central toroidal recirculation zone and the core of the flame were expected.

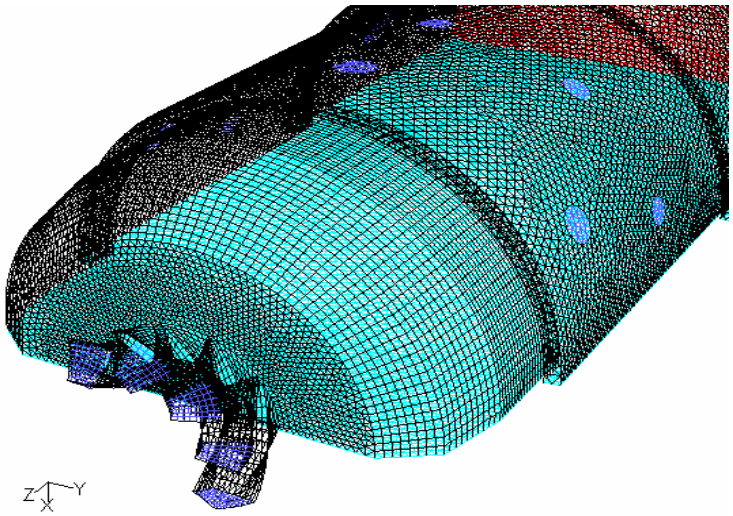

Figure 5.11. Computational grid of the combustor

Since geometric modelling and grid generation are the most time-consuming and labour-intensive processes in computational fluid dynamics-based design systems, GAMBIT journalling toolkit has been intensively used to replay model building for different computational fluid dynamics sessions. The procedures were written in parametric form in Appendix A, such that when a variation of the particular analysis case is generated, one only needs to change the value in the parameter file, and then re-run the procedures.

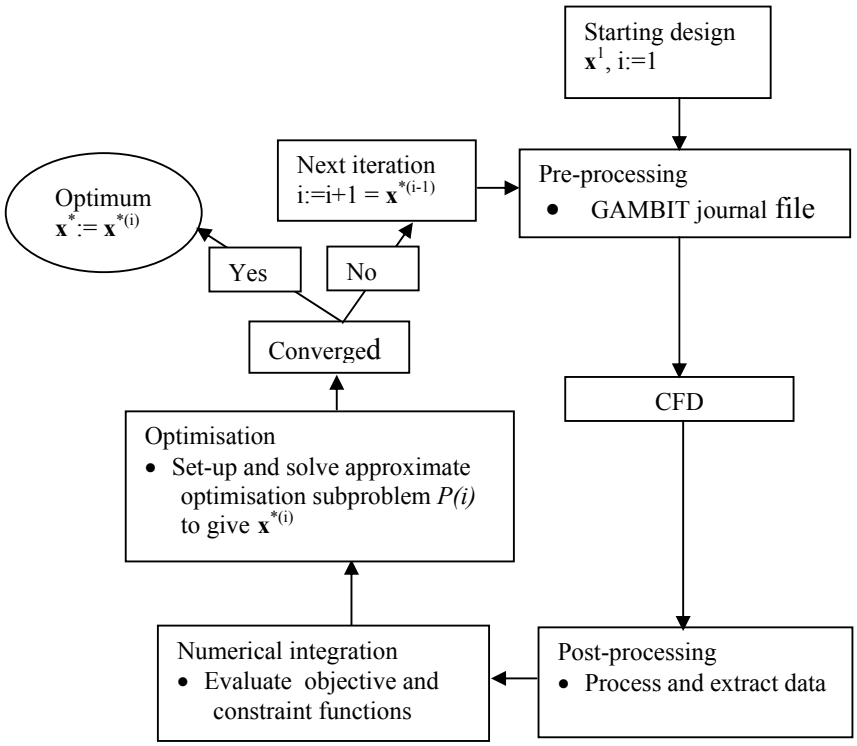

Figure 5.12. Flow diagram of FLUENT coupled to optimiser

The flow diagram of the above procedure is shown in Fig. 5.12. For every iteration or given starting design $\boldsymbol{x}^i$, i=1,2,3…, the mathematical optimiser generates a set of variables that needs to be evaluated. A journal file is then generated with the current variables and passed to GAMBIT to generate the mesh used in FLUENT. After computational fluid dynamics simulations converged, a file is written to a hard disk , which is then processed to derive the data that will be processed with the numerical integrating code to yield the objective function. The mathematical optimiser obtains all the data, sets up a new approximate optimisation subproblem *P(i),* and predicts a new optimum design $\boldsymbol{x}^{*i}$. For the next iteration i:=i+1, the process is repeated until

convergence. With this implementation, the time required to generate a variation of a particular geometry has been reduced from the order of days to minutes.

5.6 BOUNDARY CONDITIONS

Boundary conditions that need to be specified are the mass flow inlets through the swirler, primary holes, secondary holes and dilution holes. The combustor outlet plane is modelled as a pressure outlet boundary. The symmetry boundary planes are modelled as rotational periodic boundary conditions. The air flow distribution boundary conditions were obtained from measurements [101] and are shown in Table 5.4.

Inlet	Radial component	Tangential component	Axial component	I [%]	L_e [m]	T [K]	ρ [kg.m^{-3}]
Swirler	0	0.5	0.5	10	1.250^{-4}	300	1.001
Primary	-0.864812	0	-0.502095	10	$1.97\text{x}10^{-4}$	300	1.001
Secondary	-0.837064	0	-0.547106	10	$1.53\text{x}10^{-4}$	300	1.001
Dilution	-0.913757	0	-0.406262	10	$3.39\text{x}10^{-4}$	300	1.001

Table 5.4. Boundary conditions at the various inlets

The total mass flow rate of air into the combustor is 0.1 kg/s. The mass flow splits are as follows: 8.4% through the swirler, 12.5% through the primary holes, 15.3% through the secondary holes and 60.5% through the dilution holes.

5.7 FUEL SPRAY INJECTION MODEL

Considering that a spray consists of a huge number of drops, it is common practice to gather similar droplets (same diameter, velocity and liquid properties) in a parcel and calculate the trajectory of the parcel to represent that category of drops. According to Tap *et al.* [83], this approach (known as the discrete droplet model) is widely used in computational fluid dynamics codes and was used in the current study. The discrete droplet model was explained in section 3.7.

A spray from the atomiser had to be characterised experimentally for the discrete-phase modelling. The drop breakup and atomisation processes are not modelled and the liquid spray is assumed to be dilute [102], and other thick spray effects are not present [103]. If the spray cannot be considered dilute it might affect the properties of the carrier fluid. In this case, the spray is dense enough to affect the carrier flow field via momentum exchange between the droplets and the carrier fluid. The liquid is assumed to enter the combustor as a fully atomised spray comprised of spherical droplets. The spray modelling was explained in section 3.7.

In order to characterise the spray for computational fluid dynamics modelling, a Malvern Phase Doppler Particle Analyzer (model 2600) was used to obtain the droplet size and distribution of the spray. The spray measurement was taken at a pressure setting of 825 kPa, which produced a flow rate of 0.77g/s. The nozzle used was a Monarch 1.0 USGPH, 80° R. This nozzle produced a solid cone spray. A 300 mm focal length lens that made the instrument sensitive to droplets of between 5.8 and 564 μm in diameter was used to take the measurements. The data was taken at room temperature and pressure, and the fluid used was kerosene. The density, surface tension, and viscosity of this fluid at standard pressure and temperature are 780 kg/m^3, 0.0263 N/m and 0.0024 kg/ms.

Size group	Mean droplet size in group [μm]	Volume fraction	Mass flow [mg/s]
1	7.21	0.014	0.01078
2	8.34	0.003	0.00231
3	10.4	0.003	0.00231
4	12.9	0.007	0.00539
5	16	0.024	0.01848
6	19.9	0.077	0.05929
7	24.8	0.149	0.11473
8	30.8	0.187	0.14399
9	38.4	0.179	0.13783
10	47.7	0.158	0.12166
11	59.3	0.107	0.08239
12	73.8	0.053	0.04081
13	91.7	0.021	0.01617
14	114	0.01	0.0077
15	142	0.004	0.00308
16	176	0.002	0.00154

Table 5.5. Discretised fuel spray data

Before measurements were taken, the instrument was aligned, and the base point measurement for the prevailing conditions (air) was taken. Then a search was made of the spray obscuration to find the ideal distance in which to position the atomiser away from the laser beam. The distance was found to be 0.06 m, with an obscuration of 0.3234. At a distance less than 0.06 m, the sauter mean diameter (SMD) increased, which showed that the atomisation was not fully complete. This can have an adverse effect on combustion if the data is used for combustion modelling. Beyond that location (0.06 m), there was an indication of drop coalescence and fine droplet evaporation. In short, obscuration decreased up to 0.06 m and increased as the atomiser was moved further than 0.06 m. Therefore, 0.06 m gave a lower obscuration value, and measurements were performed when the atomiser was placed in this position.

The experimental results of a fuel spray nozzle produced a Rossin-Rammler drop size distribution function [104,105], as shown in Fig. 5.13. This is characterised by a minimum diameter of 5.8 μm, the SMD of 27.37 μm, a maximum drop size of 204 μm, X = 38 μm and drop size spread parameter of 1.78. The droplets were divided into 16 different size ranges and were introduced into the combustor at 36 discrete circumferential injection points equally spaced at the centre of the combustor. Table 5.5 shows the discretised fuel spray data used in the computational fluid dynamics spray model.

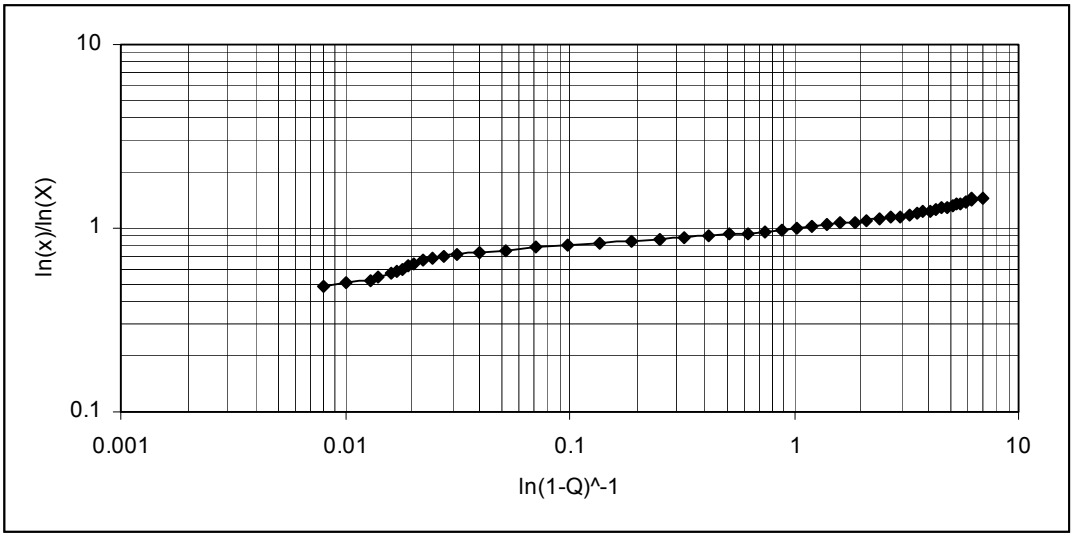

Figure 5.13. The modified Rossin-Rammler plot of spray

Cone	Injection velocity magnitude [m/s]	Half angle [°]	Fuel flow rate [g/s]	Drop size range [microns]
1	32.522	5	0.1283	7.21 – 176
2	32.522	12	0.1283	7.21 – 176
3	32.522	19	0.1283	7.21 – 176
4	32.522	26	0.1283	7.21 – 176
5	32.522	33	0.1283	7.21 – 176
6	32.522	40	0.1283	7.21 – 176

Table 5.6. Prescribed cone fuel nozzle pattern

The non-atomiser model used, involved building a cone. A cone was constructed for 5, 12, 19, 26, 32 and 40 degree cone angles with spray boundary conditions as shown in Table 5.6.

5.7.1 Experimental errors and equipment limitations

There are generally some differences in spray, even when using the same atomiser at nominally the same flow conditions [58]. The errors are due to varying reasons: i.e. the instrumentation used to measure pressure (flow rate) caused some unsteady flow due to the pump unsteadiness, failure to properly align the instrumentation and errors due to obscuration. Some errors caused by alignment and obscuration can be avoided by careful work. Other errors such as detector sensitivity, multiple scattering and vignetting are inherent to the Malvern instrument, and are the major causes of inconsistency in measurement [58].

Multiple scattering is caused by spray with high densities, when light that is scattered by a drop may be scattered by a second drop before reaching the detector. Since the theory of laser diffraction-based instruments assumes scattering from a single droplet, this multiple scattering introduces errors in the computed size distribution. This problem causes the indicated sizes to be broader in distribution and smaller in average size than the actual distribution. These errors can be minimised by keeping the obscuration as low as possible. Chin *et al.* [106] suggest an obscuration of not more that 0.4 (40%). It is suggested that below this obscuration value, SMD does not vary much, but above 0.6 (60%), the SMD varies much and there is need for a correction. In this experiment, the obscuration fell below 0.4 (0.3234) and, therefore, the results are only affected minimally by multiple scattering.

5.8 CONSISTENCY AND CONVERGENCE

It was not possible to perform strict consistency tests, because of the heavy computations that were required. However, a compromise was found between the number of cells that give satisfactory accuracy within a reasonable time ideal for the design optimisation study. In a consistency test, it is expected that as the grid is shrunk indefinitely, the accuracy of the original partial differential equation is recovered. This drives the process to an unconditionally consistent numerical scheme.

Convergence is a familiar mathematical concept in the case of sequences of numbers that here, however, refers to whether and how sequences of the solution approach the true solution of a continuum differential equation. Convergence and accuracy are closely linked to stability, while it is totally incorrect to believe that numerical instability problems can be removed and accuracy increased simply by using a finer grid. The relation between flow parameters and grid scales is essentially what matters, for stability and its associated accuracy. The convergence matrix used for the analyses was based on flow field parameters as opposed to solver residuals. Convergence of the combusting flow field was demonstrated when the area-weighted temperature at the combustor exit plane remained unchanged to within 1 000 iterations.

5.9 COMBUSTOR NUMERICAL FLOW FIELDS

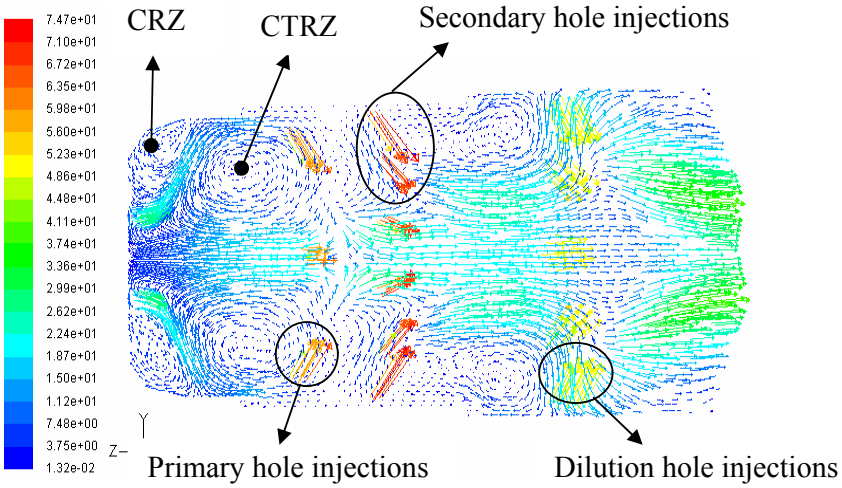

Figure 5.14. Combustor velocity (m/s) vectors

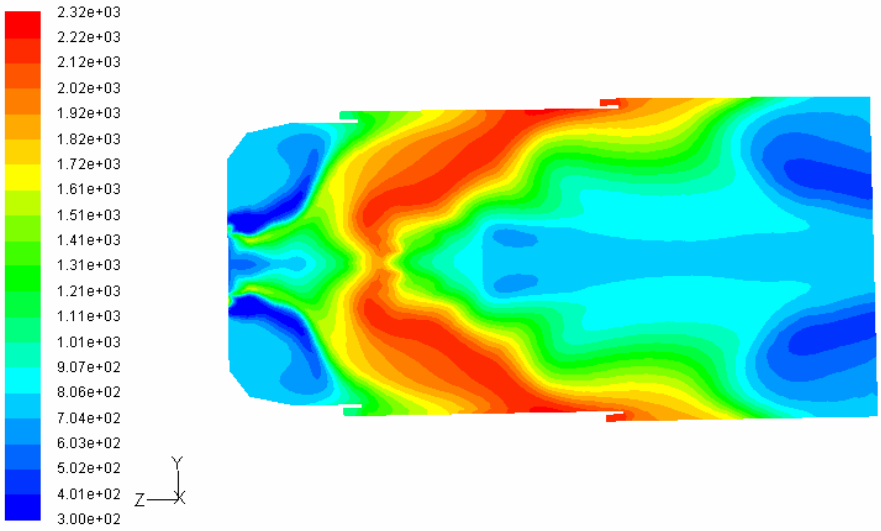

Figure 5.15. Combustor temperature [K] contours

The computational results of the velocity vectors and temperature contours on a longitudinal planar section under the base case design are shown in Fig. 5.14 and Fig. 5.15. The velocity profiles display the swirling flow, as well as the primary, secondary and dilution penetration. The recirculation zone in the combustor primary zone is caused by the joint effect of the primary jet impingement and shearing, upstream of the jet. The mixing and recirculation in this zone provide an ideal aerodynamic condition for evaporation of the fuel spray and ignition of the mixture. It is shown in Fig. 5.15 that the combustion process is basically not completed in the primary zone. This normally happens with atmospheric experimental combustors because of low heat release rates [2]. But in order to increase the combustion efficiency and improve the uniformity of the exit temperature distribution, flow fields in the primary, secondary and dilution zones should be carefully controlled.

Satisfactory combustion is achieved when the spray is enclosed in the swirling recirculation zone, as explained in sections 2.1.2 and 2.1.4. Actually, the swirling recirculation is designed to induce combustion products to flow upstream to meet and merge with the incoming fuel and air. This action also assists in stabilising the flame. When sprays are trapped in recirculation zones, droplets are sufficiently mixed with the high temperature gas, heated by the surrounding area and vaporised, and finally react with the air. Otherwise, the combustion is incomplete due to the poor

distribution and mixing. When the spray is within the recirculation zone, the evaporation of droplets and the combustion of mixtures are complete.

For the current study, the central toroidal recirculation zone is shifted slightly off-axis near the location of the primary jet injection. According to Durbin *et al.* [34], this is a sign of low swirl and is caused by the absence of vortex breakdown due to low swirl. Experimental results showed that the central toroidal recirculation zone is a quasi-axisymmetric bubble developed by vortex breakdown, which is associated with swirling flow exceeding a certain swirling strength [2,107]. Multiple factors, including inlet conditions and geometries, tangential and axial velocities have been found to affect the process of vortex evolution and breakdown [107].

The presence of a corner recirculation zone is also a sign of low swirl and when swirl is high, corner recirculation zones are reduced. The corner recirculation zone is caused by the fact that the tangential velocity distribution at the swirl exit is such that the peak velocity occurs radially outwards away from the centreline. This peak in tangential velocity profile towards the corner, results in a strong corner recirculation zone in conjunction with a weak central toroidal recirculation zone.

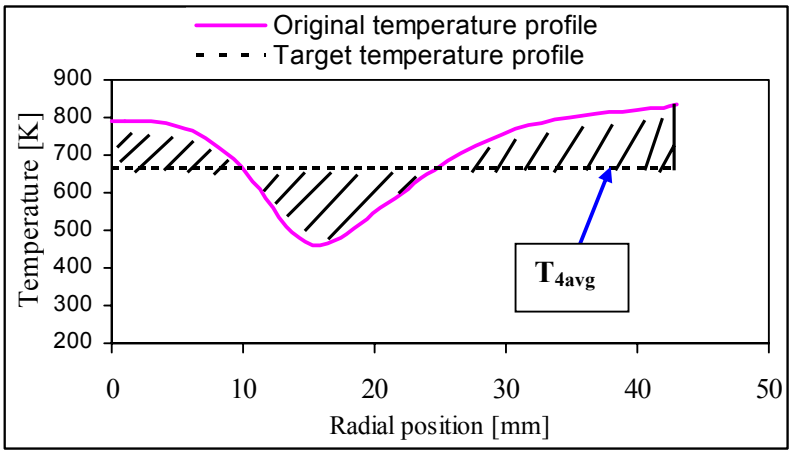

Figure 5.16. Target and actual combustor exit temperature profile

In the high-swirl case, the flow expands rapidly soon after entering the combustor, unlike the low-swirl case. This divergence of streamlines in the high-swirl case leads to the reduction in size of the corner recirculation zone as compared with low swirl. A

carefully controlled primary flow field creates an on-axis central toroidal recirculation zone. Due to the lack of optimised flow fields, a non-uniform combustor exit temperature profile (Fig. 5.16) has resulted, and in order to get a uniform combustor exit temperature profile, the combustor flow fields must be optimised.

5.10 OPTIMISATION PROBLEM DEFINITION AND FORMULATION

The formulation of an appropriate and consistent optimisation problem (or model) is the most important part of mathematical optimisation. The correct formulation of both the objective function and constraints ensure that the solution is feasible.

5.10.1 Numerical integration

In this work, the mathematical optimiser gathers all the data and predicts a new optimum design, and the process is repeated until convergence is reached. The objective function of this case is not known analytically, therefore, an approximation has to be performed from the simulation results.

After the solution had been obtained with computational fluid dynamics simulations, data was extracted from the results of the exit plane of the combustor, and a file was written to a hard disk that was then processed in order to obtain the objective function for a specific design configuration. A rake with 43 data points was created at the exit of the combustor in order to extract temperature data. The number of data points can affect the accuracy of the numerical integration result. As the number of data points increases the accuracy also increases. However, there is a cut-off point where the accuracy just changes negligibly with increase in the of data points and for this research 43 was the optimal number of data points. The purpose of the proposed design optimisation is to obtain dimensions for the combustor in Fig. 5.10 that would give a flatter (uniform) combustor exit temperature profile which closely matches an imposed target temperature profile.

Optimisation with these variables is the same as using momentum-flux ratio as an optimisation design variable, since the variables used have a direct effect on momentum-flux ratio. The mass flow rate of the air to the liner holes is kept constant

by the use of a mass flow inlet boundary condition. This boundary condition ensures that the liner holes always share the same mass flow rate of the air equally. It is possible that during the optimisation process the pressure drop increases, and this is avoided by applying a constraint for pressure drop.

Figure 5.16 shows the numerical integration technique that is used to derive the objective function (function value) for mathematical optimisation. The trapezoidal rule [108] was implemented in a computer code (Appendix B) for numerical integration of the combustor exit temperature profile curve (Fig. 5.16). This code was also extended to calculate the area between the non-optimised (original) combustor exit temperature profile and the target temperature.

The target temperature, T_{4avg}, is 667 K, and it is represented by the target temperature profile in Fig. 5.16. This is equivalent to the mass-weighted temperature at the outlet of the combustor. T_{4avg} is also related to the final temperature of the products of combustion. This temperature can also be determined from the following simple thermodynamic relationship:

$$\left(\dot{m}C.V\right)_{fuel} = \left(\dot{m}c_p(T_2 - T_1)\right)_{products} \qquad (5.1)$$

where $\dot{m}$ is mass flow rate, $C.V.$ is the calorific value of fuel, c_p is the specific heat capacity of air and T_1 and T_2 are initial and final temperatures. Since the flow rate of fuel is negligible when compared with the flow rate of air, it has been assumed that heat is transferred to air from T_1 to T_2.

The final temperature of products as calculated from the analytical equation 5.1 is 652 K, and this value compares very well with 667 K, which is obtained from simulation results and the difference is 15 K. A possible reason for the difference could be the effect of the standard k-ε turbulence model and some minor effects related to discretisation procedures. The standard k-ε turbulence model has certain deficiencies when applied to highly swirling flows particularly in the prediction of mixing levels. Also, the combustion model used in this code assumes a fast chemical reaction and

does not account for possible finite-rate chemical reaction effects that may contribute to the difference. The above discrepancies are explained in Chapter 3.

The other curve in Fig. 5.16, is the temperature distribution across the radius at the exit of the combustor. In order to flatten the original temperature profile so that it follows the target temperature profile closely, one can reduce the area between the two curves (shaded area). Although it is recognised that a uniform temperature distribution may not always be desired, optimum is generally used herein [47] to identify flow and geometric conditions, which lead to a uniform combustor exit temperature profile. The procedure of optimising for a uniform combustor exit temperature profile also has a direct impact on the pattern factor and profile factor. This is due to the fact that they all depend on jet penetration and mixing efficiency. However, it is more appropriate to optimise for combustor exit temperature profile because the pattern factor and profile factor just provide a measure of the quality of the combustor exit temperature profile.

5.10.2 Mathematical optimisation

The most important thing in optimisation is the ability to properly formulate the optimisation problem: i.e. determination of design variables, a way of judging the design (objective function), and provision of constraints that satisfy a feasible design space.

Objective function

The objective of this study is to obtain a flatter (uniform) combustor exit temperature profile that closely matches the target profile. The combustor exit temperature profile is not the only performance parameter that is important for the design of gas turbine combustors, but, it is a key parameter of an optimised combustor that is related to the power output and durability of the turbine. The combustor exit temperature profile is a function of jet penetration and mixing efficiency, which are all functions of momentum-flux ratio. This momentum flux ratio is a function of combustor geometric parameters. Having derived the objective function $f(\mathbf{x})$, the next task is to optimise the objective function.

The method that is employed here is geometric optimisation, where geometric parameters are used as design variables to optimise the objective function.

Design variables

The design variables for this study can include process variables and geometric variables. The process variables can include parameters such as flow rate and inlet temperature. The process variables are usually not a preferred choice for optimisation as they are dictated by the operation of the combustor, such as air-fuel ratio. The design variables that directly affect the combustor exit temperature profile are used: i.e. the number and the radius of primary, secondary and dilution holes and swirler angle. These design variables control the combustor exit temperature profile due to their direct impact on momentum-flux ratio, which subsequently controls jet penetration and mixing efficiency.

Design constraints

The most important constraint for design optimisation studies is the pressure drop. Though other constraints related to emissions could be considered, injection velocities have drastic effects on combustor pressure drop. As geometric parameters (design variables) are varied by the optimiser, it is possible for the combustor pressure drop to increase. This would, therefore, make it necessary for pressure drop to be limited to a certain value. The design variables are also confined to certain limits to ensure that the realistic and practical considerations are accounted for. An equality constraint that would maintain the total surface area of the specific holes would be necessary. This equality constraint would ensure that the surface area through which the quantity of mass of air passes does not vary, hence keeping the pressure drop constant.

Handling integer variables

In this research, it is required that some of the design variables (number of holes) be integers. In other words, the requirement that those design variables should be integers at every design iteration must be added to the optimisation formulation. This problem, therefore, becomes a mixed integer optimisation problem, because there is a mixture of continuous and integer variables. Any particular variable can be represented in two parts: the greatest integral part and the corresponding fractional part. The variables can be represented as follows:

$$x_i = gr_i + fr_i \text{. where } 0 \leq fr_i < 1 \text{, and } i = 1,2,3,\ldots\ldots,n \qquad (5.2)$$

gr = greatest integral part and fr = fractional part.

In order to satisfy the condition that x_i should always be integer variables, necessary steps have to be performed, as shown below:

- The problem can be solved by rounding off the integers constrained either up or down [108,109]. This procedure as suggested by Kuffman and Henry-Labordere [109] has the potential of producing a solution that violates the constraints. The optimal solution without integer solution can be very different from solutions of the same when integer solutions are mandatory.

- There are special algorithms and heuristics, such as the Gomory algorithm cited in [109-111] that have been accepted as best fitted to solve a class of combinatorial problems comprising integer and mixed variables. More often than not, these algorithms are very computationally expensive and sometimes fail to converge to the solution, especially when the number of design variables is large.

Since Dynamic-Q does not have a specific feature for handling integer constraints, an appropriate method of handling constraints has been devised. In this work, it has been decided that a rounding-off procedure would be used to produce integer design variables from optimisation solutions [109,110]. The rounding-off procedure will be performed in this way:

$$\text{If } fr_i \geq 0.5 \text{ then round up and if } fr_i < 0.5 \text{ then round down} \quad (5.3)$$

The method of rounding off can cause the integer design variable to rock up and down between two values of design variables, especially when the variables have reached their optimum, because the optimum will be between the two integer values.

5.11 CONCLUSION

This chapter focused on development of the design optimisation methodology that is used for this study. Computational fluid dynamics simulation results were compared with experimental results for documented experimental burner. The submodels used for computational fluid dynamics were also discussed. Finally, the design optimisation methodology which entails coupling computational fluid dynamics to mathematical optimisation was presented.

CHAPTER 6

RESULTS

6.1 PREAMBLE

This chapter presents the results of the design optimisation for the different case studies introduced in the previous chapter. In particular the mathematical optimisation formulations for all the case studies are also presented.

6.2 OPTIMISATION CASE STUDIES

The computational time required for one computational fluid dynamics simulation on a Pentium IV (with 1 GB RAM and 2.6 Hertz) was four days. Thus for the gradient-based design optimisation methodology implemented here, n+1 computational fluid dynamics simulations or function evaluations are required at each design point $\boldsymbol{x}$ to determine all the components of the objective and constraints gradient vectors. Therefore, the total optimisation time required for each case appears to be prohibitively high, hence making automatic linking of the Dynamic-Q optimisation and computational fluid dynamics infeasible. For this reason, computational fluid dynamics simulations were performed on a few computers simultaneously for different perturbed design variable settings, from which the approximations of the objective and constraint functions and the gradient vectors were obtained. The approximations of the subproblem *(P(i))*, were then solved with Dynamic-Q which is implemented in the Toolkit for Design Optimisation (TDO) software [112]. This manual process greatly reduces the total computational time required since the use of many computers in parallel resulted in greater overall economy in performing the computational fluid dynamics simulations.

The Toolkit for Design Optimisation (TDO) [112] has been used with Dynamic-Q to perform design optimisation for the approximated objective function. The Dynamic-Q method needs first-order gradients of the objective and constraint functions with respect to each of the design variables. The complete theory of the Dynamic-Q

method is given in Chapter 4. Due to the computational expense of the problem to be optimised, gradient sensitivity investigations could not be performed in order to determine the perturbation size (Δx) for each design variable. The perturbations sizes for the design variables were used as suggested by Snyman *et al.* [112]. The size of the admissible range was determined from performing some computational fluid dynamics simulations and by using engineering judgement. The results of the simulations beyond the determined range were unrealistic. Move limits were determined according to reference [21], where it is suggested that the move limits should be approximately 20% of the range, and perturbation size be 10% of the range.

The complete mathematical formulation of the optimisation problem will be given for each case. Constraints will be written in the standard form $g_j(\boldsymbol{x}) \leq 0$ (inequality) and $h_k(\boldsymbol{x}) = 0$ (equality), where $\boldsymbol{x}$ denotes the vector of the design variables $(x_1, \ldots, x_n)^T$.

The objective is to minimize the shaded area, $f(\boldsymbol{x})$, in Fig. 5.16, so that the original combustor temperature profile and target combustor temperature profile follow each other closely. By so doing the temperature difference will be reduced and the combustor exit temperature profile can be made more uniform.

6.3 TWO DESIGN VARIABLES (Case 1)

This case considers the widely used approach of optimising combustor exit temperature profile by selecting dilution hole parameters as design variables [2], specifically the number of dilution holes and the diameter of dilution holes. The number of dilution holes was allowed to vary between two and seven and the diameter between four and eight. Therefore, the limits are set as $2 \leq x_1 \leq 7$ and $4 \leq x_2 \leq 8$, where x_1 = number of dilution holes and x_2 = diameter of dilution holes. The explicit optimisation problem is therefore:

Minimise $f(\boldsymbol{x})$ = Shaded Area in Fig. 5.16

such that: x_1 an integer, $x_2 \in R$

where x_1 = number of dilution holes and x_2 = diameter of dilution holes.

The original temperature profile (non-optimised) in Fig. 6.1, was generated with initial (starting) values of $x_1 = 5$ and $x_2 = 6$. The move limits for x_1 and x_2 are 2 and 1, respectively and the perturbation sizes for calculating the gradients are 1 and 0.4, respectively. No explicit inequality or equality constraints have been used, so that the minimum found is essentially for an unconstrained problem, although limits have been set on design variables to ensure that the problem remains realistic. This is intended to show where the best possible optimum lies, so that later when constraints are used, the optima can be compared. The integer solutions were selected by the rounding off of the continuous approximate solutions obtained.

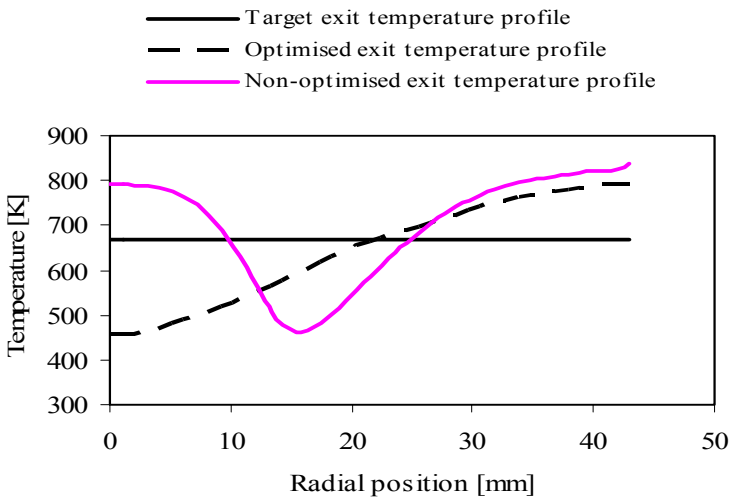

Figure 6.1. Target, non-optimised and optimised combustor exit temperature profile for Case 1

6.3.1 Results for Case 1

The results of the optimised combustor exit temperature profile are shown in Fig. 6.1 for Case 1, where two design variables are used. In this figure, the corresponding target, optimised and non-optimised combustor exit temperature profiles are shown.

A comparison of the non-optimised and the optimised combustor exit temperature profiles shows an improvement, because the severe sinusoidal nature of the non-optimised (original) combustor exit temperature profile has been lessened. Though the optimised temperature profile in Fig. 6.1 is still not very close to the target

temperature profile, the exit temperature profile is more uniform than before design optimisation. The area-weighted average amount of $C_{12}H_{23}$ or unburnt hydrocarbons (UHC) at the exit of the combustor was zero before and zero after design optimisation. For CO, the area-weighted average was 0.00035 before optimisation and 0.00034 (2.9% difference) after optimisation, and this shows that the CO is almost constant. The presence of CO is due to dissociation in the high-temperature combustion zone, as confirmed by the non-existence of $C_{12}H_{23}$, which can be interpreted as complete combustion. The pattern factor was 0.50 before design optimisation and 0.36 after design optimisation, showing some improvement.

Figure 6.2 shows the optimisation history of the objective function. The objective function essentially levels out after seven design iterations, showing that the objective function has converged. The objective function has converged to a local optimum, with the global optimum for this case probably corresponding to the lower value (F=4.8) of the objective function reached at iteration 6 (see Fig. 6.2). The objective function has decreased from 5.3 to 4.8 at iteration 6, which represents a decrease of 9.5% and corresponds to a feasible design. At this minimum objective function, the design variables are given as $x_1 = 4$ for the number of dilution holes, and $x_2 = 4$ for the diameter of dilution holes. It can be observed in Fig. 6.3 that both design variables are still changing after the eighth iteration, although the objective function in Fig. 6.2 has levelled off. This indicates that the last three designs in the optimisation run are effectively equivalent having the same objective function value, although the design variables differ slightly.

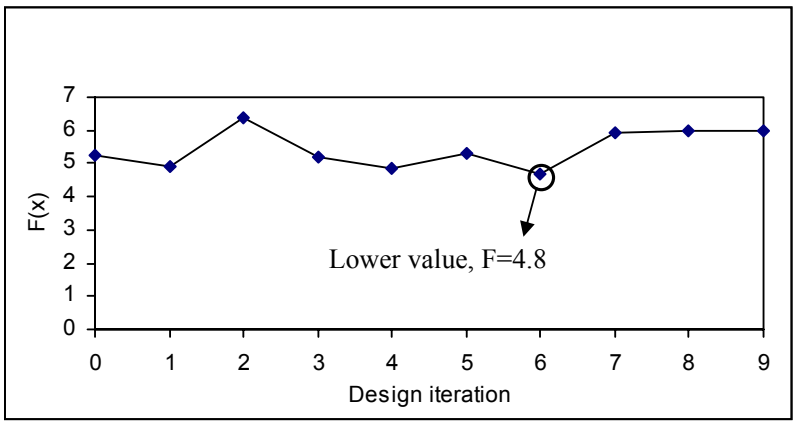

Figure 6.2. Optimisation history of the objective function for Case 1

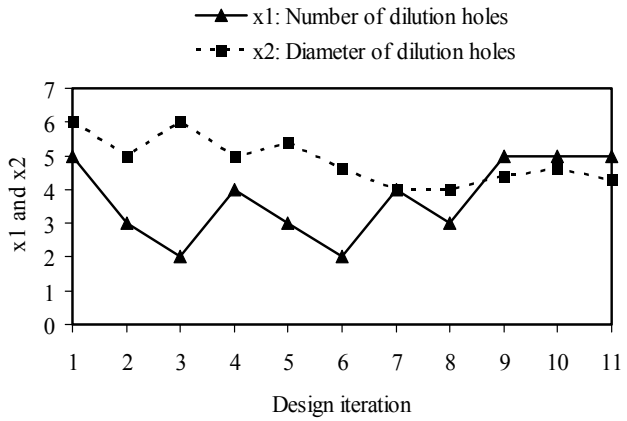

Figure 6.3. Optimisation history of design variables for Case 1, where x_1 = number of dilution holes and x_2 = diameter of dilution holes

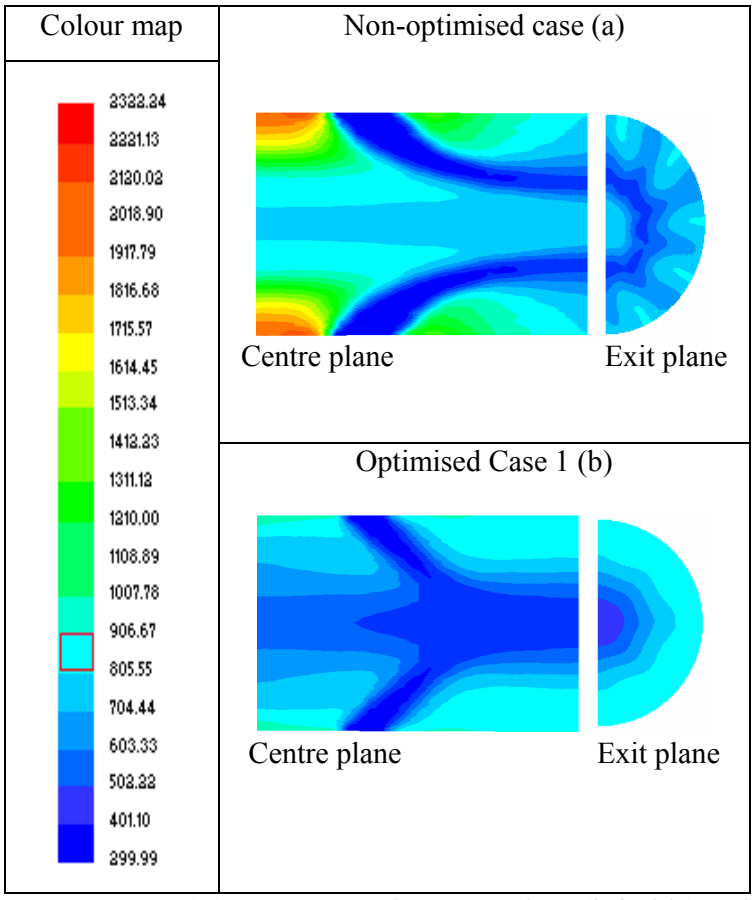

Figure 6.4. Temperature (K) contours on the centre plane (left side) and exit plane (right side) of the combustor for the non-optimised case (a) and optimised Case 1 (b)

Figure 6.4 shows temperature contours at the centre plane (left side) and exit plane of the combustor (right side) for both non-optimised and optimised cases. The combustor exit temperature contours in Fig. 6.4b (right side) are better than in Fig. 6.4a (right side). In Fig 6.4a, there is a hot section in the centre and a cold section midway section and a variation of cold and hot sections close to the wall of the combustor. This is caused by poor mixing due to an unoptimised flow field, which is improved in Fig. 6.4b. Figure 6.4a and Fig. 6.4b on the left side show how the jet penetrates the combustor. It can be noticed that the jet in Fig. 6.4a under-penetrates, whereas the one in Fig. 6.4b penetrates deeper into the combustor, causing an improvement in mixing. This has caused an improvement in the non-optimised pattern factor for Case 1 from 0.50 to 0.36.

In Case 1, the pressure drop has increased by 37%, which is an undesirable feature, though it is beneficial to combustion and dilution processes. This is because a high pressure drop results in high injection air velocities, steep penetration angles and a high level of turbulence, which promotes good mixing [2]. These results show that the optimum design creates high pressure drop in the combustor. Due to the fact that high pressure drop was experienced in Case 1, a pressure loss constraint was imposed in Case 2.

6.4 FOUR DESIGN VARIABLES (Case 2)

As already explained, a common procedure for optimising the combustor exit temperature profile involves the use of design variables related to the dilution holes as in the previous Case 1. This is the case when most of the combustor performance requirements were achieved during the preliminary design phase. However, in the current study, combustion proceeded into the secondary zone, which is an undesirable feature that would undermine the primary purpose of the secondary holes. This means the secondary holes would have some influence on the flame structure and hence the quality of the combustor exit temperature profile. Based on the above reason, it has been decided that the parameters related to the secondary holes be included as optimisation design variables. The other reason is that the optimum lies in the region where pressure drop is high, as explained in the Case 1 results. Therefore, including secondary holes may provide a better optimum with improved pressure drop.

In Case 2, four design variables are considered for design optimisation and they include: the radius of the secondary holes *(x_1),* number of secondary holes *(x_2),* number of dilution holes *(x_3)* and radius of dilution holes. An inequality constraint is imposed so that the pressure drop does not exceed the initial pressure drop by 8% ($\Delta p \leq 160$ Pa). The equality constraint has also been imposed so that the mass flow through the secondary holes should not change during the design optimisation runs, therefore, the total surface area must be the same. The optimisation parameters for Case 2 are given in Table 6.1. The formulation of the optimisation problem is now as follows:

Minimise f(**x**) = Shaded Area in Fig. 5.16

such that:

$$g_1 = \Delta p - 160 \leq 0 \quad \text{(inequality constraint)}$$

$$h_1 = x_1 x_2 - 37.5 = 0 \quad \text{(equality constraint)}$$

$$g_j = -x_j + x_j^{\min} \leq 0, \qquad j = 1, 2, ..., 4$$

$$g_{j+2} = -x_j - x_j^{\max} \leq 0, \qquad j = 1, 2, ..., 4$$

where $x_j^{\min}$ and $x_j^{\max}$ denote the upper and lower limits on the variation of variables.

In addition move limits (Table 6.1) are also imposed.

Here x_2, x_3 are integers, and x_1, x_4, $\in$ R

	x_1	x_2	x_3	x_4
Initial values	2.5	6	5	6
Move limits	0.4	2	2	1
Perturbations sizes	0.2	1	1	0.4
Lower limit	1.9	3	2	4
Upper limit	3.9	10	7	8

Table 6.1. Optimisation parameters for Case 2

6.4.1 Results for Case 2

The results of the optimised combustor exit temperature profile are shown in Fig. 6.5 for Case 2. In this figure the corresponding target, optimised and non-optimised

combustor exit temperature profiles are shown. The results show an improvement in the non-optimised (original) combustor exit temperature profile when compared with the non-optimised exit temperature profile. Though the optimised exit temperature profile is still not close to the target temperature profile, the exit temperature profile is more uniform than before optimisation. The area-weighted average of $C_{12}H_{23}$ or unburnt hydrocarbons (UHC) at the exit of the combustor was zero before optimisation and zero after optimisation. For CO, the area-weighted-average was 0.00035 before optimisation and 0.00036 (2.9% difference) after optimisation, and this shows that the CO is almost constant. As in Case 1, the presence of CO is due to dissociation in the high-temperature combustion zone, as confirmed by the non-existence of $C_{12}H_{23}$, which can be interpreted as complete combustion.

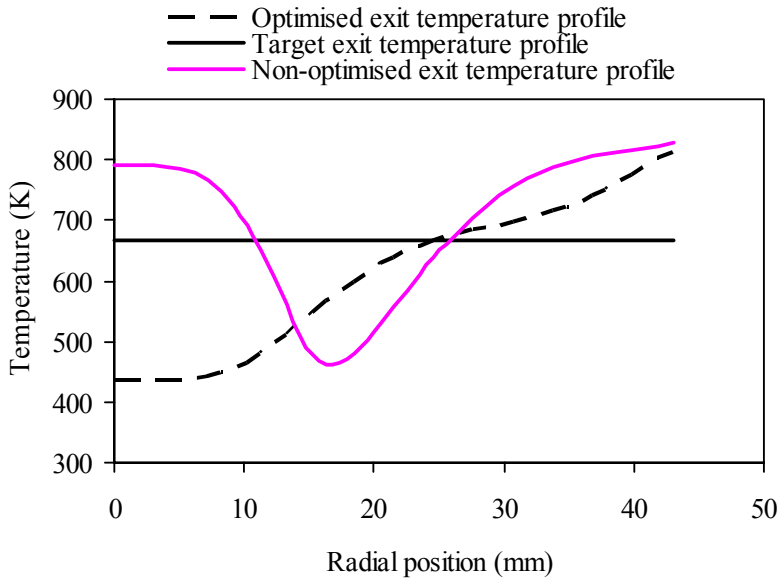

Figure 6.5. Target, non-optimised and optimised combustor exit temperature profile for Case 2

Figure 6.6 shows the optimisation history of the objective function. The objective function essentially levels out after 14 design iterations, showing that the objective function has converged to a local minimum. The lower value of the objective function (F=4.2) is at iteration 8, however, the design is not feasible because the inequality constraint function which is related to pressure drop has been violated. The objective function appears to reach a value closer to the global minimum at iteration 13, which

corresponds to a feasible design. This value of 4.6 represents a decrease of 13% relative to the value for the initial design of 5.3. At this minimum objective function value, the design variables are given as the diameter of secondary holes (x_1) = 2.1, number of secondary holes (x_2) = 8, number of dilution holes (x_3) = 6, and diameter of dilution holes (x_4) = 5.5. In Fig. 6.7, it can be observed that the design variables are still changing (though with small magnitudes) after the fourteenth iteration, although the objective function has almost levelled off. This indicates that the last three designs in the optimisation run are effectively equivalent.

Figure 6.8 shows that during the optimisation run, both the inequality and equality constraints were violated at certain design points. The inequality constraint ($g(\boldsymbol{x})\leq 0$) in Fig 6.8 is violated when it exceeded zero, and the equality constraint was violated as long as the curve representing $h(\boldsymbol{x})$ is not a horizontal straight line coinciding with the x-axis. It is acceptable for constraints to be violated by the optimiser, but the extent of violation should be limited to a reasonable value. The design at iteration 13 is acceptable. The validity of the design at the point where the results are violated can be considered in terms of the designer's engineering judgement. For example, if designers accept the design at iteration 4, then the inequality constraint has been violated by 5% and equality constraint by 1.7% and both these values may be acceptable. If the results were not acceptable, considering the fact that it is a requirement that engineering judgement should be used when looking at the results, the next best design point would be looked at.

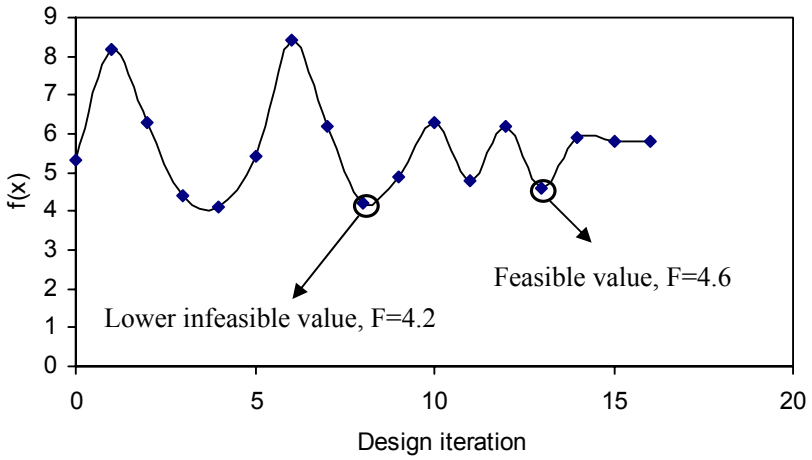

Figure 6.6. Optimisation history of the objective function for Case 2

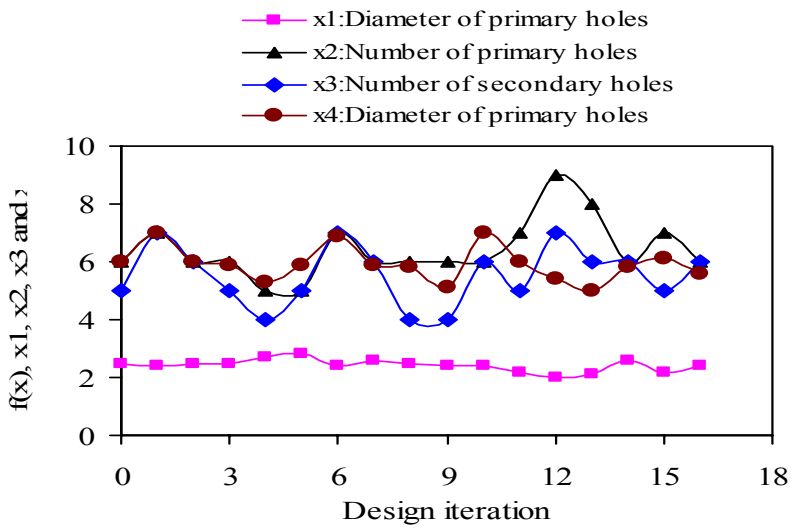

Figure 6.7. Optimisation history of the design variables for Case 2, where x_1 = diameter of secondary holes, x_2 = number of secondary holes, x_3 = number of dilution holes, x_4 = diameter of dilution holes

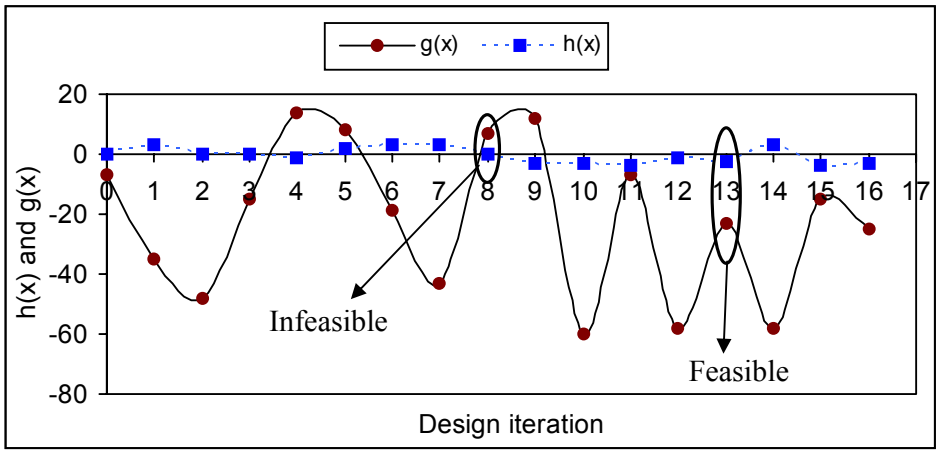

Figure 6.8. Optimisation history of constraints for Case 2

Figure 6.9 shows temperature contours of the combustor exit plane for both non-optimised and optimised cases. The combustor exit temperature contours in Fig. 6.9b are better than in Fig. 6.9a. In Fig 6.9a, there is a hot section in the centre and a cold section midway and a variation of cold and hot sections close to the wall of the combustor. This is caused by poor mixing due to an unoptimised flow field, which is improved. Improved mixing has caused an improvement in the pattern factor for Case 2 from 0.50 to 0.42.

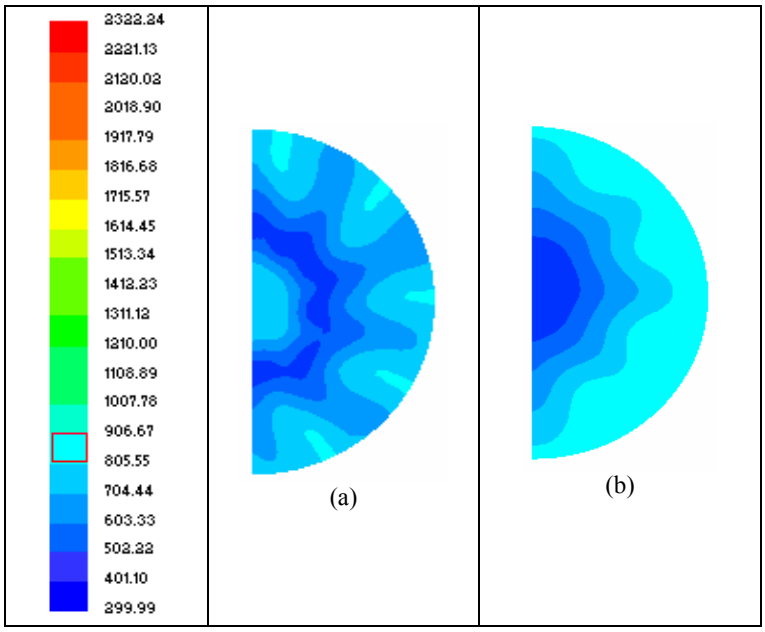

Figure 6.9. Temperature (K) contours (exit plane) for non-optimised and optimised for Case 2

6.5 FIVE DESIGN VARIABLES (Case 3)

In Case 3, five design variables are considered for design optimisation and they include: the radius of the primary holes *(x_1),* number of primary holes *(x_2),* number of dilution holes *(x_3),* radius of dilution holes *(x_4)* and swirler angle *(x_5).* The primary hole parameters and swirler angle have been considered because the recirculation zone has tremendous effects on various combustion processes as explained in sections 2.2.3 and 2.2.5, of which combustor exit temperature profile is a result. An inequality constraint is imposed so that the pressure drop does not exceed the initial pressure drop by 8% ($\Delta p \leq 160$ Pa). The formulation of the optimisation problem is now as follows:

Minimise f(**x**) = Shaded Area in Fig. 5.16

such that:

$$g_1 = \Delta p - 160 \leq 0 \quad \text{(inequality constraint)}$$

$$g_j = -x_j + x_j^{\min} \leq 0, \qquad j = 1,2,...,5$$

$$g_{j+2} = -x_j - x_j^{\max} \leq 0, \qquad j = 1,2,...,5$$

where x_j^{min} and x_j^{max} denote the upper and lower limits on the variation of variables. In addition, move limits (Table 6.2) are imposed.

Here x_2, x_3 are integers, and x_1, x_4, $\in$ R

where x_1 is the diameter of primary holes, x_2 is the number of primary holes, x_3 is the number of dilution holes, x_4 is the diameter of dilution holes and x_5 is the swirler angle. The optimisation parameters for Case 3 are given in Table 6.2.

	x_1	X_2	x_3	x_4	x_5
Initial values	3.3	3	5	6	45
Move limits	0.4	2	2	1	0.5
Perturbation sizes	0.2	1	1	0.4	1
Lower limit	2.3	2	2	4	45
Upper limit	2.9	6	7	8	65

Table 6.2. Optimisation parameters for Case 3

The design variable x_5 is of different dimensions and expressed in a different unit from the other four design variables. It is, therefore, necessary to scale x_5 so that difficulties in calculating numerical gradients and distortion of the objective function can be avoided. The design variable x_5 (swirler angle) is scaled through the use of range equalisation factors (θ) as:

$$\theta_i = \frac{x_{5i} - x_{5LL}}{R} \quad , R = x_{5HH} - x_{5LL} \qquad (5.4)$$

$$i = 1,2,3,\ldots\ldots n.$$

where R represents the range width, HH represents higher limit and LL represents lower limit. Due to the scaling process, the new limits of variable x_5 are; $0 \leq x_5 \leq 5$.

6.5.1 Results for Case 3

The results of the optimised combustor exit temperature profile are shown in Fig. 6.10. In this figure, the corresponding target, optimised and non-optimised combustor exit temperature profiles are shown. A comparison of the non-optimised

and the optimised combustor exit temperature profiles shows an improvement, because the severe sinusoidal nature of the non-optimised (original) combustor exit temperature profile has been lessened. Although the combustor exit temperature profile is improved by optimisation, the pattern factor has increased from 0.50 to 0.55. Pattern factor has increased because the maximum temperature of the optimised combustor exit temperature profile in Fig. 6.10 is more than for the non-optimised combustor exit temperature profile. However, a more uniform combustor exit temperature profile shows an improvement in mixing due to the inclusion of swirler angle and primary holes as optimisation design variables. The area-weighted average of $C_{12}H_{23}$ or unburnt hydrocarbons (UHC) at the exit of the combustor was zero before optimisation and zero after optimisation. For CO, the area-weighted average was 0.00035 before optimisation and 0.00034 (2.9% difference) after optimisation, and this shows that CO is almost constant. As in Case 1 and Case 2, the presence of CO is due to dissociation in the high-temperature combustion zone, as confirmed by the non-existence of $C_{12}H_{23}$, which can be interpreted as complete combustion.

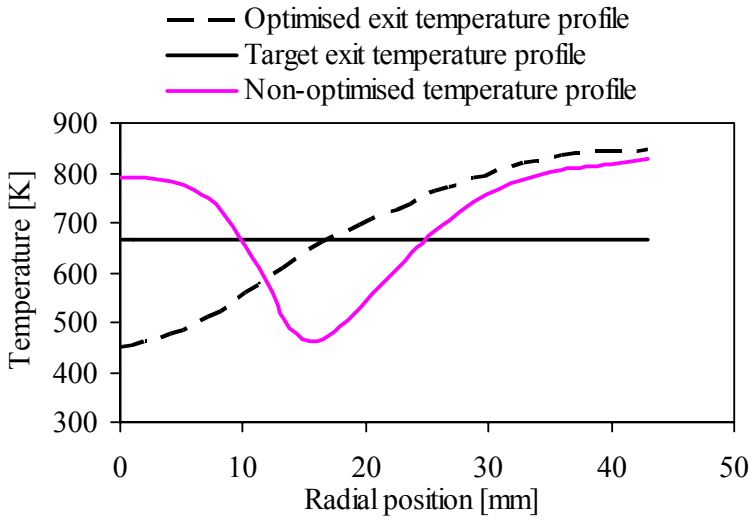

Figure 6.10. Target, non-optimised and optimised combustor exit temperature profile for Case 3

Figure 6.11 shows the optimisation history of the objective function. It can be noticed that the objective function essentially levels out after nine design iterations, showing that the objective function has converged to a local minimum. Again the objective function has probably reached the neighbourhood of the global minimum at iteration 8

where it attains the value of 3.9, representing a decrease of 26% relative to its initial value of 5.3. At this minimum objective function value, the design is feasible with variables given as diameter of primary holes (x_1) = 3.9, number of primary holes (x_2) = 2, number of dilution holes (x_3) = 3, diameter of dilution holes (x_4) = 4.3 and swirler angle (x_5) = 47.3°. In Fig. 6.12, it can be observed that some design variables are still changing (though with small magnitudes) after the ninth iteration, although the objective function has almost levelled off. This indicates that the last three designs in the optimisation run are effectively equivalent having almost the same objective function values (shaded area between the curves), although their geometries differ slightly. Figure 6.13 shows that during the optimisation process, the pressure drop (inequality constraint) mostly remained within the limits.

Figure 6.14 shows the temperature contours of the combustor exit plane for both the non-optimised and optimised cases. The combustor exit temperature contours in Fig. 6.14b are better than in Fig. 6.14a. In Fig 6.14a, there is a hot section in the centre and a cold section midway and a variation of cold and hot sections close to the wall of the combustor. This is caused by poor mixing due to an unoptimised flow field, which is improved in Fig. 6.14b.

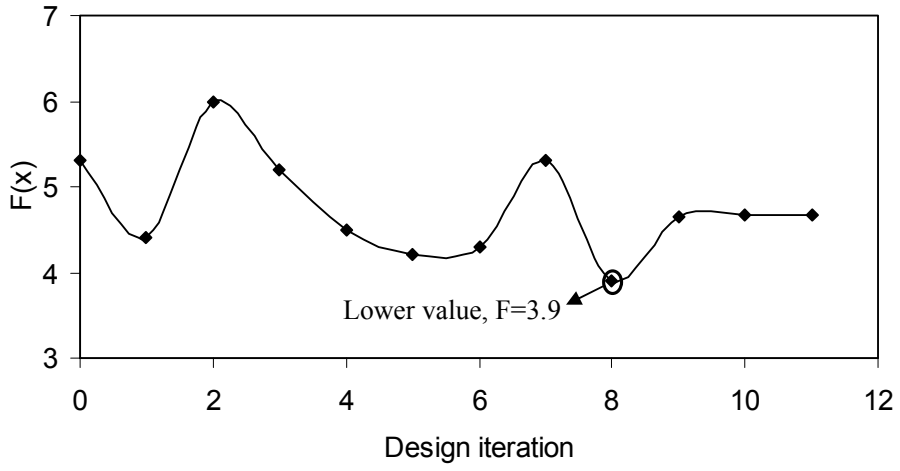

Figure 6.11. Optimisation history of the objective function for Case 3

The swirler angle and the number and diameter of primary holes were used because the primary zone flow field has some effects on the combustor exit temperature

profile. Figure 6.15 shows the non-optimised and optimised tangential velocities. The tangential velocity for the optimised case is increased, hence, modifying the size of the central toroidal recirculation zone. The central toroidal recirculation zone is also a function of the interaction of swirling flow and the number and diameter of primary holes [1,113]. Decreasing the number of holes and increasing the diameter of holes, increase the size of the central toroidal recirculation zone. In this case, the optimiser increased the tangential velocity by an increased swirl angle and provided bigger and fewer primary holes. This has the effect of increasing the size of the central toroidal recirculation zone.

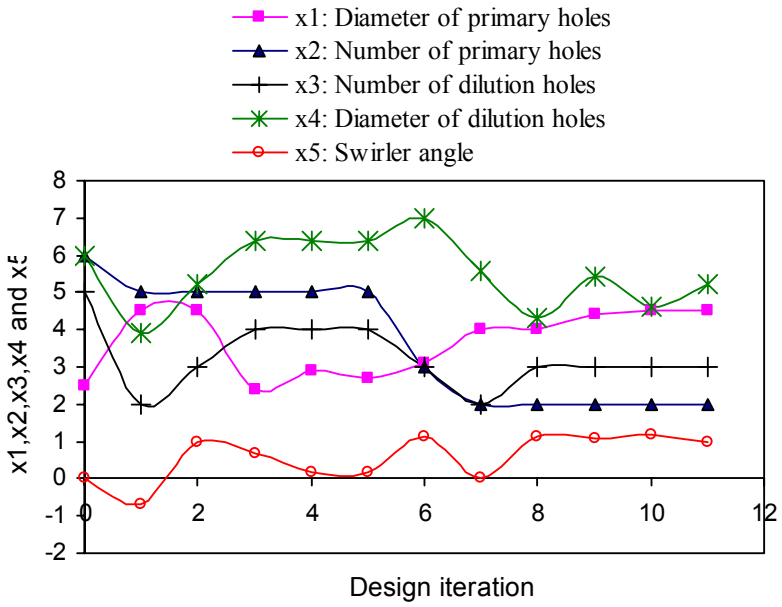

Figure 6.12. Optimisation history of design variables for Case 3, where x_1 = diameter of primary holes, x_2 = number of primary holes, x_3 = number of dilution holes, x_4 = diameter of dilution holes and x_5 = swirler angle

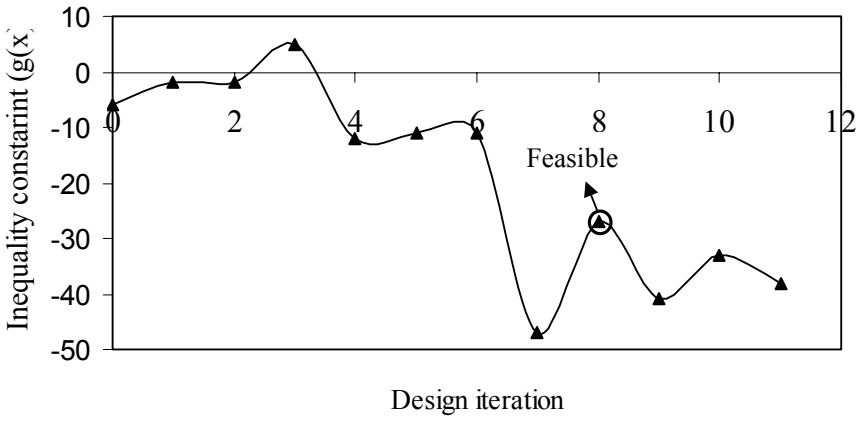

Figure 6.13. Optimisation history of inequality constraint for Case 3

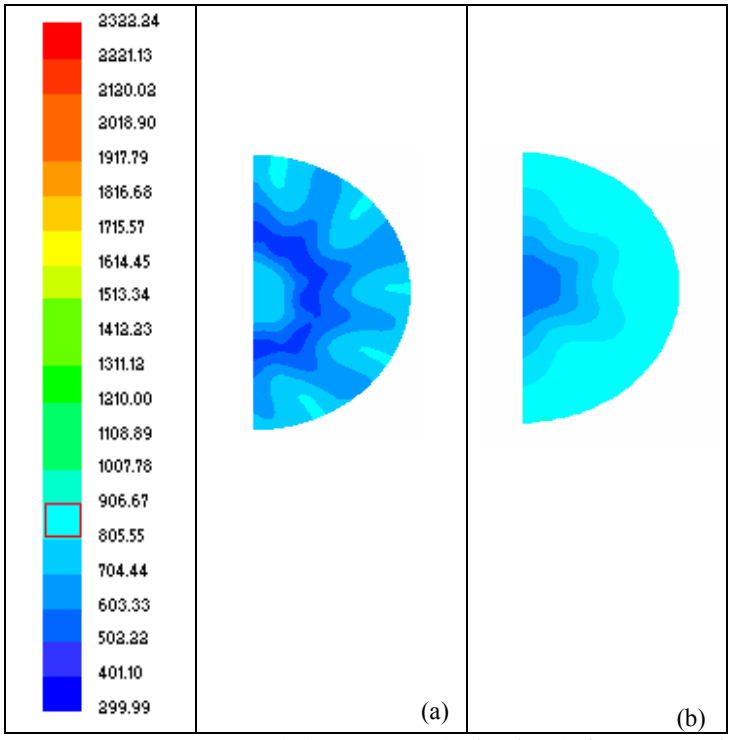

Figure 6.14. Temperature (K) contours (exit plane) for non-optimised and optimised for Case 3

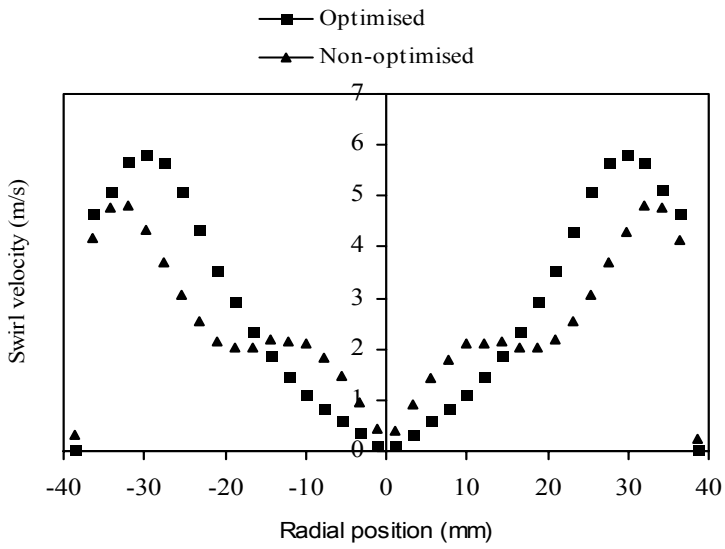

Figure 6.15. Swirl velocity at 30 mm from the dome face for non-optimised case and optimised Case 3

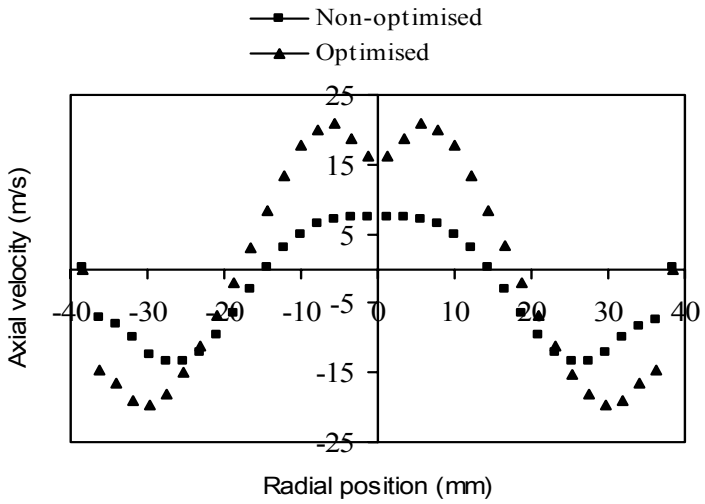

Figure 6.16. Axial velocity at 30 mm from the dome face for non-optimised case and optimised Case 3

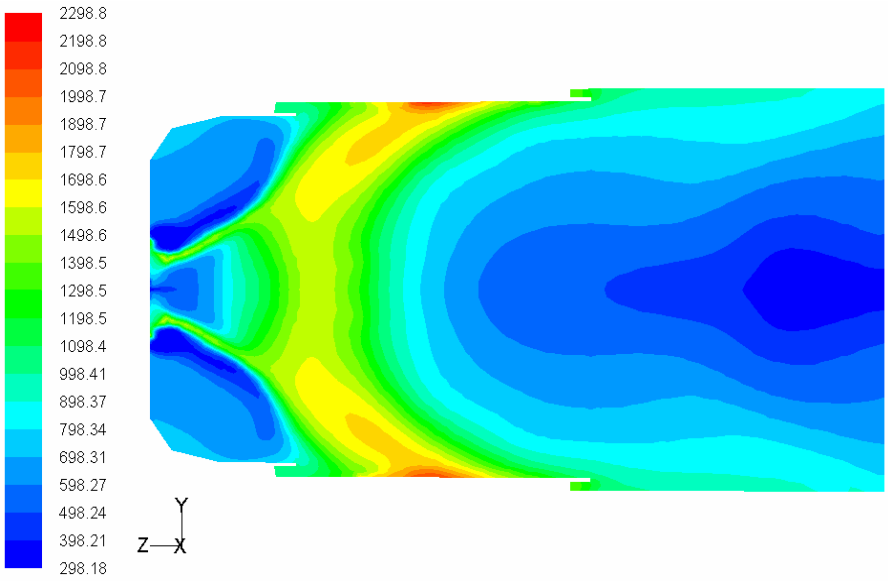

Figure 6.17. Temperature (K) contours of optimised Case 3 on the symmetrical plane

The formation of the central toroidal recirculation zone is shown in Fig. 6.16. The optimised Case 3 has high peaks of positive and negative axial velocities. Due to the fact that the size of the central toroidal recirculation zone is increased, the flame in Fig. 6.17 also became shorter than in Fig. 5.15. This is consistent with the observations of Lefebvre [2] and Vanoverberche *et al.* [113] that strong recirculation zones provide shorter flames. Very high values of swirl are, however, not appreciated because the flame can be located very close to the nozzle and dome causing damage to them and it can also affect flame stability [113]. This interaction subsequently influences emissions. Therefore, tight design variable limits have to be placed on the swirler angle and on the number and diameter of primary holes. These observations could also discourage the inclusion of these parameters in the optimisation problem for combustor exit temperature profile. Therefore, care must be taken when selecting the limits of design variables related to the geometry of the swirler and the primary holes, particularly when dealing with reacting flows.

6.6 CONCLUSION

The design optimisation methodology was used to get a more uniform combustor exit temperature profile by optimising the combustor with design variables related to the combustor geometry. In Case 1, a common procedure of optimising the combustor

exit temperature profile with dilution holes was used. Though the combustor exit temperature profile was improved, it was at the expense of high pressure drop. This case revealed that it might not be possible to get the optimum combustor exit temperature profile, especially when pressure loss is one of the constraints.

In Case 2, optimisation returns improved results at a considerably reduced pressure drop with four design variables that are related to the dilution holes and secondary holes. Increasing the design variables resulted in getting a better optimum within design constraints. A better combustor exit temperature profile was achieved and the pattern factor also improved.

In Case 3, a better optimum at lower pressure drop was achieved with design variables that are related to swirler, primary holes and dilution holes. Though the combustor exit temperature profile was improved the pattern factor increased.

In all three cases, optimisation returns a significant modification in the combustor exit temperature profile. The optimiser started with an extremely non-uniform combustor exit temperature profile, but a more uniform combustor exit temperature profile was achieved in each case.

A better pattern factor has been obtained in Case 1 where only the dilution hole parameters were used. This is a common procedure used in trying to shape the combustor exit temperature profile, by mixing cold air with hot combustion products. Another improved pattern factor is provided by Case 2, where the secondary hole and dilution hole parameters are used for design optimisation. This case has provided results which are within pressure drop limits. The pattern factor in Case 3 has increased, though the combustor exit temperature profile is more uniform. This might be due to the fact that a lot of combustor flow non-linearities are taking place in the primary zone, where vaporisation processes and heat generation take place. Alteration of the flow field in the primary zone has affected this non-linearly related and coupled flow processes.

CHAPTER 7: CONCLUSIONS AND RECOMMENDATIONS

7.1 CONCLUSIONS

From the literature survey, presented in Chapter 1, it can be concluded that it is necessary to search for better alternatives for the optimisation of gas turbine combustors. Any design optimisation methodology that is based exclusively on experimental methods is considered too time-consuming and expensive to be a viable method for producing an optimum result. Although the use of computational fluid dynamics provides some improvements in cutting cost and time, it is unable on its own to give an optimum design. Both the above methods are based on trial and error and depend heavily on the skills and experience of the designer. Other methods which have recently been employed utilise genetic algorithms in which one-dimensional semi-empirical equations are used. These methods do not provide three-dimensional solutions and cannot perform parametric variations.

The following paragraphs summarise the optimisation methodology which is based on gradient-based successive approximation mathematical optimisation developed in this study and also highlights the main conclusions drawn from the study:

(a) A methodology is developed to optimise a combustor exit temperature profile by using combustor geometric parameters as design variables. The methodology makes use of mathematical optimisation and computational fluid dynamics to give near-optimal combustor exit temperature profiles subject to certain constraints as specified by the designer. Relevant literature that describes computational fluid dynamics modelling of combustion and the mathematical optimisation techniques used in this work is presented in Chapter 3 and Chapter 4.

(b) The first step towards implementing the methodology was to validate the computational fluid dynamics results. This part was achieved by comparing the numerical results with experimental results obtained from a representative model of a combustor. This also gives the designer confidence in the use of the numerical tool. The second and most important step was the formulation of the optimisation problem. This step involved deciding on the design variables and the objective and constraint functions. The third step involved creating journal files and data extraction techniques.

(c) The methodology developed in this thesis was tested on three cases as described in Chapter 6. The first case (Case 1) optimised the combustor exit temperature profile with two design variables and without explicit constraints. The second case (Case 2) optimised the combustor exit temperature profile with four design variables, one equality constraint and one pressure drop inequality constraint. In the third case (Case 3), five design variables were used to optimise the combustor exit temperature profile. The swirler and the primary hole parameters were included to allow for the effect of the central toroidal recirculation zone on the combustor exit temperature profile.

(d) The methodology worked well in all three cases, obtaining near-optimal designs in relatively few optimisation iterations. The results show improvements in the combustor exit temperature profile and the pattern factor. From these results, it can be concluded that the proposed optimisation methodology can be considered as a strong alternative in designing for optimal combustor exit temperature profiles. This methodology can be extended to other combustor performance parameters as long as a feasible optimisation problem can be formulated.

(e) For the methodology to be successful, the correct formulation of the optimisation problem is important. This, however, is heavily dependent on the skill, understanding and experience of the designer.

(f) The proposed methodology has two drawbacks. First, the methodology is computationally expensive, especially with regard to combustion modelling. This is compounded by the fact that *n+1* computational fluid dynamics simulations are performed for one optimisation iteration. However, the effective computational time can be greatly reduced by using multiple computers to run the simulations in parallel. Increasing computational power will also allow less simulation time and more refined computational fluid dynamics simulations to be performed. In terms of design optimisation, the computational drawback is offset to a larger extent by the fact that a near-optimal design may be reached in relatively few (~10-15) optimisation iterations. This would most probably not be possible when using traditional experimental or trial-and-error numerical modelling.

(g) It is noteworthy, that the study shows that the Dynamic-Q algorithm may readily and successfully be adapted to handle integer variables.

(h) The methodology can be applied generally to the design optimisation of gas turbine combustors, provided a realistic optimisation problem can be formulated.

7.2 RECOMMENDATIONS

Although the design optimisation methodology presented in this work is fully functional, it is possible to identify the following three main directions for further work:

- Improvement of the simulation capabilities.
- Further development of the optimisation capability.
- Extension of the design optimisation process.

The following sections will present these three possible ways of improving and extending the usefulness of the design optimisation methodology.

7.2.1 Improvement of simulations capabilities

As mentioned in the previous chapters, the k-ε turbulence model was used to model turbulence in this work, because it is more stable and quicker to converge. This is despite the fact that it has inherent problems when it comes to calculating flows with non-linearities. For these reasons, poor predictions are expected when the non-linearity of the flow field is high, such as in the presence of chemical reactions and high swirling flows. Using better turbulence models such as the Reynolds stress method may improve the simulation results because of more accurate calculation of the flame zone. As the computer power increases, it is expected that this will be achievable.

7.1.2 Further development of optimisation capability

In addition to simulation capabilities, the optimisation performance has the potential for improvement in the way it handles the integer design variables. In particular, Dynamic-Q is not tailored to explicitly handle mixed integer problems, and currently has to be adapted in an ad hoc manner to treat such cases. Special algorithms that can handle the mixed integer nature of the problem more effectively should be developed and incorporated into the Dynamic-Q algorithm. Such a feature should have the potential of improving the convergence of the integer design variables. The current ad hoc approach has the unsatisfactory tendency to rock up and down when the rounding-off technique is applied to the integer variables.

7.2.3 Extension of the design optimisation process

This work was performed on an atmospheric research combustor that is representative of a real combustor. Further complicating issues may, however, arise when dealing with a real combustor. This would necessitate the inclusion of more constraints in the optimisation formulation, such as the following:

- CO, UHC and soot emissions. For high-pressure real combustors, the emissions of pollutant become critical parameters of design.
- NOx model. The NOx model can benefit from the mixing information and more detailed chemistry.